Hidden Communication Mechanisms between Functional Regions of the Myosin Motor Domain

Thesis by

Bálint Kintses

for the Degree of Doctor of Philosophy

Advisor: András Málnási-Csizmadia PhD.

Structural Biochemistry Doctoral Program,
Doctoral School in Biology

Program Leader: Prof. László Gráf DSc.
Head of the School: Prof. Anna Erdei DSc.

Eötvös Loránd University
Budapest, Hungary
2008

Acknowledgement

First of all, I would like to thank my whole family for their support and for providing such ideal circumstances for my growth and education over the last 28 years. A special thank you goes to my wife, Andi who joined the supporting team 6 years ago. Without her I would not have been able to come this far.

I am forever grateful to András Málnási-Csizmadia, alias Málna, my adviser. It is difficult to say in a few words how much he has given me. Besides introducing me into molecular biology and reaction kinetics I learnt very much from him during our common daily routine, seeing a good example of how to focus your attention on finding a solution to a problem, be unwaveringly hard-working, obsessive in scientific questions, and always optimistic. I would like to thank Mihály Kovács, alias Stoci, for his continuous help. The idea that he has a supercomputer in his head often occurs to me. Fortunately, he is well-equipped with output interfaces thus, students always have the opportunity to download the necessary information. I am forever grateful to Máté Gyimesi, on whom I can always count and who helped me with much valuable advice and many inspiring insights during our long studentship. Furthermore, I would like to thank all members of the lab, especially Zoltán Simon for his continuous help in solving computer problems, Balázs Jelinek for management activity, and Judit Tóth for her help. A special thank you goes to Boglárka Várkuti, Yang Zhenhui, and László Végner, Kata Sarlós, and Nikolett Nagy for their contribution to our common projects.

I would like thank Prof. László Gráf, László Nyitray, and Prof. György Hegyi for operating such a successful Biochemistry Department, giving the opportunity for many students to study. Finally, I am grateful to all my teachers who taught me and people with whom I worked together at Eötvös University and at other universities as well. I am especially grateful to Clive R. Bagshaw and Mike A. Geeves for their help and for their critical readings of our manuscripts.

Summary

Myosin is an ATP-driven molecular motor that generates force and moves along an actin filament. During this complex process, the acto-myosin system goes through more than a dozen reaction steps that are performed in distant functional sites of the myosin motor domain. These distant functional regions have to communicate with each other in order to harmonize their actions, otherwise the energy to be converted into mechanical work dissipates as heat. Consequently, the understanding of the enzyme cycle of myosin requires both the exploration of the workings of each region and the mapping of their communication mechanisms.

For this purpose we use site-specific fluorescence signals placed in functional regions of *Dictyostelium* myosin II motor domain in combination with transient kinetic measurements. With this technique the fluorescent states of the observed region can be identified and the energetic of its transitions can be characterized. Furthermore, the effects of these transitions on the workings of the other functional regions can be investigated. Due to the crystal structures we can assign our fluorescent states to known conformations, this approach complements well the static structural data. Moreover, the lack of the acto-myosin crystal structure inhibits the identification of the actin-induced conformational changes and strengthens the importance of this kinetic approach.

In myosin nucleotide and actin binding is generally antagonistic, but actin affinity strongly depends on the type of the bound nucleotide. This phenomenon has been known for a while, however the molecular mechanism of the allosteric communication between the nucleotide and actin binding sites is still unknown. Recent structural studies have identified two states of switch 1 loop in the nucleotide binding site, implying a mechanism that transmits the information on the bound nucleotide towards the actin binding site. In order to investigate this concept, we introduced single tryptophan residues into the switch 1 region of myosin II motor domain and studied them by rapid-reaction methods. We identified the two functional states of switch 1 and found that the equilibrium constant between these states is coupled with the strength of the actin-myosin interaction. We found that the received thermodynamic model, describing an equilibrium shift mechanism between the pre-

existing states of switch 1, is also applicable for the nucleotide-controlled interactions of other P-loop NTP-ases and seems to be general.

Another question is how actin binding induces the force generating lever arm movement, the power stroke. According to the currently accepted conformational cascade, actin binding opens the nucleotide binding site, resulting in phosphate (P_i) release and the inducement of the power stroke. However, muscle fiber experiments suggest that the force generating lever arm movement precedes the P_i release. In order to solve this contradiction and to achieve a better integration of the mechanical step into the biochemical cycle, we conducted a detailed kinetic, mutational, and structural investigation of the lever arm movements. Based on the received findings we suggest a direct communication path between the actin binding region and the lever arm, which induces the power stroke without primary nucleotide binding site opening and P_i release.

In summary, our studies are a significant contribution to the understanding of how the nucleotide binding site, the actin binding region, and the lever arm of myosin communicate with each other.

Összefoglalás (Summary in Hungarian)

A miozin egy ATP-hajtott molekuláris motor, ami erőkifejtésre és az aktin filamentum mentén való mozgásra képes. E komplex folyamat végrehajtása közben az akto-miozin rendszer több mint egy tucat reakciólépésen halad keresztül, amelyek a miozin motor domén egymástól távol eső részein mennek végbe. E távoli funkcionális részeknek kommunikálniuk kell egymással, hogy összehangolják működésüket, különben a mechanikai munkává alakítandó kémiai energia hőveszteséggé alakul. Következésképpen, a miozin ATP-áz ciklusának megértése érdekében elengedhetetlen minden funkcionális régió működésének felderítése és a köztük lévő kommunikációs mechanizmusok feltérképezése.

Ennek vizsgálatára mi *Dictyostelium* miozin II motor domén funkcionális részeibe elhelyezett fluoreszcens szenzorokat használunk tranziens kinetikai módszerekkel kombinálva. Ezzel a technikával a vizsgálandó régió fluoreszcens állapotai azonosíthatóak, és az egymásba való átalakulásuk energetikája jellemezhető. Továbbá, ezzel a módszerrel vizsgálható egy funkcionális rész átalakulásának hatása más részek működésére. Mivel a kristályszerkezetek segítségével a fluoreszcens állapotokat hozzárendelhetjük ismert térszerkezetekhez, ez a megközelítés jól kiegészíti a statikus szerkezeti adatokat. Sőt, az akto-miozin kristályszerkezet hiánya gátolja az aktin kötés okozta térszerkezeti átalakulások azonosítását, és növeli a kinetikai megközelítés fontosságát.

A nukleotid és az aktin kötése a miozinhoz általában véve antagonisztikus, viszont az aktin affinitás erősen függ a nukleotid γ-foszfát jelenlététől. Ez a jelenség régóta ismert, viszont a nukleotid kötőzseb és az aktin kötőrész közötti kommunikáció molekuláris mechanizmusa ezidáig ismeretlen volt. Új szerkezeti eredmények a nukleotid kötőzsebet alkotó *switch 1* hurok két térszerkezeti állapotát azonosították, ezáltal szolgáltatva egy lehetséges mechanizmust a nukleotid γ-foszfát jelenlétének érzékelésére, és az információ aktin kötőrégió felé való továbbítására. A modell kinetikai vizsgálatához triptofán szenzorokat építettünk be miozin II motor domén *switch 1* régiójába. Így azonosítottuk a *switch 1* hurok két funkcionális állapotát, és azt találtuk, hogy a két állapot közötti egyensúlyi állandó kapcsolt az akto-miozin interakció erősségével. Továbbá azt találtuk, hogy a kapott termodinamikai modell, amely leírja *a switch 1* régió állapotai közötti egyensúlyok eltolódását, alkalmazható

más p-hurok NTP-ázok nukleotid kontrolált fehérje interakcióira, és általánosnak tűnik.

Továbbá azt is vizsgáltunk, hogy hogyan indukálja az aktin a miozin erőkifejtési lépését. A jelenleg elfogadott térszerkezet-változás kaszkád alapján az aktin kötés indukálja a nukleotid kötőzseb nyílását, ami viszont a foszfát felszabadulást és az erőgenerálási lépést indukálja. Ezzel szemben, izomrostban végzett és egyedi molekula kísérletek azt mutatják, hogy az erőgenerálási lépés megelőzi a foszfát felszabadulást. Az ellentmondás feloldásához és a mechanikai lépés biokémiai ciklusba való jobb integrálásához, az erőkar mozgásainak mélyreható kinetikai, mutációs és szerkezeti vizsgálatait végeztük el. A kapott eredmények alapján azt állítjuk, hogy az aktin kötő rész egy direkt kommunikációs útvonalon keresztül indukálja az erőgenerálást, elkerülve az elsődleges nukleotid kötőzseb nyílást és foszfát felszabadulást.

Összességében elmondhatjuk, hogy e munka jelentősen hozzájárul a nukleotid kötőzseb, az aktin kötőrégió és az erőkar közötti kommunikáció megértéséhez.

Contents

Review of Literature

The myosin

Myosins are molecular motors that move along actin filaments by converting ATP-stored chemical energy into mechanical work. They were first discovered in muscle fiber ref (5), however it was later revealed that every eukaryote cell expresses myosins. Cytoplasmic transport processes, cell movements, cytokinesis, membrane trafficking, and signal transduction are some examples from the repertoire of the myosin-driven cell functions (3, 61). The great variability among myosin genes allows their divers functions. The human genome for example, contains over 40 different active myosin genes. In spite of this great variability, the chemo-mechanical transduction, the mechanism that converts the ATP-stored energy into mechanical work, seems to be conserved among myosin families.

The conservation of the chemo-mechanical transduction is due to the fact that all myosin isoforms contain very similar N-terminal motor domains. Figure 1 shows the structure of conventional myosin molecules (myosin II [1]), such as striated muscle or smooth muscle myosins.

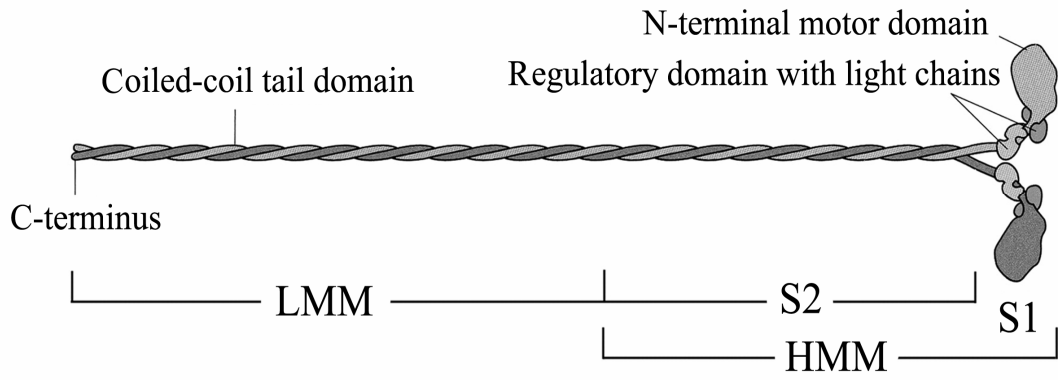

Figure 1. The homodimer myosin II molecule with indication to its proteolytic fragments (84). The head of the myosin (subfragment 1, S1) consists of the catalytically active N-terminal motor domain and a light chain binding regulatory domain. The long coiled-coil tail serves for dimerization and myosin filament formation. S1 together with S2 create the heavy meromyosin (HMM), while the C-terminal fragment is the low meromyosin (LMM) (23, 84).

[1] Myosin superfamily contains 18 classes marked with roman numerals.

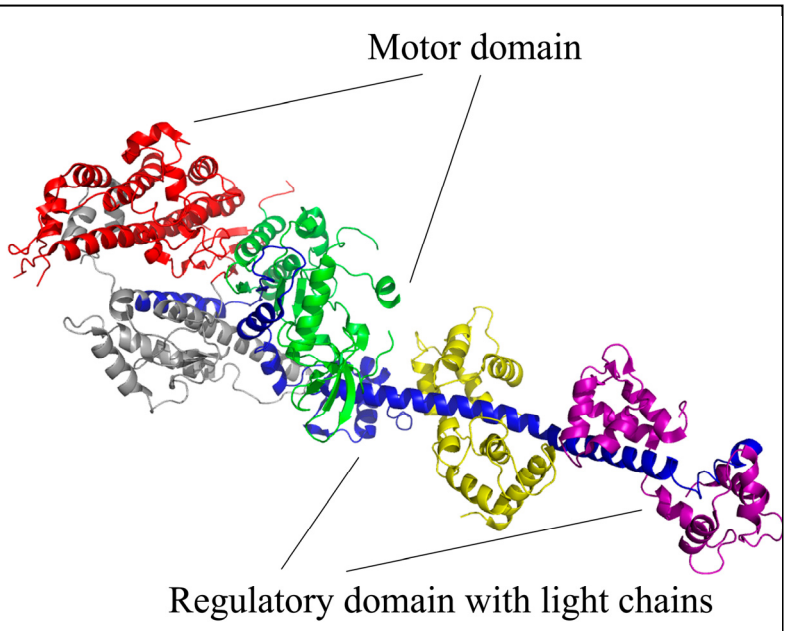

Figure 2. Crystal structure of scallop myosin II S1 with the light chains (purple and yellow) (Protein Data Bank code 1KK7).

The myosin head consists of the N-terminal motor domain and the regulatory domain (Figure 2). The motor domain is responsible for the catalysis of ATP hydrolysis, for cyclic interaction with actin, and for force generation. Consequently, those restricted forms of myosin which contain just the myosin head (Subfragment 1, S1) or the motor domain show complete motile functions making them successful objects of experimental investigations aiming at the understanding of the motor function (51). The regulatory domain is the lever arm that amplifies movement. All myosin II molecules contain a long C-terminal coiled-coil tail domain after the myosin head, serving for dimerization and filament formation. Other myosin isoforms contain other tail domains, such as cargo binding domain, depending on their function.

We use *Dictyostelium* myosin II motor domain for our investigations because it shows high similarity to skeletal and smooth muscle myosins, it can be expressed in high quantity in *Dictyostelium* recombinant expression system (59), and its globular structure allows it to crystallize (17).

The working models of the acto-myosin system

The 1942 discovery that muscle contraction is based on the interaction of two proteins, actin and myosin, can be tied to the Hungarian Nobel Laureate's name, Albert Szent-Györgyi (5). However, it took further thirty years for the principles of

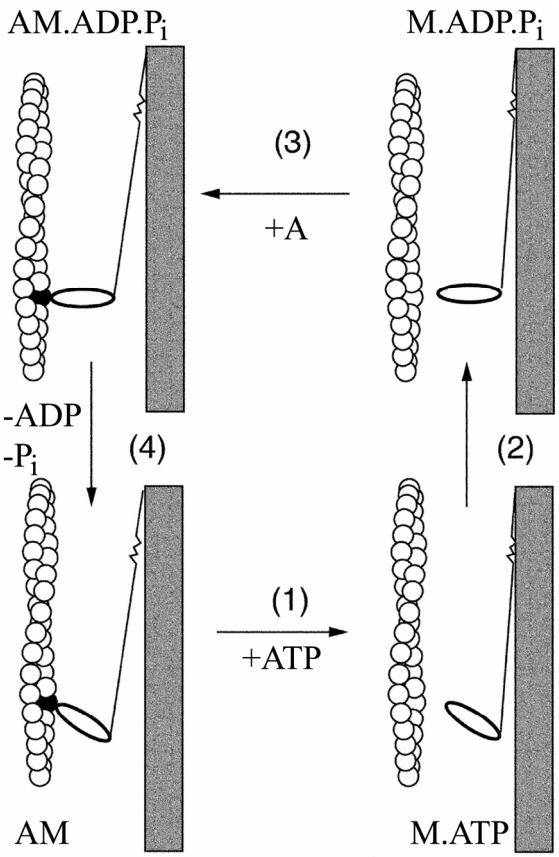

Figure 3. The classic model of the myosin enzyme cycle proposed by Lymn and Taylor (ref). ATP binding to the myosin cross-bridge dissociates from the acto-myosin complex. Then in the detached state the myosin cross-bridge goes through a conformational change, of which the reversal movement after rebinding to actin causes displacement along the actin filament.

the myosin enzyme cycle to be explored (84). Figure 3 shows the Lymn-Taylor model, which represents a four-step enzyme cycle for the acto-myosin system (54). According to this model, in rigor state (state 1) the myosin cross bridge carrying the myosin head interacts strongly with the actin filament in the absence of nucleotide. The first step is the MgATP binding into the nucleotide binding site of myosin, which induces allosterically the acto-myosin dissociation. In step 2 the myosin cross bridge undergoes a large conformational change with the priming of the myosin for force generation and MgATP hydrolysis. Then actin binds back to myosin in step 3 when ATP has already been hydrolyzed and MgADP.P_i is bound into the nucleotide binding pocket. The actin re-attachment activates the enzyme cycle of myosin, leading to a rapid hydrolytic product release and the reversed conformational change of the cross bridge (step 4). In spite of the fact that the Lymn-Taylor model does not contain some newly discovered intermediates, the essential four steps are still valid.

Also in the seventies Clive R. Bagshaw during his PhD work and David Trentham developed a kinetic model for the enzyme cycle of the myosin in the absence of actin that is still valid as well (Scheme 1) (2). By using intrinsic fluorescence of skeletal myosin, they found that the nucleotide binds to myosin in two steps corresponding to an induced fit binding mechanism (Step 1 and 2). This step is analogous with the first step of the Lymn-Taylor model in the presence of actin. They found that the MgATP binding is almost irreversible however, the affinity for the

hydrolytic products is not so strong ($K_{d\ MgADP}$=1-100 µM, $K_{d\ Pi}$=10-50 mM). This asymmetry of the cycle allows the great free energy change of the MgATP binding needed to drive forward the enzyme cycle. The further significance of this finding is that ATP hydrolysis energy for the enzyme is not directly supplied by the breakage of the high-energy phosphate anhydride bond. The next conformational change observed by the intrinsic tryptophan fluorescence change was supposed to be coupled to the priming of the cross bridge and the hydrolysis step of myosin (step 3 in Bagshaw-Trentham scheme and step 2 of the Lymn-Taylor). In the next steps the reversed conformational change of the cross bridge (step 4) allows Pi release (step 5) and MgADP release (step 6 and 7).

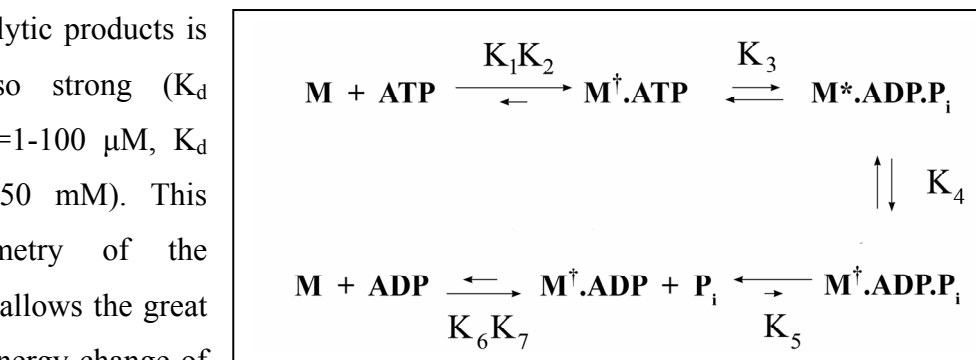

Scheme 1. Bagshaw-Trentham scheme, representing the myosin enzyme cycle in the absence of actin.

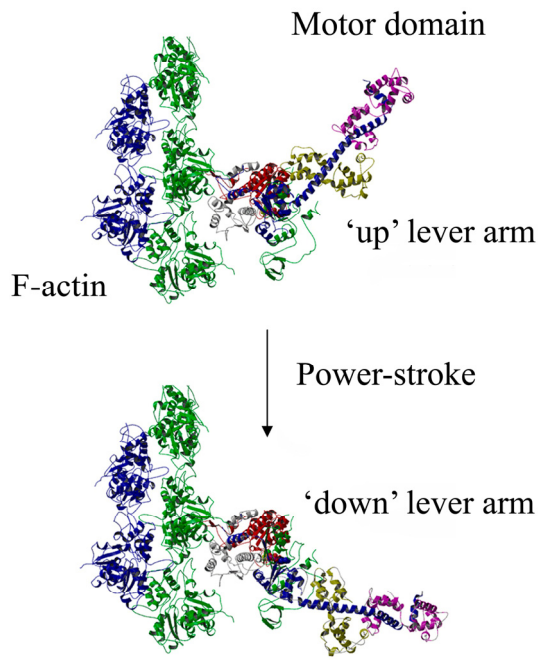

Figure 4. The swinging lever arm model. The crystal structures of myosin S1 show that the force generation is due to a swing of the lever arm formed by the regulatory domain from its primed or up conformation to its down position (20).

The lack of the high resolution structures inhibited the identification of the force-generating parts and it was believed that the change in the orientation of the myosin cross bridge is what provokes the force (swinging cross bridge theory (38), see Figure 3). However, such orientation change could not be detected. Furthermore, the low resolution structures suggested that the conformational change leading to the power stroke happens distal to the actin binding sites. 20 years later the atomic structures of myosin provided structural insight into the cross bridge.

The first atomic structures of the myosin head led to the swinging lever arm model (32, 70, 75) (Figure 4). These structures showed that the head consists of the catalytically active motor domain and the regulatory domain, which was the moving part of the myosin cross bridge. The regulatory domain forms the lever arm. This has two positions: a primed or "up" and a "down" position. The lever arm swing starting from the primed or up position and going to the down is the force generating step (step 4 in Lymn-Taylor), the power stroke that results in the displacement of the myosin motor domain along the actin filament. This model allows displacement without the orientation change of the whole motor domain in relation to the actin filament (20).

Functional regions of the myosin motor domain

The core region of myosin is a seven-stranded β-sheet, which is surrounded with loops and helixes that connect the strands to each other along the polypeptide chain. The core β-sheet is an evolutionary conserved platform for P-loop NTP-ases (52) and comparative protein evolution results reveal that this kind of structure is the most "successful" protein structure in general (7). Figure 5 shows the motor domain, indicating its four subdomains in different colors [2].

The lower and the upper 50 kDa subdomains (colored in gray and red respectively, amino acid sequence according to *Dictyostelium* myosin II numbering of the lower 50 kDa: 478-614 and the upper 50 kDa: 207-477) form an extensive actin binding surface in which several surface loops of the 50 kDa subdomains take part. The cognition of the exact actin binding surface is based on mutational analyses (18, 28) and on rigid docking of actin and myosin structures fitted into electron microscopic map of the acto-myosin complex (Figure 6) (36, 68). The two 50 kDa subdomains are divided by a large cleft called the actin binding cleft, so the two subdomains can move relative to each other. Actually, there are two known conformations. The actin binding cleft can be closed due to a rotation of the upper 50 kDa subdomain toward the lower 50 kDa subdomain (9, 33, 36, 71)

[2] The subdomain nomenclature is based on limited proteolysis carried out by Prof. Miklós Bálint and his co-workers (4).

This movement results in strong acto-myosin interaction, such as in the rigor state (nucleotide absence) (~0.05 μM).When the cleft is opened, the actin affinity decreases with about three orders of magnitude (50 μM).

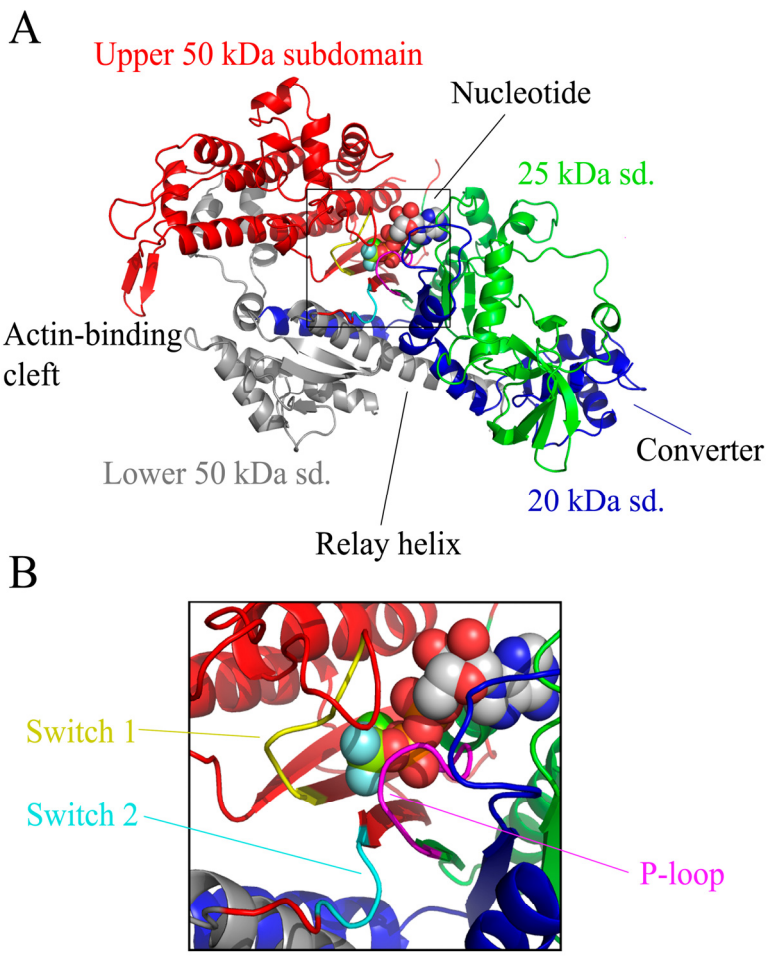

Figure 5. A: functional regions of the myosin motor domain. The lower (gray) and the upper (red) 50kDa subdomains form the actin binding region and they are separated by the actin binding cleft. Between the upper 50kDa and 25kDa subdomains there is the nucleotide binding site. The 20kDa subdomain forms the C-terminal converter region that carries the lever arm. **B:** The nucleotide binding site is formed by the conserved P-loop and by the γ-phosphate sensors switch 1 and switch 2 loops.

The second functional region of the motor domain is the nucleotide binding pocket situated between the upper 50 kDa and the 25 kDa subdomains (green, 1-206). Three functionally important loops form the binding site: the P-loop (magenta, 179-186), switch 1 (yellow, 233-240), and switch 2 (cian, 454-459). The P-loop is an evolutionary conserved structure, which enables the protein to bind the nucleotide. It is a characteristic of all P-loop NTP-ases (52). While the role of P-loop is restricted to the binding, switch 1 and switch 2 have two conformations that enable them to sense the γ-phosphate of ATP as real switches. Their switch functions control other functional regions in myosin. While switch 1 seems to influence the actin binding region, switch 2 communicates with the lever arm. Since a great part of my work was to investigate the

workings of these regions, a more detailed introduction is presented in Chapter 1 and 2.

The third functional region is the converter/lever arm region. The lever arm belongs to the regulatory domain, while the converter to the C-terminal 20 kDa subdomain of the motor domain (blue, 615-761), which carries the lever arm. The converter domain has many interactions with the lower 50 kDa subdomain, especially with the relay region (relay helix and relay loop). The relay helix (465-498) transmits the conformational changes from the nucleotide binding site to the converter region. This module (relay/converter/lever arm region) also has two states, the primed or "up" and the down lever arm states. The lever arm swing between these two states results in the displacement of the motor domain along the actin filament (32). The role of the α-helical lever arm is to amplify the rotation of the converter domain to a bigger movement. Thus the 5 Å displacement of switch 2 loop is converter to a 10 nm movement of the end of the lever arm.

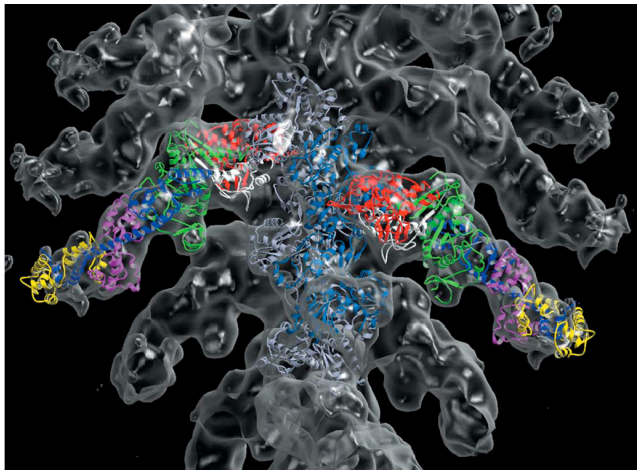

Figure 6. The actin and rigor-like myosin S1 crystal structures fitted into the cryo-electron microscopic envelope of the acto-myosin complex (36).

The above mentioned conformational transitions, such as the actin binding cleft closure and lever arm rotation can be described most fittingly as rigid subdomain movements which are driven by the conformational changes of small hinge regions, such as switch 1 and 2 that connect the subdomains to each other (13). Thus, small changes in these hinge regions can be amplified to large subdomain movements. However, we will see that this is a very reductionist approach.

Communication between functional regions

The previously presented functional regions, responsible for nucleotide binding, sensing and hydrolysis, actin binding and movement amplification, have to

cooperate with each other in order to harmonize their actions, otherwise the energy to be converted to work dissipates as heat. The question arises how this cooperation can be imagined? From a mechanical point of view, communication between two regions is when the conformational change of one site alters that of another through their interacting surfaces. However, on the molecular level where heat movement makes the whole protein a very dynamic system, things can work differently.

The potential conformational space of each functional region can be described with a hypothetical energy landscape in which funnel-like local energy minimums are the stable macroscopic conformations (Figure 7). According to the dynamic energy landscape model, the shape of the energy landscape depends strongly on the surroundings of the region (50). Thus, communication between two regions could be the process when the alteration of one region changes the energy landscape of another, leading to the appearance of new stable conformations or re-distribution between pre-existing local energy minimum conformations [3]. Myosin has several communicating functional regions however, the situation is simplified by the fact that they always have only two functional states, as it was presented in the previous section. Switch 1 and switch 2 are supposed to be opened and closed just like the actin binding cleft and the converter/lever arm region can be in up and down positions [4].

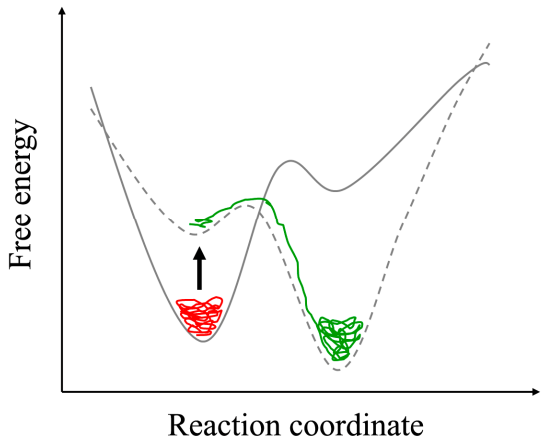

Figure 7. Dynamic energy landscape of a conformational change. A transition of a functional region is able to change the energy landscape of another functional region with which it communicates. The sets of the red and green spots represent the populated states of the influenced functional region before and after the transition of the influencing region. This energy landscape transition represents an equilibrium shift between the two states of the influenced region.

[3] The difference between the two cases is analog with the difference between the induced fit substrate binding and the population-shift model (48, 64).

[4] Interestingly, the working of electronic circuits is also based on the binary system. In such a system each element of the whole set contains only two values, “yes” and “no”, “1” and “0”, or “on” and “off”. However, the transition from one state to the other is very different on the molecular level in a protein and between macroscopic states of an electronic element.

The transitions between these states, which are driven by ATP binding, hydrolysis and actin binding, have to be well synchronized in order to achieve displacement along the actin filament. According to this, each step of the Lymn-Tylor model supposes at least one communication pathway between functional regions. The first step, when ATP binding dissociates the acto-myosin complex, requires communication between the nucleotide binding site and the actin binding region. A similar path toward the lever arm is required when ATP induces lever arm movement in step 2. Furthermore, in step 3, actin rebinding has to be harmonized with the events of the lever arm and the nucleotide binding site, in order for actin to bind back to a myosin having primed lever arm and ADP.Pi in its binding pocket. Otherwise actin rebinding leads to a futile cycle. Finally, in step 4 the actin binding region has to induce the lever arm movement and the release of the hydrolytic products from the nucleotide binding pocket, which also supposes communication toward the nucleotide binding site and the lever arm.

The two states of each site are in equilibrium in every condition regardless of how populated they are and can be described as a complex network (Scheme 2 as in (91)).

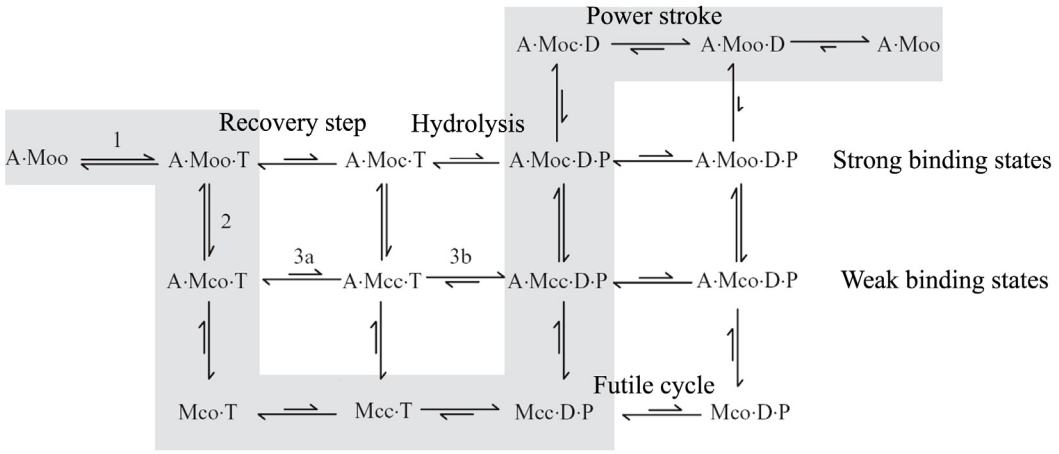

Scheme 2. Possible reaction paths of the acto-myosin system. $_O$ and $_C$ indicate the open and closed conformations of switch 1 and switch 2 in this order. Switch 1 states are supposed to be coupled with the strength of the acto-myosin interaction, while switch 2 states are coupled with lever arm movement and hydrolysis. The main reaction path (gray) is the actin activated ATP-ase cycle of myosin. The question arises, how the functional regions are harmonized to perform the efficient reaction path, resulting in movement, dominantly.

The productive enzyme cycle of myosin is the main reaction flux in this network (indicated by gray), which is determined by the energetic parameters of these equilibriums. Thus, in order to understand the enzyme cycle of myosin, we have to characterize all equilibriums between the two functional states of all functional

regions in every conditions (presence of different nucleotides and actin) and we have to understand which region influences which equilibrium step and how.

The next four chapters are assigned to the four steps of the Lymn-Tyalor model. I will present our contribution to the understanding of each step with a special emphasis on the inter-regional communication.

Chapter 1

Step 1 of the Lymn-Tyalor model – Communication between the nucleotide binding site and the actin binding region

Introduction

Nucleotide dependent interaction of the acto-myosin complex

In 1942 the Hungarian Nobel Laureate, Albert Szent-Györgyi brought forth the idea that muscle contraction is based on the ATP-controlled interaction of two proteins. They found that myosin can be extracted from muscle in two different forms. They got a less and a more viscous myosin extract, depending on whether they prepared it from the rabbit immediately or 24 hours after the animal died (5). When they gave ATP to both extracts their viscosity fell to a similar value. They supposed the presence of a substance that detaches from myosin due to MgATP binding. Later they isolated this substance and named it actin, the protein that "activates" myosin. Today it is generally accepted that the energy stored in nucleoside triphosphates is used for the operation of dynamic protein networks, however this experiment was perhaps the first observation of a nucleotide dependent protein interaction.

In the acto-myosin system the nucleotide and actin binding are antagonistic, a general characteristic of myosins although the actual dissociation constant of the acto-myosin complex depends on the type of the nucleotide bound to myosin. The free energy change resulted from the MgATP-induced conformational change produces enough energy for the endergonic actin dissociation, however that of the MgADP binding does not. Consequently, actin and myosin interact weakly in the presence of MgATP or MgADP.P_i, but more strongly in the presence of MgADP (18), implying the presence of a γ-phosphate sensor in the nucleotide binding site. Furthermore, not just the nucleotide weakens actin affinity, but actin also weakens the nucleotide affinity (during the fourth step of the Lymn-Tyalor model actin accelerates the release of the hydrolytic products). These phenomena suppose a bidirectional communication between the nucleotide and actin binding sites, however its mechanism has remained hidden until recently.

It was recently pointed out that the actin-binding cleft of myosin II is closed in the strongly bound rigor complex based on the docking of myosin crystal structures into electron-microscopic envelops of the rigor acto-myosin complex (Figure 6) (33). Kinetic investigations prove that this cleft closure is induced by the actin binding process (9). Furthermore, it was proposed that in the apo atomic structures of myosin II (PDB:1q5g) and V (1OE9) the closure of the actin-binding cleft opens switch 1 loop in the nucleotide binding site (13, 71), explaining the allosteric communication between the actin binding region and the nucleotide pocket (Figure 8A).

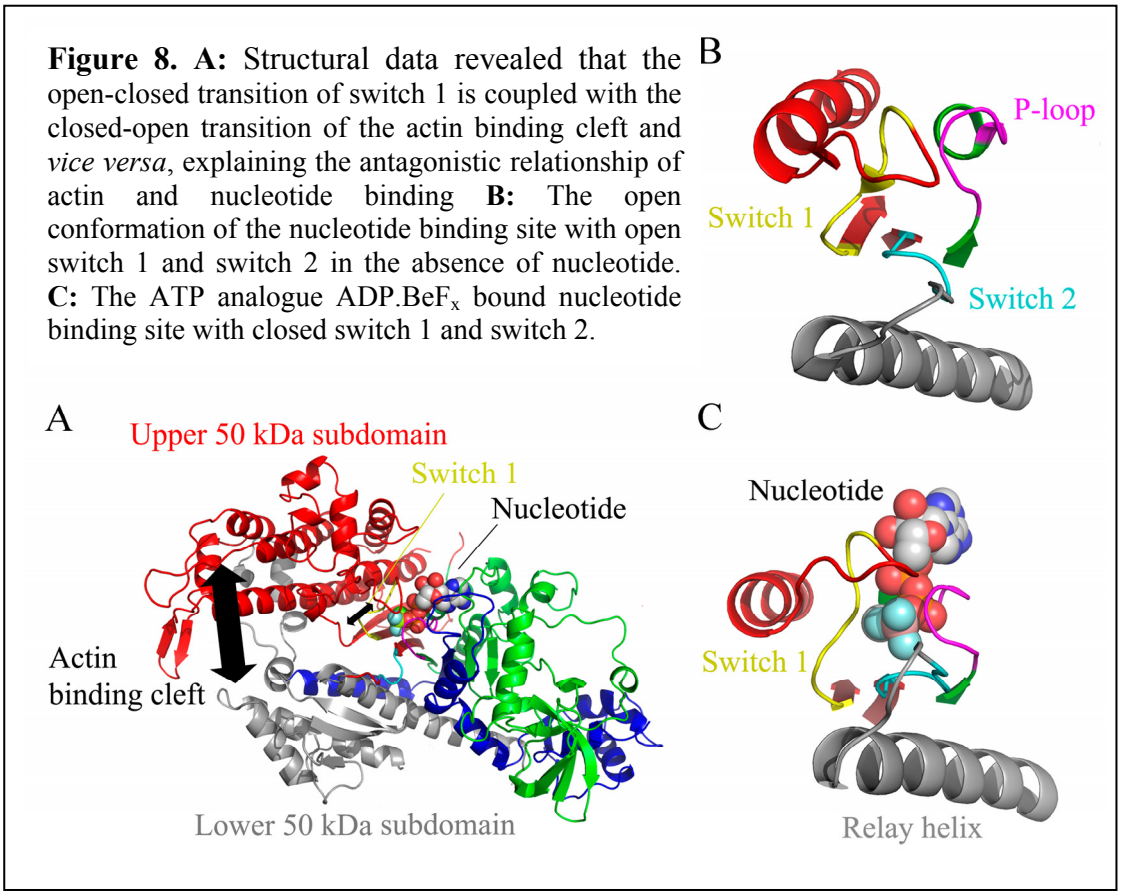

Figure 8. A: Structural data revealed that the open-closed transition of switch 1 is coupled with the closed-open transition of the actin binding cleft and *vice versa*, explaining the antagonistic relationship of actin and nucleotide binding **B:** The open conformation of the nucleotide binding site with open switch 1 and switch 2 in the absence of nucleotide. **C:** The ATP analogue ADP.BeF_x bound nucleotide binding site with closed switch 1 and switch 2.

These structural data gave validity to the assumption that the open-closed transition of switch 1 upon ATP binding is also coupled with the closed-open transition of the actin binding cleft, supposing the bidirectionality of the mechanism. This structural explanation for the antagonistic relationship of actin and nucleotide binding remained hidden for a long time since all previous structures contain switch 1 in the same closed conformation, regardless of the fact whether the bound nucleotide is MgATP or MgADP (26). Thus, only the new apo structures suggested that switch 1 has two different conformations (Figure 8B). In the strong actin binding states (in nucleotide

absence, MgADP-bound) switch 1 can be opened if actin binds to the myosin, while in the weak binding states (MgATP, MgADP.P_i) it cannot.

However, the action of switch 1 and its movements has to be explored in solution in order to prove this structural assumption. The question arises, are there really two states of switch 1? If yes, what is the equilibrium constant between the two states in different nucleotide- and actin-bound states and how do the nucleotide and actin affinities depend on them?

Nucleotide dependent interaction of other P-loop NTP-ases

The literature shows that many P-loop NTP-ases have nucleotide dependent protein interactions (Figure 9). For example, the heterotrimeric G-proteins, the intracellular signaling partners of the GPCRs (G-protein-coupled receptors), have three subunits (GαGβγ), which interact strongly when MgGDP (guanosine diphosphate) binds to the Gα subunit, but more weakly when MgGTP (guanosine triphosphate) does (66). The elongation-factor-Tu, which brings the aminoacylated t-RNA to the ribosome binds to the ribosome strongly in the MgGTP-bound form, but more weakly when MgGDP binds to it (87). The nucleotide dependent interaction of

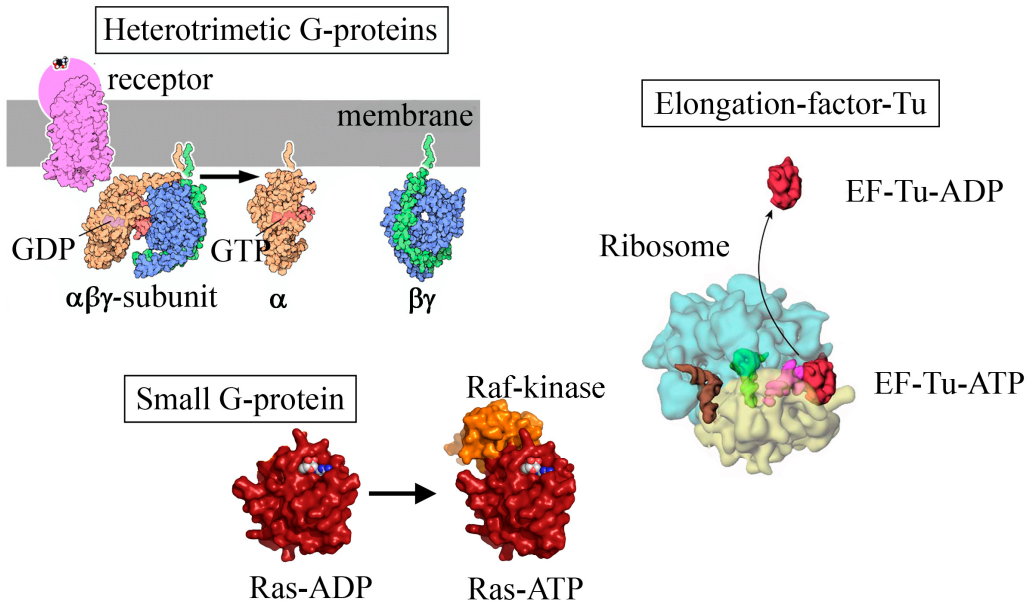

Figure 9. Nucleotide dependent interactions of other P-loop NTP-ases. The nucleotide binding sites of these proteins sense the presence of the γ-phosphate by conserved switch regions, which influence their affinity to the partner protein. The question arises, does the control mechanism remains conserved during their divergent evolution?

the small G-protein Ras with Raf-kinase is the most studied among the listed interactions because these proteins are involved in the regulation of many signal pathways that control cell proliferation. They are found to be the most frequent oncogenes in human tumors (8). The affinity of Ras for its effector protein Raf is high when MgGTP is bound to Ras and low in the case of MgGDP (25).

Interestingly, not just myosin but the homologue switch 1 loops of small G-proteins and kinesin are also thought to be the regions responsible for the antagonistic relationship between the nucleotide binding pocket and the binding region of a partner protein (65, 78). Hence, the mechanisms of action of switch 1 loops in these proteins need to be compared with those of the myosin to explore the potential similarities. It is an interesting question, weather such a control mechanism is able to be conserved despite the fact that these proteins have been bearing a long-standing evolutionary transformation since the deviation from their last common ancestor (52).

Aims

Our concept was that the complete understanding of switch 1 action requires both kinetic and structural information. In order to investigate in solution the states and transitions of switch 1 by using switch 1 specific intrinsic fluorescent signals, tryptophan residues were engineered into the switch 1 loop of *Dictyostelium* myosin II motor domain (M761) null tryptophan construct by replacing Phe-239 (M_{W239+}) or Phe-242 (M_{W242+}). Due to the similar side chains of tryptophan and phenylalanine, the most minimal structural perturbation might be caused by these substitutions. Phe-239 is in a central position, because it is very close to the R238-E459 salt bridge which connects switch 1 to switch 2. Phe-242 is located at the C-terminal end of switch 1, at the beginning of the β-sheet strand that extends from the switch 1 loop. We expected that these residues provide information on switch 1 states in different nucleotide and actin-bound forms when investigated with steady-state and transient kinetic fluorescence experiments.

Results

Steady-state fluorescence of M_{W239+} and M_{W242+}

First we tested weather these tryptophans are able to distinguish between MgADP and MgATP, as it is required from a γ-phosphate sensor switch. Thus, we measured the fluorescence emission spectra of M_{W239+} and M_{W242+} in different nucleotide-bound forms. We found that nucleotides caused a large fluorescence quench in both constructs. All of the nucleotides have the same effect on M_{W242+} fluorescence by causing 20% fluorescence quench (Figure 10B). However, the M_{W239+} construct bears a 37% quench upon MgATP binding, while MgADP causes a 20% quench at 20 °C. (Figure 10A). Furthermore, the studied nucleotide analogues (AMP.PNP, ATPγS, $ADPBeF_x$, $ADPV_i$)[5], which occupy the γ-phosphate site in the nucleotide-binding pocket, show the same spectra as MgATP with M_{W239+} indicating that the fluorescence of W239 is not sensitive to the open-closed transition of switch 2 (since the equilibrium constant of the open-closed transition of switch 2 is different in these nucleotides (56). Furthermore, in the absence of Mg^{2+} the M_{W239+}.ADP complex has different fluorescence than in the presence of Mg^{2+}. However, the other

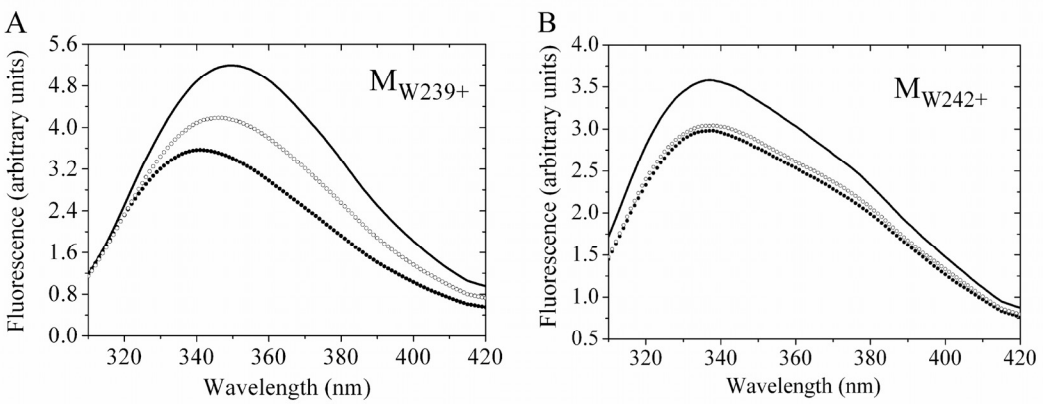

Figure 10. Fluorescence emission spectra of 3 μM M_{W239+} (A) and M_{W242+} (B) in the absence (—) and presence of 0.5 mM MgADP (◦◦◦) or 0.5 mM MgATP (•••) at 20 °C. Tryptophan was excited at 297 nm. M_{W239+} is able to distinguish between MgATP and MgADP.

[5] The AMP.PNP (adenylyl-imidodiphosphate) having a N containing anhydride bound between the β-γ Pi groups and the ATPγS (adenosine 5′-O-(3-thio)triphosphate) having thio-group instead of a γ-Pi oxo-group are ATP analogues. They are not or slowly hydrolysable. The BeF_x is also thought to be an ATP analogue, however its fluoride stoichiometry is in equilibrium between the 3 and 4 fluoride. $ADPV_i$ is an ADP.Pi analogue.

nucleotide-bound forms do not show such difference.

In summary, M_{W239+} senses the difference between MgATP and MgADP and the large fluorescence changes of M_{W239+} and M_{W242+} upon adding nucleotides create good signals for the investigation of switch 1 movements.

Nucleotide binding to M_{W239+} and M_{W242+}

We characterized nucleotide binding kinetics to the single tryptophan constructs. Tryptophan fluorescence was followed during the reaction with nucleotides by using a stopped-flow device. Single exponential functions can be fitted to the MgATP or MgADP binding transients of M_{W239+} under pseudo first-order conditions at 20 °C. The concentration dependences of the observed rate constants show that both MgATP and MgADP binding to M_{W239+} follow two-step-binding kinetics, describing an induced-fit mechanism (Figure 11 and Table 1).

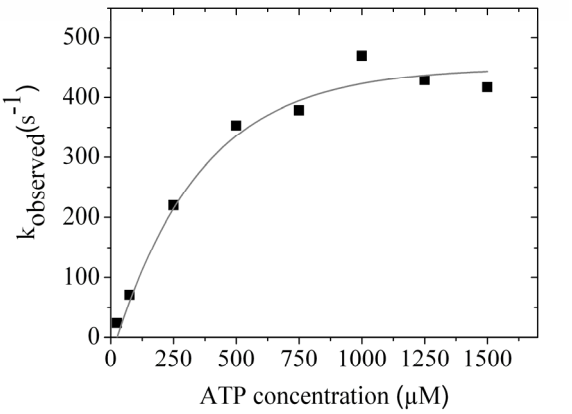

Figure 11. The observed rate constants of MgATP binding to M_{W239+} at 20 °C plotted against MgATP concentration. 3 μM motor protein was mixed with different MgATP concentrations in stopped-flow, while tryptophan fluorescence was detected at 340 nm. Kinetic data are presented in Table 1.

On the contrary, at lower temperatures (12 °C and 5 °C) the stopped-flow records of M_{W239+} MgADP binding are markedly different. The fast quenching phase corresponding to the binding event (Table 1) is followed by a slower fluorescence enhancement with an observed rate $k_{iso\ switch\ 1\ observed}$ = 55 s^{-1} and 32 s^{-1} at 12 °C, and 5 °C, respectively (Figure 12A and B, Table 2). This slower phase implies the presence of a further equilibration step after the nucleotide binding step. This transition was not detected with M_{W242+}, since it showed simple two-step-binding kinetics for MgATP and MgADP at all temperatures, indicating that this isomerization is a characteristic of the middle of switch 1.

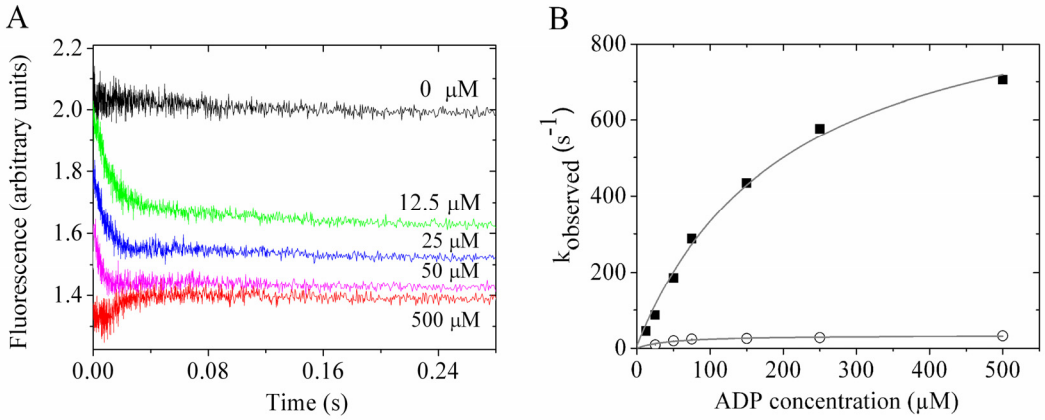

Figure 12. MgADP binding to M_{W239+} at 12°C. **A:** Stopped-flow records of the fluorescence signals for the reaction of 2 µM M_{W239+} with different concentration MgADP. The quench phase is MgADP binding, which is followed by a fluorescence increase. The amplitude loss becomes significant at higher ADP concentrations. **B:** The MgADP concentration dependence of the observed rate of the fitted exponential functions to the fluorescence change. The maximum rate constant of ligand binding (■) is estimated to be between 1000 and 1500 s^{-1}. At high MgADP concentration, the fluorescence enhancement separates from the quenching phase, showing a maximal observed rate 55 s^{-1} at 12 °C. This fluorescence enhancement corresponds to the equilibration between the two ADP states.

Furthermore, the mutations have no dramatic effect on the nucleotide affinity. The MgADP affinity of M_{W239+} is practically unchanged because both the second order binding constant ($3.9x10^6$ $M^{-1}s^{-1}$ for M_{W239+}, $1.4x10^6$ $M^{-1}s^{-1}$) and dissociation constant were slightly faster than for the wild type (58) [6].

The isomerization step of switch 1 loop in the myosin-MgADP complex

Since the stopped-flow records of MgADP binding to M_{W239+} reveal the existence of a first order equilibrium step, we measured the steady-state fluorescence of M_{W239+}.MgADP on different temperatures to detect the temperature dependence of the equilibrium constant. Figure 13A shows the temperature dependence of the steady-state fluorescence of M_{W239+} measured in the absence and presence of different nucleotides. The temperature dependence of the apo and MgATP forms' fluorescence are parallel [7], but that of the MgADP complex differs from the others above 8 °C.

[6] The second order binding constant or on-rate is the slope of a fitted line to MgADP concentration dependence of the observed rates of the binding at low MgADP concentration (Figure 11). The dissociation constant or off-rate is the y-intercept of the same function.

[7] The temperature dependence of the fluorescence of the MgAMP.PNP is also parallel with the apo and MgATP, however this data is not shown.

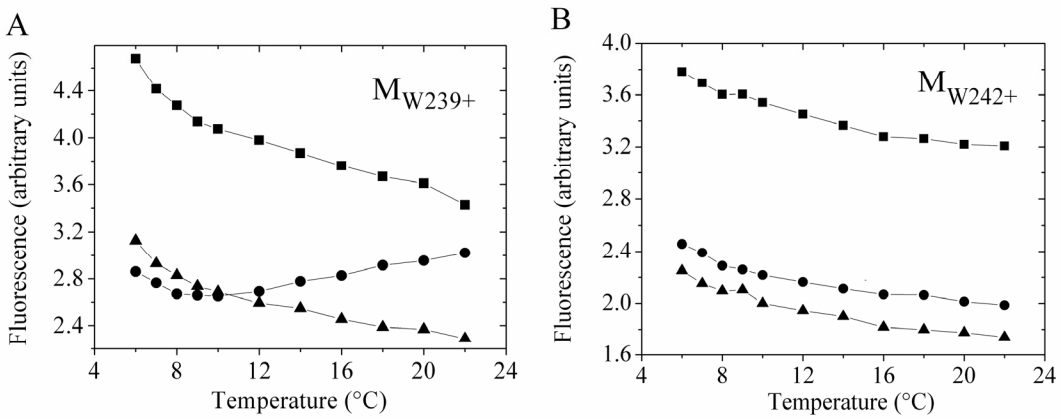

Figure 13. Temperature dependence of M_{W239+} (**A**) and M_{W242+} (**B**) fluorescence in the absence of nucleotide (■) and in the presence of MgATP (1mM) (▲) and MgADP (1mM) (●). The temperature dependence of the Trp-239 fluorescence in the MgADP bound form reveals the presence of a temperature dependent equilibrium. At low temperature the fluorescence intensities in the presence of MgATP were slightly higher than in MgADP however, in ATP turnover experiments a fluorescence intensity change cannot be detected after ATP consumption. M_{W242+}.MgADP does not show such an equilibrium.

However, at lower temperatures it has the same fluorescence as the MgATP form. This is in sync with the observation that the fluorescence spectrum of M_{W239+}.MgADP complex is the same as that of the MgATP form at 5°C.

These findings also indicate that the M_{W239+}.MgADP complex exists in at least two states of equilibrium. The two MgADP states are denoted as †M.ADP and *M.ADP for the quenched and the high fluorescent states respectively. The same fluorescence level of the low-fluorescent MgADP state (†M) and the MgATP-bound form indicates that these states have switch 1 in similar conformation. Because of the fractional occupancy of the high fluorescent *M.ADP state at all accessible temperatures, its fluorescence intensity cannot be determined from these experiments.

In contrast, the temperature dependence of the M_{W242+}.MgADP-bound form is identical to the other forms (apo, MgATP, MgAMP.PNP) hence, only one MgADP state can be detected (Figure 13B).

The presence of the temperature dependent equilibrium of the M_{W239+}.MgADP complex was also confirmed with temperature-jump experiments. Figure 14 shows the temperature-jump records of M_{W239+} in the presence of saturating MgADP or MgAMP.PNP. In the presence of MgADP a 4.7 % fluorescence increase can be observed with an observed rate 70 s^{-1} induced by a 6 °C temperature-jump to 20 °C.

In the other states (apo, rigor, MgAMP.PNP-bound and Mg^{2+}-free ADP states) no fluorescence change was detected. Interestingly, in the presence of actin and

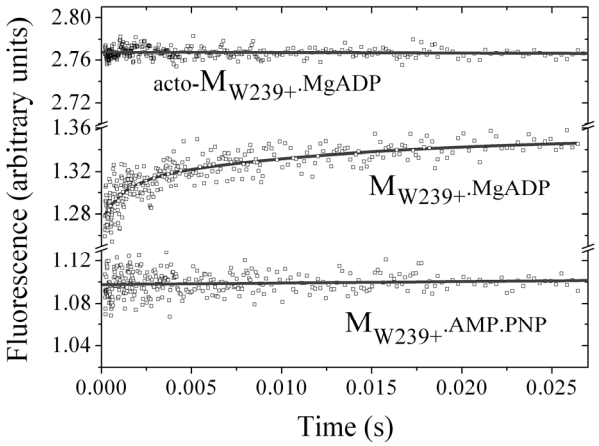

Figure 14. Temperature-jump perturbation experiment of M_{W239+} in the presence of MgADP, actin, and MgADP, AMP.PNP at 20°C. Trp-239 fluorescence was followed after a 6°C temperature jump. These experiments show that acto-M_{W239+}MgADP is locked into a single state.

MgADP the acto-M_{W239+}.MgADP complex is also locked into a single state because no transition was detected (Figure 14). Pressure-jump experiments done by our collaborators, Professor Mike A. Geeves and David S. Pearson (University of Kent), confirmed these findings (41). Based on these experiments, we can state that there are at least two MgADP states in equilibrium. In contrast, in the absence of Mg^{2+} and in the presence of actin or γ-phosphate site occupation Trp-239 shows only a single fluorescent state. Note that the two MgADP states are marked with similar nomenclature as the pre- and post-recovery states in Chapter 2 i.e. $M^{\dagger}$ and M* (58) but here the signs corresponding to switch 1 states are written before M i.e. the †M and * M

Mg^{2+} binding to M_{W239+}.ADP allowed us to determine the equilibrium constant between the myosin-MgADP states

We found that removing Mg^{2+} from M_{W239+} caused a significant fluorescence change only in the presence of ADP and absence of actin. In the absence of Mg^{2+} the addition of ADP to M_{W239+} causes a 45% quench in tryptophan fluorescence although the fluorescence quench was just 20% in the presence of Mg^{2+}. This Mg^{2+}-free M_{W239+}ADP complex is a single fluorescent state because neither temperature nor pressure perturbed the fluorescence (see previous section). Stopped-flow measurements showed that the (Mg^{2+}-free) ADP affinity of myosin is similar to that of MgADP however, the binding and dissociation in the absence of Mg^{2+} is faster (see kinetic data in Table 1). This fluorescent state (††M) is different from the †M.ATP state because the emission maximum is 9 nm red shifted (349 nm) compared to that of the †M state (340 nm).

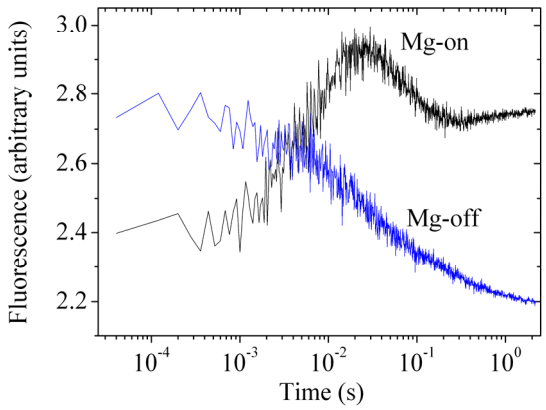

Figure 15. Stopped-flow records of Mg^{2+} dissociation and binding of M_{W239+}.MgADP complex at 11°C. **Mg-off**: 2 µM M_{W239+}, 1 mM ADP was mixed with 5 mM EDTA, 1 mM ADP. The fluorescence quench shows two phases with a rate constant 89 s^{-1} and 18 s^{-1}. **Mg-on**: 2 µM M_{W239+}, 1 mM ADP, 3 mM EDTA was mixed with 10 mM $MgCl_2$, 1mM ADP. The observed rate of the increasing and quenching phase is 120 s^{-1} and 20 s^{-1} respectively. These records are consistent with the concept that the main flux of Mg^{2+}-binding and dissociation occurs through the high fluorescence MgADP-myosin state and the second phases of the binding and dissociation reactions correspond to the equilibration of the two MgADP states. This mechanism (Scheme 3) was confirmed by modeling with Berkeley Madonna software (Table 1).

Mg^{2+} dissociation from M_{W239+}.MgADP complex was monitored by mixing it with EDTA. The observed fluorescent quench has two phases (k_{obs} = 89 s^{-1} and 18 s^{-1} at 11 °C) (Figure 15). When Mg^{2+} (5mM) was mixed with M_{W239+}ADP in a stopped-flow in order to follow Mg^{2+} binding the fluorescence profile of the record was dramatically different from what was expected from the emission spectra. Mg^{2+} binding is accompanied by a rapid enhancement phase that is followed by a slow quench phase (k_{obs}=120 s^{-1} and 20 s^{-1}, respectively at 11 °C) (Figure 15). This fluorescent profile can be explained if Mg^{2+} binding occurs predominantly to the high fluorescent *M.ADP state and the slow phase represents the equilibration between *M.MgADP and †M.MgADP states (Scheme 3). This concept is also supported by the fact that the rate of the second phase of the Mg^{2+} dissociation is equal with the rate of the second phase of the Mg^{2+} binding trace (equilibration between *M.MgADP and †M.MgADP states). Consequently, Mg^{2+} dissociation also happens predominantly through the *M.MgADP state. The observed rates of the quenching phase at different temperatures were in line with the observed rate of the same equilibration detected by the temperature-jump, the pressure-jump, and the MgADP binding stopped-flow experiments. However, here the equilibration is a bit slower.

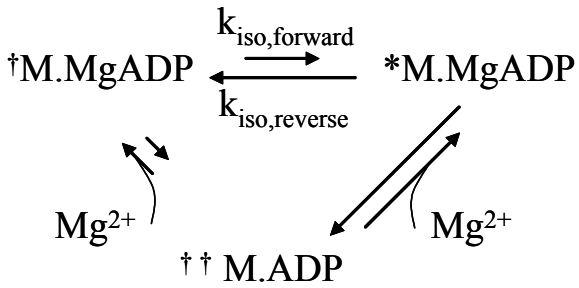

Scheme 3. Mechanism of Mg^{2+} binding to the M_{W239+}.ADP complex. K_{iso} refers to the isomerisation of switch1

Since the fast phase of Mg^{2+} binding is significantly faster than the subsequent equilibration step accompanied by the fluorescence quench, at the end of the fluorescent enhancement the *M state is almost 100% populated and its fluorescence intensity can be determined. By using the binding mechanism described in Scheme 1, the measured Mg^{2+} binding stopped-flow records at different temperatures were modeled by a global fit method (Berkeley Madonna software) and we determined precisely the relative fluorescence intensities of the states. Since the relative fluorescence intensities of the Mg^{2+} free ††M.ADP state and the M.MgADP mixture are determined by the starting and end points of these stopped-flow records (just like by the fluorescence spectra) their fluorescence difference can be used to convert the fluorescence intensities of the stopped-flow records to those of the fluorescence spectra. Thus, the fluorescence of the *M state can be compared to that of the †M and apo states. Hence, if the fluorescence intensity of the apo state is taken as unity the relative intensities of *M and †M states are 1.13 and 0.63, respectively. Since we know the fluorescence intensities of the M_{W239+}.MgADP mixture at each temperature and the relative fluorescence of the *M.MgADP and †M.MgADP states, we can calculate the equilibrium constants of the isomerization ($K_{iso\ switch\ 1}$) between the *M.MgADP and †M.MgADP forms. At 20 ºC $K_{iso\ switch\ 1}$=[*M]/[†M] is 0.7 and the calculated thermodynamic parameters are: ΔG_0=0.9kJ/mol, ΔH_0=44kJ/mol, ΔS_0=0.15kJ/mol·K. Below 8 °C the fluorescence intensity of the M_{W239+}.MgADP complex reaches the fluorescence of the †M state because the lower the temperature the smaller the equilibrium constant of $K_{iso\ switch\ 1}$=[*M]/[†M].

Based on these findings, a general mechanism for MgADP binding to M_{W239+} (Scheme 4) can be determined. According to this scheme both the †M and *M states are able to bind MgADP. However, the fluxes through the two routes may different. At low temperature, where the fluorescence of the MgADP-bound form is similar to that of the †M.ATP state, the population of the *M.ADP state is very low ($K_{iso\ switch\ 1}$<0.1). Furthermore, the MgADP binding stopped-flow record showing a 30% and

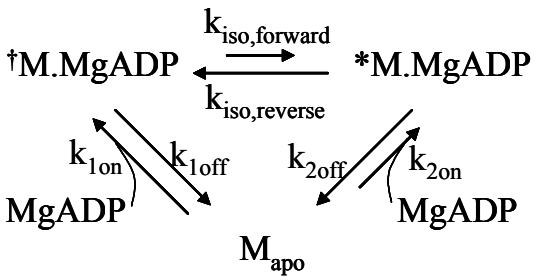

Scheme 4. Mechanism of MgADP binding to M_{W239+}.

fast fluorescent quench (faster than $k_{iso\ switch\ 1}$) reveals that only the low fluorescent †M.ADP state is formed upon binding. This indicates that the ADP affinity of the high fluorescent state is weaker than that of the low fluorescent state at low temperature. However, the higher the temperature, the smaller the amplitude of the fluorescence quench upon MgADP binding. This indicates that MgADP now also induces the formation of the *M.ADP state directly.

Actin binding to M_{W239+} and M_{W242+}

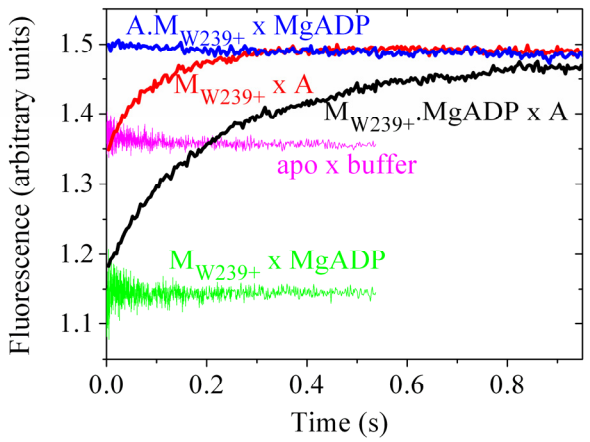

Figure 16. Time courses of the reaction of M_{W239+} with actin in the presence (black) and absence (red) of MgADP, the reaction of M_{W239+} with MgADP (green), and that of the acto-M_{W239+} with MgADP (blue) at 20°C. The fluorescence intensity of the apo M_{W239+} is represented by the magenta trace. Actin fluorescence was subtracted from the records if actin was present. The concentration of M_{W239+} and actin was 2 µM, MgADP 1mM. In the record of the reaction of M_{W239+} mixed with 1 mM MgADP (green), the fast quenching phase occurred in the dead time of the stopped-flow.

In the previous sections we determined the fluorescent states of switch 1 in the absence of actin. Another important question is whether actin binding induces a change in switch 1 conformation as implied from structural data (12, 13). To test this presupposition, actin was mixed with M_{W239+} in stopped-flow and the fluorescence change of Trp-239 was monitored in parallel with the light-scattering signal. As a result, a 4.3% increase in protein fluorescence was observed. Since actin contains four tryptophans, this fluorescence change corresponds to an approximately 15% fluorescence change relative to the fluorescence of Trp-239 if we subtract all of the actin fluorescence and light scattering artefact (10), Now the

changes can be compared with the records measured in the absence of actin (Figure 16, red trace). Interestingly, *M has the same fluorescence intensity as the rigor state, since the fluorescence of *M was determined to be 13% higher than that of the apo state. In contrast, M_{W242+} shows only 1.5% fluorescence change upon actin binding, being the same as with the tryptophan free motor domain construct (10), indicating that the fluorescence of M_{W242+} does not change upon actin binding. These findings indicate that the conformation of the switch 1 loop or the environment of Trp-239 change upon actin binding.

We also measured the effect of actin binding on Trp-239 fluorescence in the presence of MgADP. This stopped-flow record also shows a fluorescence increase, but with larger amplitude than in the absence of MgADP (Figure 16, black trace). The fluorescence intensity of actin is subtracted from the records, similarly to the previous experiment. Thus, Figure 16 shows the actin-induced fluorescence changes of M_{W239+} in the presence and absence of MgADP and it also shows the MgADP-induced fluorescence changes in the presence (blue trace) and absence of actin (green trace). At 20 °C MgADP binding is so fast as the signal change lost in dead time thus, the record shows only the fluorescence intensity of the M_{W239+}.MgADP complex. These fluorescence levels reveal that actin binding induces the same fluorescent state regardless of the presence of MgADP. Importantly, there was no significant fluorescence change when actoM_{W239+} was mixed with MgADP and the light scattering signal shows that actin dissociation is also negligible (Figure 17B).

Furthermore, we found that the mutation has no dramatic effect on the actin affinity of M_{W239+}. In the presence of MgADP it is slightly stronger (0.04 μM) than in the case of the wild type construct (0.12 μM) however, in the absence of MgADP the actin affinities are similar to each other (0.03 μM). Moreover, actin cannot activate the ATP-ase cycle of M_{W239+}. This is due to the fact that F239W mutation reduces the rate of the hydrolysis step significantly that becomes the rate limiting step of the basal enzyme cycle (data not shown). However, the hydrolysis is not directly coupled with the interactions of actin and myosin (10), thus M_{W239+} is a suitable construct for the investigation of the relationship between actin binding and switch 1 movements.

Coupling between switch 1 movement and actin dissociation

We studied the ATP-induced actin dissociation reaction to test the coupling of switch 1 movement and actin dissociation (step 1 in the Lymn-Taylor model). Acto-M_{W239+} was mixed with MgATP under pseudo first-order conditions. The received fluorescence change is a large quench, similar to that observed upon MgATP binding in the absence of actin. The light-scattering signal change follows the fluorescence quench immediately, showing the acto-myosin dissociation. In contrast, upon mixing acto-M_{W239+} with MgADP neither the fluorescence nor the light scattering signal decreased (Figure 17B).

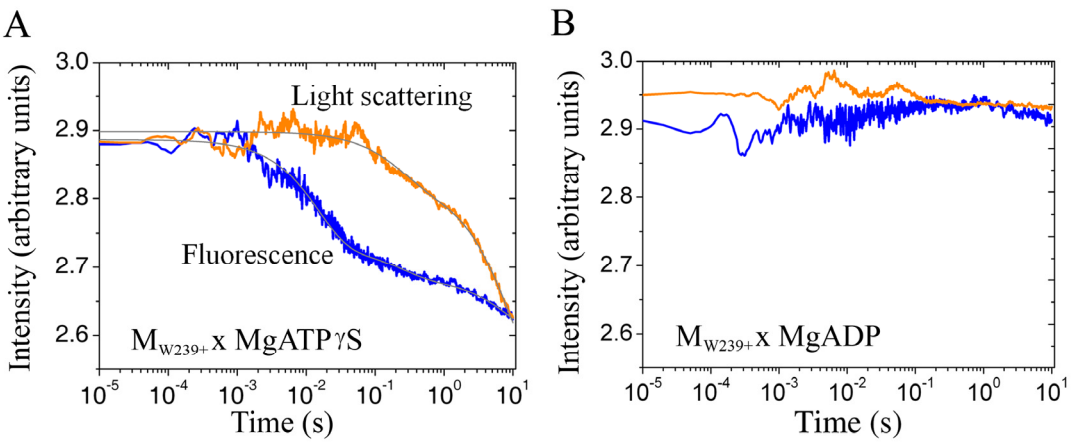

Figure 17. Stopped-flow records of the reaction of acto-M_{W239+} with ATP analogue MgATPγS (**A**) and MgADP (**B**). Fluorescence and light scattering signal were followed after mixing 2 µM M_{W239+} with 100 µM nucleotide in stopped-flow at 20°C. The light scattering signal, which follows the acto-myosin dissociation, is normalized to the fluorescence change. **A:** in case of MgATPγS, the light scattering signal has two phases ($k_{obs,light\ scatt\ 1}$ = 4.2 s^{-1}, $k_{obs,light\ scatt\ 2}$ = 0.11 s^{-1}) however, the fluorescence change has three ($k_{obs,fluor\ 1}$ = 68 s^{-1}, $k_{obs,fluor\ 2}$ = 4.3 s^{-1}, $k_{obs,fluor\ 3}$ = 0.10 s^{-1}). During the fastest phase of fluorescence change no significant acto-myosin dissociation occurs, indicating that the conformational rearrangement of switch 1 precedes actin dissociation. **B:** MgADP binding to the acto-M_{W239+} does not induce either fluorescence or light scattering signal change.

We also studied the reaction of acto-M_{W239+} with MgATPγS in stopped-flow (Figure 17A). Since MgATPγS induces slower acto-myosin dissociation this ATP analogue is a useful substrate for the study of the coupling of actin dissociation and switch 1 movement (9). Here the tryptophan fluorescence and light scattering signal were also detected in parallel. The tri-phasic fluorescence decrease shows a dominant fast phase ($k_{obs,fluor\ 1}$ = 68 s^{-1} relative amplitude 53%) that is missing in the light scattering signal, but the two slow phases correspond to the two phases of the light scattering change (their relative amplitudes and their rates are the same). The light

scattering change is similar to previous measurements of the MgATPγS-induced dissociation where pyrene-actin fluorescence was the detected signal (55). The fast

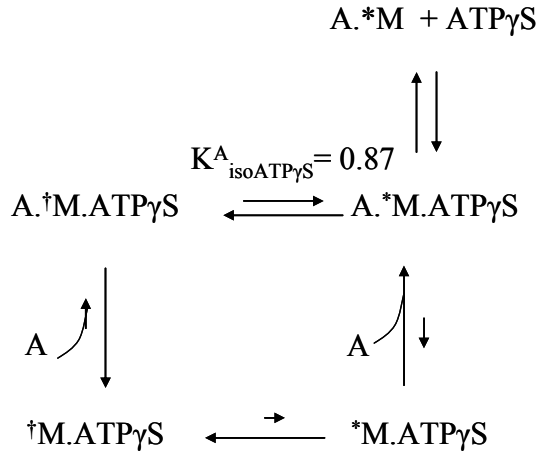

Scheme 5. Thermodynamic box of actin binding and switch 1 isomerisation in the presence of MgATPγS.

fluorescence quench in the fluorescence change most likely corresponds to a transient equilibration between the *M.MgATPγS and †M.MgATPγS fluorescence states before the occurrence of significant actin dissociation. A model describing this mechanism is shown in Scheme 5. Since the initial equilibration is much faster than the actin dissociation steps, an acto-myosin population with †M switch 1 conformation appears transiently. The relative amplitudes of the phases of the fluorescence signal change determine the equilibrium constant, $K^{A}_{iso\text{-}MgATP\gamma S}$= [A.*M.MgATPγS]/[A.†M.MgATPγS] = 0.47/0.53 = 0.87.

These results carry important indications. The conformational change of switch 1 loop can initiate actin dissociation, which is a consequence of the actin binding cleft opening (9). However, the MgATPγS induced dissociation shows that the two sites do not couple as rigid bodies to each other.

Summary of the fluorescent states of M_{W239+}

In summary, in the presence of Mg^{2+} three fluorescent states can be distinguished: †M, *M, and apo (Table 3). The high fluorescent *M is the predominant state in the presence of actin either in the presence or absence of MgADP (acto-*M, acto-*M.MgADP) and it is populated even in the M.MgADP complex in the absence of actin. The low fluorescent †M state is predominant in myosin complexed with MgATP or substrate analogues having γ-phosphate and exist in the M.MgADP state.

Discussion

Reversible movement of switch 1 loop

Since Albert Szent-Györgyi's experiments we have known that the strength of the acto-myosin interaction depends on the nature of the bound nucleotide (5). While the MgADP-bound form results in a strong binding complex, MgATP and MgADP.P_i result in weak acto-myosin interaction (18). However, the way how the nucleotide determines the actin affinity of myosin is a long-standing question (21).

Recent structural data show that switch 1 can exist in different conformational states (13, 71) and these states are presumed to play a central role in information transmission between the nucleotide and the actin binding regions (35). Solution experiments are now required to confirm the role of switch 1 and to elucidate its action. Therefore, we prepared such *Dictyostelium* myosin II motor domains that are able to produce switch 1 specific fluorescence signals. In two different constructs the F239W and F242W mutations were introduced into the switch 1 region, while native tryptophans were mutated to phenylalanine residues to reduce background fluorescence (58). Fortunately, we found that these fluorophores are really able to provide specific signals on the conformational changes of switch 1 upon nucleotide and actin binding. Furthermore, the mutations have no significant effect on the acto-myosin interaction and on nucleotide binding of myosin, thus these constructs are suitable objects for the investigation of the antagonistic relationship of actin and nucleotide binding in which switch 1 is supposed to have a central role.

In the presence of Mg^{2+} three fluorescent states of W239 were identified and a fourth state in its absence, which is the Mg^{2+}-free ADP state (Table 3). In the MgADP-bound form two states were distinguished, being in equilibrium. The low fluorescent †M.MgADP state is likely to be the same state as the MgATP-bound state. The other, high fluorescent *M.MgADP state, is different from the myosin apo state because it has a higher fluorescence. Moreover, the fluorescence intensity of this state is the same as that of the actin-bound state and actin induces this fluorescent state regardless of the presence of MgADP. This entails that actin also induces a structural change in switch 1 when it binds to the apo myosin and that the rigor acto-M_{W239+} complex could have the same switch 1 state as acto-M_{W239+}.MgADP ternary complex and *M.MgADP state.

Dictyostelium myosin II structures with bound nucleotides and nucleotide analogues, such as ADP, ATP, ADP.BeF_x and ADP.AlF_4, show switch 1 in the same, closed conformation. With the use of switch 1 specific fluorescent signals we also found that switch 1 exists in the same fluorescent state when MgATP or substrate analogs having γ-phosphate is bound to the myosin. Furthermore, this state also exists in the MgADP-bound form. Consequently, we are able to assign the closed switch 1 conformation to the low fluorescent †M with high confidence. The observation that this †M state has higher affinity to MgADP than the high fluorescent *M state and the inhibited Mg^{2+} exchange of this state also support the finding that †M is the closed switch 1 state.

The significance of the new *Dictyostelium* apo (rigor-like) structure is that in this structure switch 1 is in an open state. Furthermore, the myosin V apo structure also has opened switch 1 loop, just like an ADP-bound structure (without Mg^{2+}) (PDB: 1W7I) (12). This ADP-bound structure is called *weak ADP-bound state* because the open switch 1 state is thought to have lower ADP affinity. The further significance of the apo (rigor-like) structures is that the actin-binding cleft in these structures is in closed conformation, which is thought to be a characteristic of the strong actin-bound states (35).

In M_{W239+} switch 1 is in the *M state when actin is bound strongly to myosin, having a closed actin binding cleft (acto-M_{W239+}, acto-M_{W239+}.MgADP). This suggests that the *M state can be assigned to the switch 1 open state. However, this is different from the apo state, because that has a lower fluorescence than the high fluorescent *M state. Consequently, the switch 1 conformation or the environment of Trp-239 in the presence of actin is not the same as it is represented by the rigor like apo structures. Henceforward, we assign the open switch 1 state to the high fluorescent *M states, such as *M.MgADP, acto-*M, acto-*M.MgADP, and not the apo state.

Consequently, we found that there are two states of switch 1 in physiological conditions (in the presence of Mg^{2+}-nucleotide and/or actin): the open state and the closed state. Furthermore, between the two states there is a dynamic equilibrium. In MgADP-bound state both states are significantly populated. However, when MgATP or nucleotide analogues having γ-phosphate group are bound the equilibrium is pushed towards the closed switch 1 state. On the contrary, actin, either in the presence or absence of MgADP, pushes the equilibrium towards the open switch 1

conformation. Hannemann *et al.* also found an isomerization of the MgADP states in myosin V using mant-ADP, which is pushed predominantly to a single state upon actin binding (29). However, Rosenfeld *et al.* did not find this effect with myosin V (72). The existence of the two MgADP states of acto-myosin system is a long-standing question, and provides an explanation for the load-dependent ADP release in muscle (14).

As it was mentioned previously, the structural results reveal that switch 1 closure opens the actin binding cleft and *vice versa,* resulting in weak and strong actin binding states respectively (35). This serves as an explanation for the antagonistic relationship of actin and nucleotide binding. A similar equilibrium found in case of switch 1 has been supposed for a long time between the states of the actin binding cleft (19). If the acto-myosin interaction is strong, the equilibrium is pushed toward the closed actin binding cleft state, such as in nucleotide absence or in the ADP-bound form. When the interaction is weak (MgATP- or MgADP.P_i-bound myosin) the equilibrium is pushed to the open actin binding cleft state.

Thermodynamic model of a classical switch mechanism

Based on our experiments, we presuppose that both the open and the closed switch 1 conformations exist in solution in all Mg^{2+}-nucleotide and actin-bound forms, only the equilibrium constant is different. From this point of view there are four different states of myosin in a solution that contains actin, myosin, and a certain nucleotide in saturating amount: detached and actin-bound myosin molecules, with open and closed switch 1 (Note that actin concentration must be non-saturating). Scheme 6 shows the thermodynamic box of the four states. According to this scheme the relative concentrations of the four states are determined by the four equilibrium constants between the four states. The actin binding equilibriums are not influenced by the type of the bound nucleotide but they depend on the actin concentration and on the conformation of switch 1. Myosin binds actin strongly when switch 1 is open ($K_d \approx 0.1$ μM) but weakly when switch 1 is closed ($K_d = 50$ μM) [8]. However, the

[8] The affinity of the strong binding form is estimated from the actin affinity of the rigor complex. The actin affinity of the weak binding form is based on the K_M of the actin activated ATP-ase activity (Figure 26).

equilibrium constants between the open and closed switch 1 states depend strongly on the bound nucleotide. These equilibrium constants are measured by the use of the M_{W239+} construct: $K_{iso(MgADP)}={}_oM.ADP_{Mg}/{}_cM.ADP_{Mg}=0.7$ and $K^A_{iso(MgATP\gamma S)}=A_oM.ATP\gamma S_{Mg}/A_cM.ATP\gamma S_{Mg}=0.87$, where o and c are the open and closed forms of switch 1.

The fourth sides of the thermodynamic boxes are determined by the other three, consequently $K^A_{iso(MgADP)}=A_oM.ADP_{Mg}/A_cM.ADP_{Mg}=300$ and $K_{iso(MgATP)}={}_oM.ATP_{Mg}/{}_cM.ATP_{Mg}=0.017$, which are also consistent with the measured data.

Based on this model, the nucleotide determines the relative concentration of the four states and thus, the actual actin affinity through the equilibrium constants between the open and closed states of switch 1 as well. According to Scheme 6, in the presence of actin and MgADP the predominant state is the actin-bound myosin with an open switch 1 ($A.{}_oM.ADP_{Mg}$). This is consistent with the fact that the MgADP-myosin complex binds actin strongly.

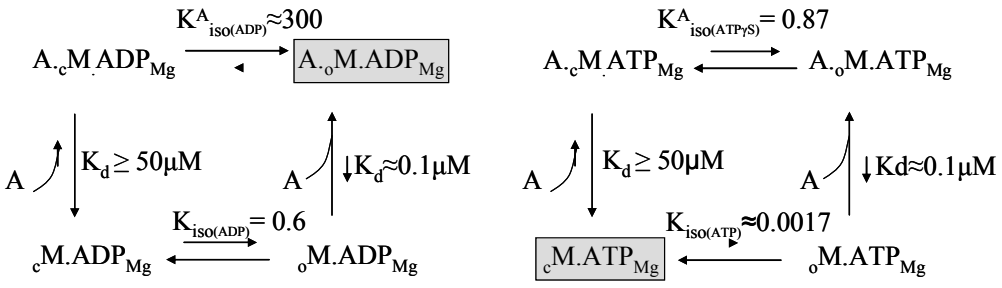

Scheme 6. Thermodynamic boxes of actin binding and switch 1 isomerisation in the presence of MgADP or MgATP.

In contrast, in the presence of actin and MgATP the thermodynamic box determines the actin detached myosin having a closed switch 1 state ($_cM.ATP_{Mg}$) as the predominant state. This correlates with the fact that acto-myosin interaction is weak in the presence of MgATP or MgADP.P_i. In other words, while MgATP is able to close switch 1 even in the actin-bound state, the lack of the γ-phosphate weakens the MgADP enough to let actin win in the thermodynamic fight.

Scheme 6 is also valid if we substitute the equilibrium constants of switch 1 with those of the actin binding cleft states in different nucleotides (19). However, the MgATPγS induced acto-myosin dissociation experiment in which switch 1 closure is

disconnected in time from actin binding cleft opening (Figure 17A) shows that switch 1 and the actin binding cleft do not move together like two parts of a rigid subdomain. Rather, the open-closed equilibrium of switch 1 influences or determines the closed-open equilibrium of the actin binding region. This is consistent with the hypothesis that the alteration of one functional region influences the conformation of the other by changing its energy landscape. In case of MgATPγS the small difference compared to MgATP perturbs the closure of switch 1, resulting in a slower actin binding cleft opening. This could be the consequence of a differently changed energy landscape of cleft movement with a higher kinetic barrier.

Nucleotide dependent interaction of P-loop NTP-ases

The minimum requirement for a nucleotide state-dependent interaction is the ability to sense the difference between the nucleotide di- and triphosphate-bound in the binding pocket. In case of P-loop NTP-ases this property is usually achieved with the help of loops in the nucleotide binding site, known as switch loops (49), working as γ-phosphate sensors. The conformations of these loops depend on the presence of the γ-phosphate and the protein is able to conduct this conformational change to the binding site of the partner protein. Just like in myosin, the switch 1 loops of small G-proteins are also known to have a central role in partner protein binding and they might share an analogous mechanism (25, 44). Switch 1 loops of small G-proteins contribute to the binding of their guanine exchange factors (GEF), such as Sos protein of Ras or RCC1 of Ran. It was pointed out that GEFs are analog proteins of actin from the perspective of GEF binding are strongly negatively coupled to nucleotide binding (25), just as actin binding to myosin. However, the mechanisms controlling their interactions are different, because MgGTP and MgGDP weaken GEF affinity of Ras by the same extent (25, 40), The similarity is more observable to the interaction of Ras and its downstream effector Raf-kinase that binds directly to switch 1 region. Switch 1 loop of Ras has two conformations as well: a closed (also called state 2) and a disordered state (state 1) (79, 80, 88). The closed switch 1 state is formed when

[9] Note that the strong binding state is the MgGTP-bound state in Ras, and the MgADP-bound form of myosin.

MgGTP is bound, allowing Ras and Raf to interact strongly and this conformation is preserved in the strongly bound Ras-Raf complex [9]. In the absence of the γ-phosphate switch 1 loop is disordered leading to 1000-fold reduction in Raf affinity. The use of the GTP analogue GPP-NH-P (guanosine-5'-(β,γ-imido)triphosphate) or GPP-CH_2-P (guanosine-5'-(β,γ-methyleno)triphosphate) allowed the detection of the equilibrium between the two states of switch 1 because it is fully reversible in these nucleotides ($K_{state12}$=2) (24, 78). Additionally, upon Raf binding the equilibrium is pushed toward the closed state (79). In the presence of MgGTP and MgGDP this equilibrium is not observable, because it is totally pushed toward the closed state ($K_{state12\text{-}GTP}$>>10) and the disordered state ($K_{state12\text{-}GDP}$<<10) respectively. These findings astonishingly resemble to the behavior of switch 1 in myosin, only the equilibrium constants between the two states of switch 1 are slightly different. Consequently, if we substitute the states and equilibrium constants of switch 1 of Ras into Scheme 6, it can perfectly describe the nucleotide regulated interaction of Ras and Raf.

The enzyme cycle of myosin and Ras from the perspective of their nucleotide dependent interactions

In myosin the time spent in actin-bound (open switch 1) or in detached states (closed switch 1) is determined by the rate limiting step of the enzyme cycle. If the rate limiting step populates predominantly weakly interacting states in the steady-state (MgATP- and MgADP.P_i-bound

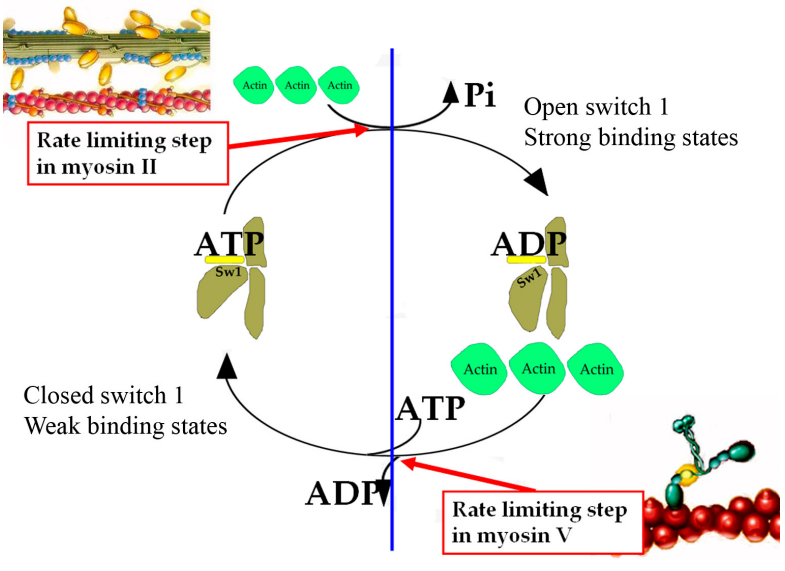

Figure 18. Enzyme cycle of myosin with regard to switch 1 states. In ATP or ADP.P_i bound forms switch 1 is closed when actin affinity is low however, actin rebinding to M.ADP.P_i opens switch 1 and dissociates the γ-phosphate. The relative time spent by myosin in actin bound and detached states (duty ratio) is determined by the rate limiting step of the cycle.

states), myosin spends most of the time detached from actin with closed switch 1 (Figure 18). This is the case with myosin II, where the rate limiting step is a conformational change that precedes P_i release (27). Upon P_i release switch 1 opens, resulting in strong actin binding (41, 71). In a multi-headed myosin filament this results in the fact that just 5 % of the myosin heads bind to actin simultaneously, so that they do not impede sterically each other. In myosin V, which is a single molecule, the rate limiting step is the MgADP release (or a conformational change that allows MgADP release), resulting in predominantly populated strong actin-bound states with open switch 1 during the steady-state (Figure 18). This property of a two headed myosin V allows the processive movement along the actin filament by creating a great possibility for binding both heads to the actin filament at the same time in each enzyme cycle.

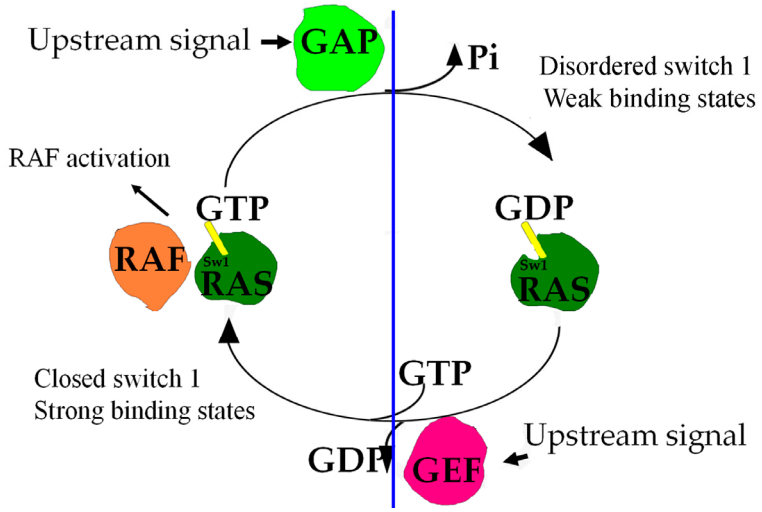

Figure 19. Enzyme cycle of ras with regard to switch 1 states. This is represented in a similar way as the enzyme cycle of myosin (Figure 18). In GTP or GDP.P_i bound forms switch 1 is closed when raf-kinase affinity is high. When γ-phosphate dissociates, switch 1 becomes disordered and raf-kinase dissociates. The relative time spent by ras in raf-bound and detached states (duty ratio) is determined by the relative rate of P_i and GDP release [10]. However, the rate of these steps is determined by the binding of the upstream elements of the signal cascade, such as GAP and GEF.

The enzyme cycle of Ras can be illustrated in the same way as that of myosin Figure 19. Here as well the relative rate of the biochemical steps determines the ratio of the strongly and weakly interacting forms of Ras. The P_i release induces the conformational change of switch 1, resulting in the dissociation of the Ras-Raf complex. The MgGDP release step

[10] Indeed the rate of MgGTP hydrolysis determines the observed rate of the P_i release in Ras and GAP activates the rate of the hydrolysis step.

allows the binding of a new MgGTP and the closure of the disordered switch 1 loop. This allows the binding of Raf with high affinity and the activation of its kinase activity. However, in the case of Ras the regulation of the conversion between the weakly and strongly interacting forms is controlled by external factors, concretely by the activity of the upstream elements of the signal pathway. GEF accelerates MgADP release, hence increases the MgGTP-bound fraction of RAS, while the other upstream regulator, GAP, accelerates the intrinsic catalytic activity of Ras and thus accelerates the subsequent P_i release, resulting in disordered switch 1 and the dissociation of Raf-kinase. The most frequent mutations in Ras oncogenes inhibit the hydrolysis of MgGTP thus, switch 1 remains closed and Raf strongly bound to Ras, activating further cell proliferation.

In summary, in spite of the fact that myosins and G-proteins have very different functions and binding partners, the mechanism regulating their nucleotide dependent interactions is very conserved.

Chapter 2

Step 2 – Communication between the nucleotide binding pocket and the lever arm: the conformational change that primes the lever arm

Introduction

The motor domain structures having down and up lever arm states support structural explanations for the mechanism of MgATP induced lever arm swing (17, 70, 75) [11]. The closure of the switch 2 loop drives a 60° rotation of the converter/lever arm region placing it to the primed or pre-power stroke position. In spite of the fact that the coupling of switch 2 movement and lever arm rotation has been known for a long time, the detailed molecular mechanism of the transition is still not fully understood.

This lever arm priming is the same conformational change (the recovery step) as that observed by Baghsaw and Trentham 25 years earlier by using tryptophan fluorescence (1). The conserved tryptophan (Trp-501 in *Dictyostelium* numbering, homologous to Trp-510 in rabbit skeletal myosin) that serves a large fluorescence increase upon the recovery step is located at the C-terminal end of the relay helix that connects switch 2 and the converter region (figure 20). Malnasi *et al.* engineered a single tryptophan *Dictyostelium* motor domain that contains only this native tryptophan (W501+ construction) (58). By the use of this construct a much better signal-to-noise ratio could be achieved than by the use of the wild type however, the elimination of the other tryptophans did not change the workings of myosin.

Scheme 7 shows the reaction steps of the myosin basal ATP-ase cycle as it can be seen by the use of the W501+ construct. Step 1 and 2 (K_1K_2 in Scheme 7) represent the two-step induced-fit MgATP binding process. $M^{\dagger}$.MgATP, which has a 20% lower fluorescence than the M apo state (PDB: 1q5g (71), corresponds to the pre-recovery (i.e. open, post-rigor, down lever arm state) structure (PDB: 1FMW, 1MMD (26).

[11] After the production of the first myosin structure in 1993 (70), the first primed or up lever arm state structure (75) was published in Biochemistry (the impact factor of this journal was

4.8 in 1996) with perhaps the most important significance of the last 25 years of myosin research.

This state has an open switch 2, and thus the lever arm in pre-recovery (down) orientation. MgADP binding (K_7K_6 in scheme 7) induces that state as well. However, when ATP binds to myosin the binding process is followed by the recovery step (step 3a in Scheme 7), when switch 2 loop closes and the relay/converter/lever arm region rotates into the post-recovery state (primed or up lever arm orientation, state M*.MgATP in scheme 1, PDB code: 1VOM, 1MND (17, 75)). The forward direction of the recovery step results in a 110% fluorescence intensity increase of Trp-501. This serves a useful signal to follow the conformational change in the relay/converter region during the recovery step.

The main finding of Malnasi *et al.* was the separation of the recovery (step 3a) and the following hydrolysis (step 3b) steps, which were represented in the Bagshaw-Trentham scheme as a single step (step 3) (58). Indeed, the recovery step results in the catalytically active conformation which can hydrolyze ATP. The post-recovery structures of the motor domain reveal that the closed

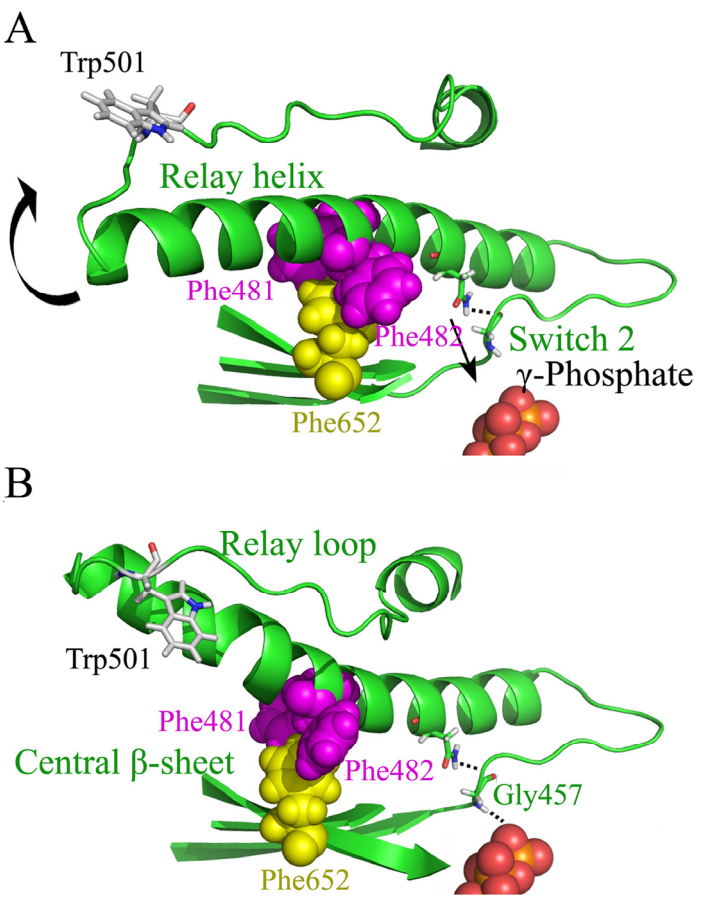

Figure 20. The conformational change of the relay region during the recovery step. Figures **A** and **B** show the pre- and post-recovery conformation of the relay region. During the recovery step, Gly-457 (switch 2) moves toward the γ-phosphate of ATP, which pulls down the N-terminal part of the relay helix via a hydrogen bond. As a result, the relay helix moves in a seesaw-like manner and then unwinds. The pivoting point of the seesaw is highlighted by spacefill modeling (Phe-652 in yellow and Phe-481 and Phe-482 in purple). Trp-501 is also shown by stick representation. Since the relay loop and thus Trp-501 is missing in the original pre-recovery structure, it is modeled. And then both structures were relaxed by applying molecular dynamics simulation.

conformation of switch 2 is required for the hydrolysis of ATP (6, 34), since in that state the amino group of the conserved Gly-457 switch 2 residue forms a hydrogen bound with a γ-phosphate oxygen. This coupling ensures that ATP hydrolysis occurs just when the lever arm is primed, avoiding wasteful hydrolysis without force generation. The hydrolysis step

itself does not cause Trp-501 fluorescence change, but its pulling effect on the equilibrium of the recovery step makes the high fluorescent states (M*.MgATP, M*.MgADP.P_i) more populated.

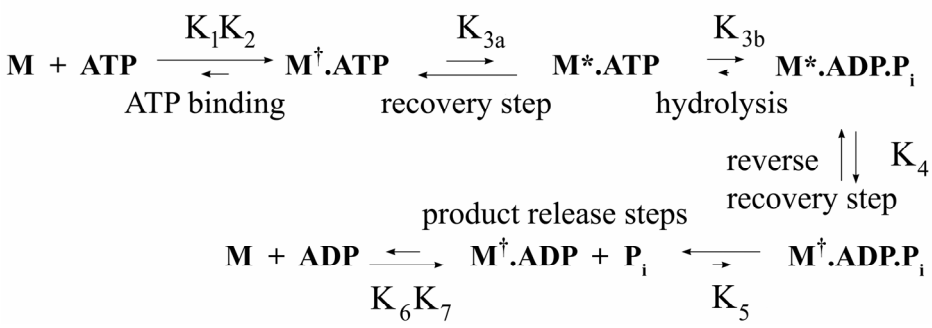

Scheme 7. The ATP-ase cycle of myosin in the absence of actin. † and * correspond to the low and high fluorescent states of Trp-501 respectively.

Nevertheless, several computer simulations have been published recently on the structural analysis of the recovery step (16, 30, 47, 62, 89, 90) . Fischer *et al*. composed a structural transition between the pre- and post-recovery states by modeling the intermediate structures using an unconstrained minimum-energy pathway simulation (16). The resulting structural trajectory shows that the relay helix movement can be separated into two phases. In the first one the relay helix moves in a seesaw-like fashion coupling the movement of switch 2 and the rotation of the lever-arm. The closure of switch 2 pulls down the relay helix near to its N-terminal end through a hydrogen bridge between Gly457 and Asn-475. Due to this pulling the C-terminal end of the relay helix swings upwards because the helix is supported by a fulcrum that serves as the pivoting point in the middle of the helix, like in the case of a real seesaw (Figure 20). The hydrophobic fulcrum of the relay helix is formed mainly by three conserved phenylalanine residues: F652 (part of the 3rd strand of the central β-sheet), F481, and F482 (relay helix). In the second phase the SH1 helix movements provoke a further 40 ° rotation of the converter/lever arm region, which causes an unwinding in the C-terminal part of the relay helix. My college, Zenhui

Yang produced a similar transition for the recovery step by using a different *in silico* method (nudge elastic bending). His results and other molecular dynamics simulations confirmed the two phases and the seesaw-like motion of the relay helix (62).

These computational simulations composed and visualized potential structural transitions of the recovery step, which might help to elucidate the communication between switch 2 and the lever arm. However, experimental validation of the model has been lacking.

Aims

Our aim was to investigate experimentally the seesaw-like movement of the relay helix suggested by the computational model of the structural trajectory of the recover step (16). We produced two mutants in the M_{W501+} construct, in which different phenylalanines from the proposed pivoting point of the relay seesaw were mutated to alanines (Figure 20). Since alanine is a significantly smaller residue than the original phenylalanine the mutations reduce the size of the fulcrum, which is supposed to lead to the loss of the supporting role of the phenylalanine cluster. The $M_{F481A,F482A}$ construct has a reduced fulcrum in the side of the relay helix, while M_{F652A} contains a reduced support for the relay helix. Since Trp-501 shows a large fluorescence increase upon the recovery step, M_{W501+} single tryptophan construct is an ideal construct to test the effect of the mutations on the recovery step.

Results

Steady-state fluorescence of $M_{F481A,F482A}$ and M_{F652A}

We measured the steady-state fluorescence emission spectra of the two mutants ($M_{F481A,F482A}$ and M_{F652A}) in the presence of different nucleotides and compared them to that of M_{W501+} (Figure 21). At 20 °C in the absence of nucleotide the three constructs have similar emission spectra (emission maximum at 342 nm), just like in the presence of MgADP when all constructs show a 15% quench and 2 nm blue shift compared to the apo state. In contrast, in the presence of ATP the mutants show smaller fluorescence enhancements than the M_{W501+}. While the fluorescence of the MgATP-bound M_{W501+} is 100% higher than that of the MgADP-bound (58), the

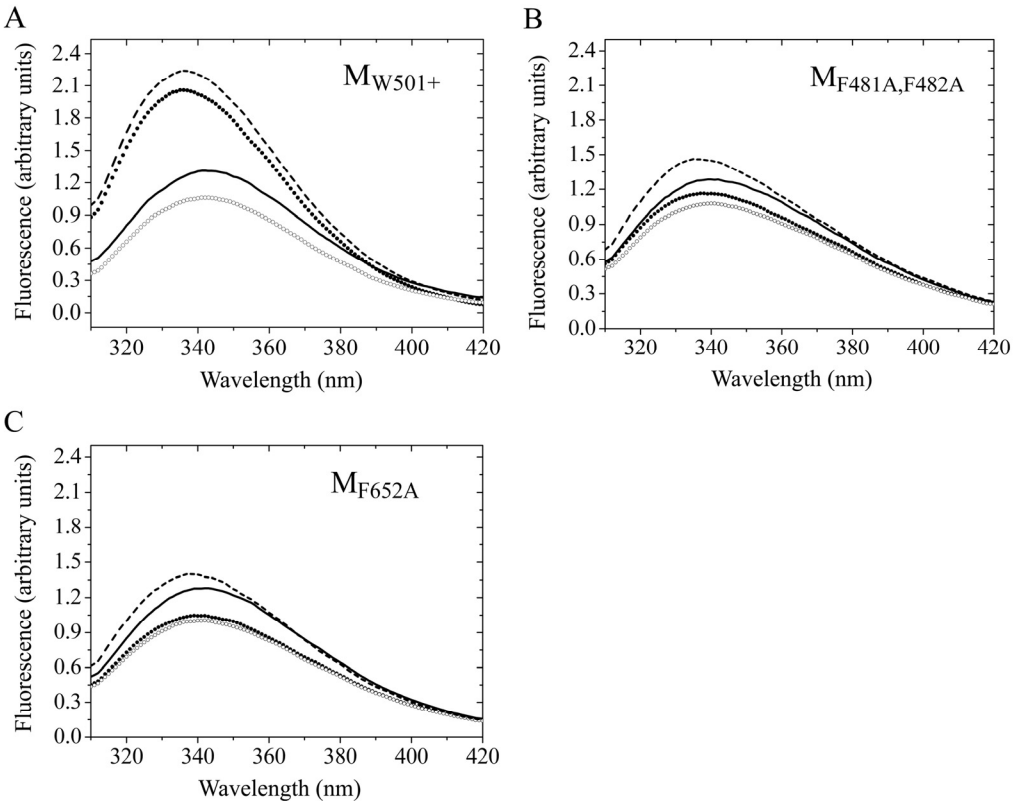

Figure 21. Fluorescence emission spectra of 3 μM M_{W501+} (**A**), $M_{F481A,F482A}$ (**B**) and M_{F652A} (**C**) in the absence (—) and presence of 0.5 mM MgADP (◦◦◦) or 0.5 mM MgATP (•••) or MgADP.AlF_4 (---) at 20 °C. Tryptophan was excited at 297 nm.

fluorescence intensity increases of $M_{F481A,F482A}$ and M_{F652A} were only 10% and 5% respectively. This observation can be the consequence of two possible scenarios. The smaller fluorescence increases of the mutants can be the manifestation of a changed conformation of the relay helix. Alternatively, the conformations sensed by Trp-501 are not changed, only the K_{3a} of the mutants are more pulled to the $M^{\dagger}$MgATP states. The ADP.AlF_4, which is an ADP.P_i analogue, induces a dominant post-recovery state (the high fluorescence state of M_{W501+}). The comparison of the fluorescence intensities of the ADP.AlF_4-bound forms (Figure 21) can help the decision. While the fluorescence level of the M_{W501+}.MgADP.AlF_4 state is 110% higher than the M_{W501+}.MgADP state, those of the $M_{F481A,F482A}$.MgADP.AlF_4 and M_{F652A}.MgADPAlF_4 are just 40% and 35% higher respectively. The fluorescence spectra of the mutants measured at different temperatures show that the relative fluorescence intensities of the apo, MgADP-, and MgADP.AlF_4-bound forms were not influenced by temperature. Whereas the apo and the MgADP-bound states are known to be single fluorescent states, $M_{F481A,F482A}$.MgADP.AlF_4 and

M_{F652A}.MgADP.AlF_4 populate predominantly a single fluorescent state, which is structurally different from the wild type post-recovery state (M_{W501+}.MgADP.AlF_4).

Structural implication to the changed post-recovery state by acrylamide quenching experiment

In the pre-recovery state Trp-501 is located on the surface of the myosin and exposed to the solvent however, during the recovery step this becomes a buried residue (58). Since the fluorescence quenching effect of acrylamide depends on the exposure of the fluorophore, we used acrylamide collisional quenching to explore the possible structural differences of the Trp-501 environment between the post-recovery states of the mutants and the M_{W501+}. We titrated the myosin constructs with acrylamide (up to 0.4 M) in the absence and presence of MgADP, MgATP, and MgADP.AlF_4 (Figure 22). The slope of the fitted line on the Stern-Volmer plot gives the Stern-Volmer constant, which is in line with the solvent exposure.

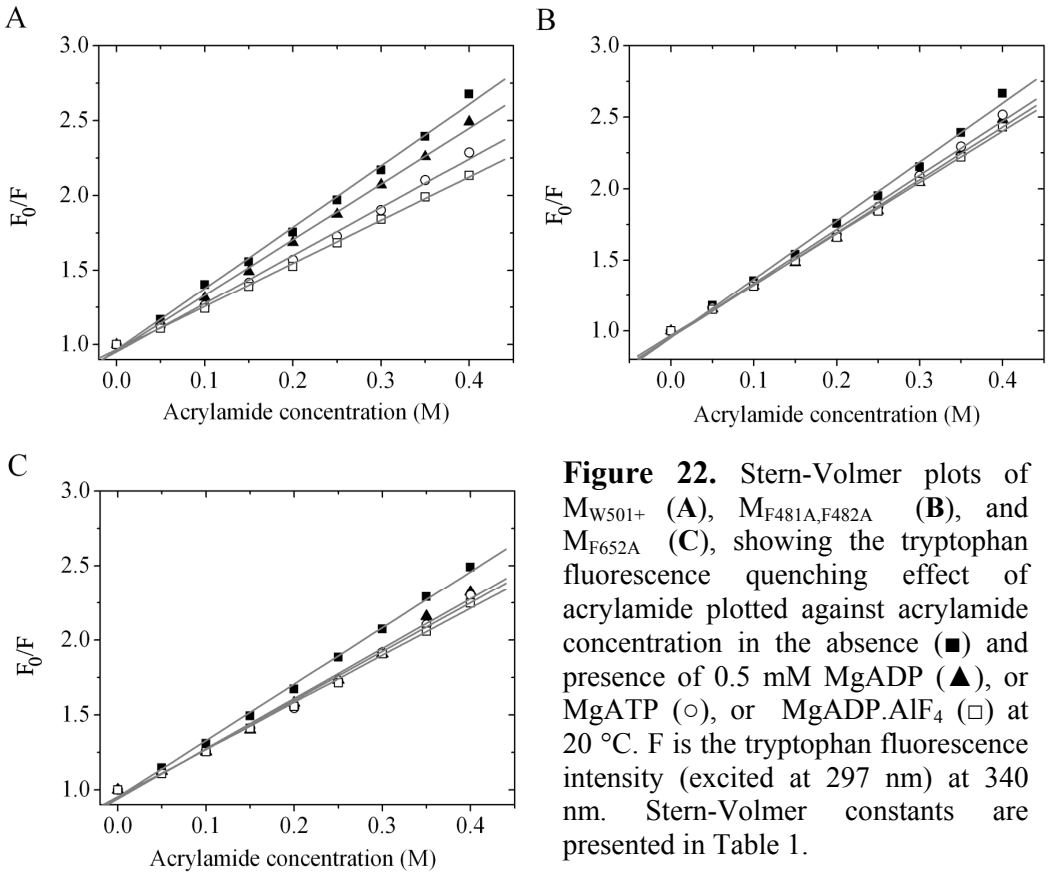

Figure 22. Stern-Volmer plots of M_{W501+} (**A**), $M_{F481A,F482A}$ (**B**), and M_{F652A} (**C**), showing the tryptophan fluorescence quenching effect of acrylamide plotted against acrylamide concentration in the absence (■) and presence of 0.5 mM MgADP (▲), or MgATP (○), or MgADP.AlF_4 (□) at 20 °C. F is the tryptophan fluorescence intensity (excited at 297 nm) at 340 nm. Stern-Volmer constants are presented in Table 1.

The smaller the slope the more buried the fluorophore. Due to this the ATP and ADP.AlF_4 complex of M_{W501+} show significantly decreased Stern-Volmer constants

compared to the apo and ADP-bound forms, indicating the more buried tryptophan fluorophore. In the mutants these differences between the MgADP.AlF_4- and MgADP-bound state cannot be observed (Table 4), indicating Trp-501 remains on the surface during the recovery step of the mutants.

Transient kinetics of Trp-501 signal change of $M_{F481A,F482A}$ and M_{F652A}

Trp-501 shows a fast fluorescence quench upon nucleotide binding, corresponding to the formation of the pre-recovery state of the lever arm. This 10-15% fluorescence quench allowed us to follow the kinetics of the nucleotide binding steps of the mutants in a stopped-flow device and compare them to M_{W501+}. At 20 °C the signal changes induced by mixing the constructs with MgADP under pseudo first-order conditions could be fitted with a single exponential function. From the ADP concentration dependence of the observed rate constant of MgADP binding (Figure 23A) both mutants follow two-step-binding kinetics, indicative of an induced-fit mechanism, as it was described earlier in the case of M_{W501+} (step 6 and 7 in Scheme 7) (58). However, the isomerization step (k_{+2} in Scheme 7) is so fast in M_{W501+} that the rate of the binding cannot be saturated in the applied ADP concentration range. The second-order rate constants of MgADP binding to the mutants are 5 fold less

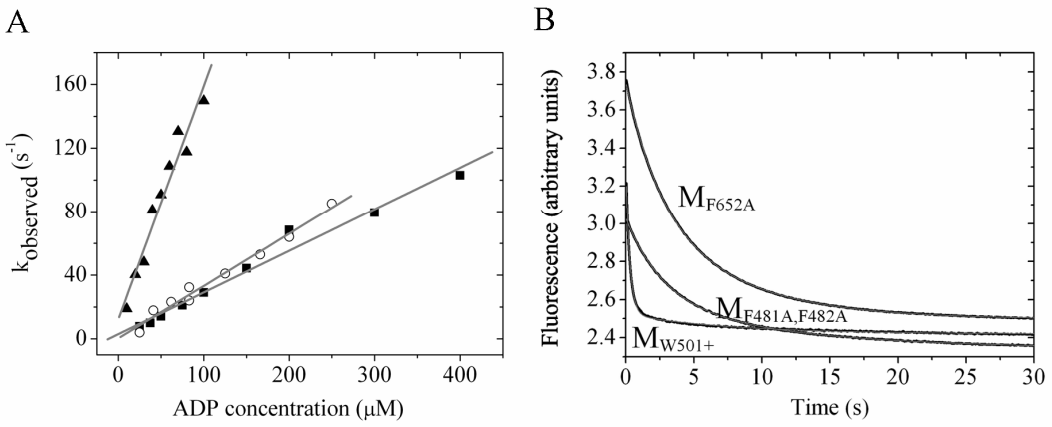

Figure 23. Characterization of MgADP affinity of M_{W501+} (▲), $M_{F481A,F482A}$ (○), and M_{F652A} (■). **A:** the observed rate constants of ADP binding (K_7K_6 in scheme 7) plotted against MgADP concentration. 3 μM motor domains were mixed with MgADP in stopped-flow at 20 °C. **B:** Stopped-flow records of mant-ADP dissociation by applying chasing experiments. 1.5 μM M_{W501+}, $M_{F481A,F482A}$ and M_{F652A} preincubated with 10 μM mant-ADP were mixed with 1mM ATP in stopped-flow. Double exponentials were fitted to the curves. A dominant fast phase (amplitude=0.76, $k_{observed}$=3.5 s^{-1} of M_{W501+}, amplitude=0.49, $k_{observed}$=0.36 s^{-1} of $M_{F481A,F482A}$ and amplitude=0.72, $k_{observed}$=0.4 s^{-1} of M_{F652A}) was followed by a slower phase (amplitude=0.10, $k_{observed}$=0.12 s^{-1} of M_{W501+}; amplitude=0.2, $k_{observed}$=0.09 s^{-1} of $M_{F481A,F482A}$ and amplitude=0.5, $k_{observed}$=0.14 s^{-1} of M_{F652A}) MgADP dissociation from M_{W501+} has similar rate constant as the fast phase of the mant-ADP dissociation. Kinetic data are presented in Table 5.

compared to the wild type (Table 5) and k_{+2} of the mutants are slower with at least 5-10 times.

We also measured the ADP off-rates of the mutants by mant-ADP chasing experiments. The ADP off-rates also decrease approximately 10 times (Table 5 and Figure 23B) in the mutants thus, MgADP affinities are only slightly affected by the mutations.

MgATP binding to M_{W501+} (step 1 and 2 in Scheme 7) is accompanied by the same fluorescence quench of Trp-501 as the MgADP binding. However, this quench can be detected only at low temperatures (e.g. 6 °C), because the higher the temperature, the faster the subsequent recovery step followed by a huge fluorescence enhancement, which does not allow the emergence of the transient fluorescence quench. At 6 °C the recovery step slows down compared to the MgATP binding so

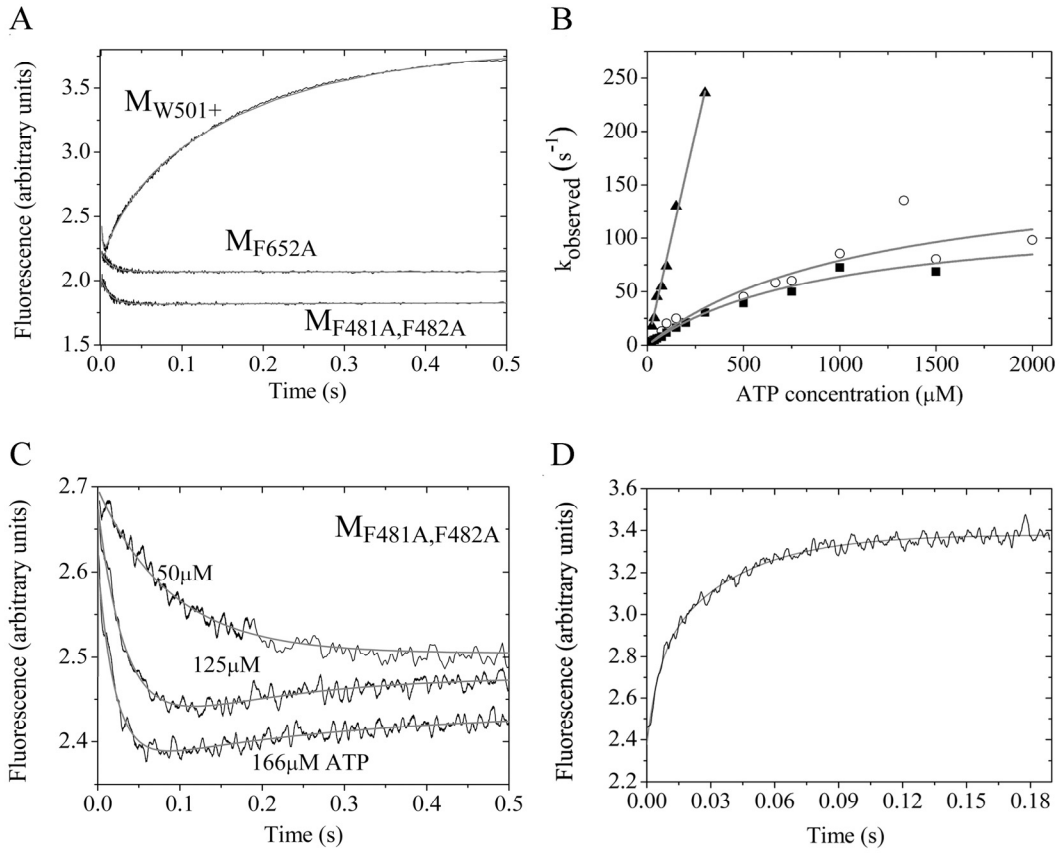

Figure 24. Stopped-flow experiments of MgATP binding. **A:** Time courses of tryptophan fluorescence change upon MgATP (1 mM) binding to 1.5 μM M_{W501+}, $M_{F481A,F482A}$ and M_{F652A} at 6 °C. The initial quench can be detected in all cases. **B:** The observed rate constants of the fluorescence quench of M_{W501+} (▲), $M_{F481A,F482A}$ (○) and M_{F652A} (■) plotted against MgATP concentration. **C:** Stopped-flow records of ATP binding to $M_{F481A,F482A}$ at 20 °C. The fluorescence quench is followed by a small enhancement phase with a rate constant $5s^{-1}$. **D**: Stopped-flow record of M_{W501+} MgATP (1 mM) binding at 20 °C. The fluorescence increment has two phases with a rate constant >150 s^{-1} and 25 s^{-1}.

much that the fluorescence quench transiently appears in the stopped-flow record (Figure 24A) (56). Figure 24A also shows the stopped-flow records of the mutants in reaction with MgATP. The binding event associated with the quench can be seen in all three cases. Single exponentials were fitted on the quenches and ATP concentration dependence of the observed rate constants show that the second order binding constant of MgATP binding is slower in the mutants than in the M_{W501+}, just like in the case of MgADP (Figure 24B, Table 5). The subsequent recovery step accompanied by the fluorescence enhancement was shown only by M_{W501+}. At 20 °C both mutants show a small increase ($M_{F481A,F482A}$ and M_{F652A} 3% and 2%,respectively) after the quench (Figure 24C). This is due to the fact that the higher the temperature, the bigger the equilibrium constant of the recovery step (56) and the high fluorescent state is more populated (it is in line with the emission spectra). At higher MgATP concentration, when the accelerating fluorescent quench has already separated from the enhancement phase, the enhancement phase does not show MgATP concentration dependence. The rate constants of these phases for $M_{F481A,F482A}$ and M_{F652A} are 5 s^{-1} and 2 s^{-1}. Compared to the mutants, the amplitude of the MgATP induced fluorescent enhancement of M_{W501+} is larger with almost two orders of magnitude and it has two phases Figure 24D. The faster phase is the recovery step (>150 s^{-1}) and the second phase corresponds to the hydrolysis step ($k_{obs}=(K_{3a}/(1+K_{3a}))xk_{3b}+k_{-3b}=25\ s^{-1}$). The hydrolysis pulls the recovery step further to the high fluorescent M*MgATP state, which results in fluorescent enhancement [12].

[12] The fast phase of the fluorescence enhancement upon the reaction of MgATP and M_{W501+} was not detected previously in stopped-flow, only in equilibrium kinetic experiments (56, 58). However, the smaller dead-time of our stopped-flow allows us to see the presence of the fast phase (see the dead-time of the stopped-flow in Material and methods). We measured the reaction of MgATP and M_{W501+} at higher temperatures, where the equilibrium constant of the recovery step is bigger. Thus, the fast phase is represented with larger amplitude. The temperature-jump/stopped-flow apparatus developed by us allows the measurement of such fast reactions even above the denaturation temperature of the protein, which is a slower process (for detailed description of the apparatus and this measurement see Appendix). These measurements confirmed the finding that the recovery step appears in the stopped-flow signal. At 50 ˚C the relative amplitude of the fast phase is 0.75 (Appendix figure 2). This has the consequence that the equilibrium constant of the recovery step has been underestimated (58).

Characterization of the ATP hydrolysis steps of $M_{F481A,F482A}$ and M_{F652A}

We carried out quenched-flow experiments to determine the hydrolytic activities of the mutant motor domains using ^{32}P-labeled ATP as a signal (Figure 25). phase is three and six times smaller in $M_{F481A,F482A}$ and M_{F652A}, respectively, than in the M_{W501+}. The amplitude of the burst phase gives the steady-state ratio of the pre- and the post-hydrolytic states thus, the apparent equilibrium constant of the hydrolysis step can be calculated ($^{app}K_{hydrolysis}$=M*.MgADP.P_i/($M^{\dagger}$.MgATP+M*.MgATP)).

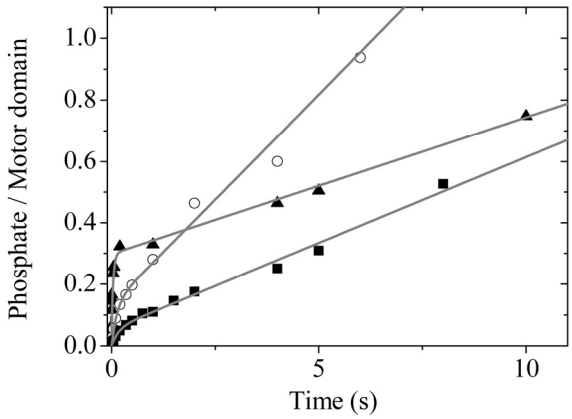

Figure 25. Phosphate production by M_{W501+} (▲), $M_{F481A,F482A}$ (○), and M_{F652A} (■). 25 μM motor domains and 180 μM γ^{32}P-ATP were rapidly mixed by quench-flow at 20˚C. All time courses show an initial burst phase followed by a steady-state phase. The relative amplitude of the burst of M_{W501+}, $M_{F481A,F482A}$ and M_{F652A} are 0.3, 0.1, and 0.05 respectively. Kinetic data are presented in Table 5

$M_{F481A,F482A}$ and M_{F652A} show 4 and 9 times smaller apparent equilibrium constants for the hydrolysis step than M_{W501+} (Table 5), respectively.

In the case of the mutants the rate of the P_i burst was also slower, as shown by the exponential fitted ($k_{observed\ hydrolysis}$=25 s^{-1} of M_{W501+}, $k_{observed\ hydrolysis}$=5.3 s^{-1} of $M_{F481A,F482A}$, $k_{observed\ hydrolysis}$=2.2 s^{-1} of M_{F652A}) The rates of the P_i bursts of the mutants are identical to the rate constants of the fluorescence enhancements induced by MgATP. In the case of M_{W501+} the second phase of the fluorescence enhancement has the same rate as the observed rate of the P_i burst (25 s^{-1}).

The rate of the steady-state phase represents the turnover rate of the enzyme cycle (k_{4+} in Scheme 7). The quenched-flow experiments show that the steady-state rates of the mutants are slightly faster than that of M_{W501+} (Table 5). This is confirmed by steady-state turnover rate measurements carried out by PK/LDH coupled assay.

Determination of the equilibrium constant of the recovery step

Trp-501 fluorescence reveals that the deletion of the phenylalanine fulcrum does not perturb the pre-recovery conformation, but it does perturb the subsequent conformational change, the recovery step. However, an analogous conformational change can be observed in the mutants, which results in a structurally distorted post-recovery conformation. Furthermore, quench-flow experiments show that the mutants are catalytically active in this changed post-recovery state, indicating a switch 2 closure that is essential for the hydrolysis of ATP. Furthermore, the P_i burst phase of the quench-flow experiments followed by a steady-state phase indicates that the observed rate of the ATP hydrolysis step is faster than the rate limiting step of the enzyme cycle (step 4 in Scheme 1), both in the mutants and in the wild type.

These findings show that the mutations do not change basically the enzyme cycle of myosin represented by Scheme 7. Hence, before the rate limiting conformational change (step 4) three states are populated ($M^{\dagger}$.MgATP, M*.MgATP, and M*.MgADP.P_i) in the steady-state (27). The steady-state fraction of the low ($M^{\dagger}$.MgADP) and the high ($M^*_{(total)}$= M*.MgATP+M*.MgADP.P_i) fluorescent states can be calculated by the steady-state fluorescence spectra: $M^{\dagger}=(F_{MgADP.AlF4}-F_{ATP})/(F_{MgADP.AlF4}-F_{MgADP})$ and $(M^*=(F_{MgATP}-F_{ADP})/(F_{MgADP.AlF4}-F_{MgADP})$, where F is the fluorescence intensities of the emission maximum of the spectra. The ratio of the two fractions gives the apparent equilibrium constant of the recovery step ($^{app}K_{recovery-step}=M^*_{(total)}/M^{\dagger}$.MgADP). The $^{app}K_{recovery-step}$ is 19 and 38 times smaller in $M_{F481A,F482A}$ and M_{F652A} than that in M_{W501+} (Table 5). Since the relative amplitude of the Pi burst of the quench-flow experiment gives the steady-state fraction of the M*.MgADP.P_i state, the relative population of the three states ($M^{\dagger}$.MgATP, M*.MgATP, and M*.MgADP.P_i) can be determined and the equilibrium constants of the recovery step (K_{3a}) and the hydrolysis step (K_{3b}) can be calculated (Table 5). The K_{3a} of the mutants show great perturbation, as it is 20 and 30 times smaller in $M_{F481A,F482A}$ and M_{F652A}, respectively, than in the M_{W501+}. K_{3b} of the mutants do not deviate from that of the M_{W501+}, although the P_i bursts of the mutants are decreased several times. This is the consequence of the changed conformation of the post-recovery state that pulls back K_{3a} and thus decreases the P_i burst. A similar effect was found in other mutants (57).

Effects of the mutations in the presence of actin

We determined the actin affinity of the mutants in the absence and presence of ADP. Pyrene-labeled actin was mixed with myosin up to 2 μM in a stopped-flow device. Single exponentials were fitted on the records and the received observed rate constants were plotted against myosin concentration (Figure 26A and B). The second order binding constant (on-rate) and the rate of the dissociation (off-rate) were determined (k_{+A} and k_{-A}, respectively in Table 6, according to the accepted myosin nomenclature). By comparing the results to M_{W501+} (28), it can be seen that the actin

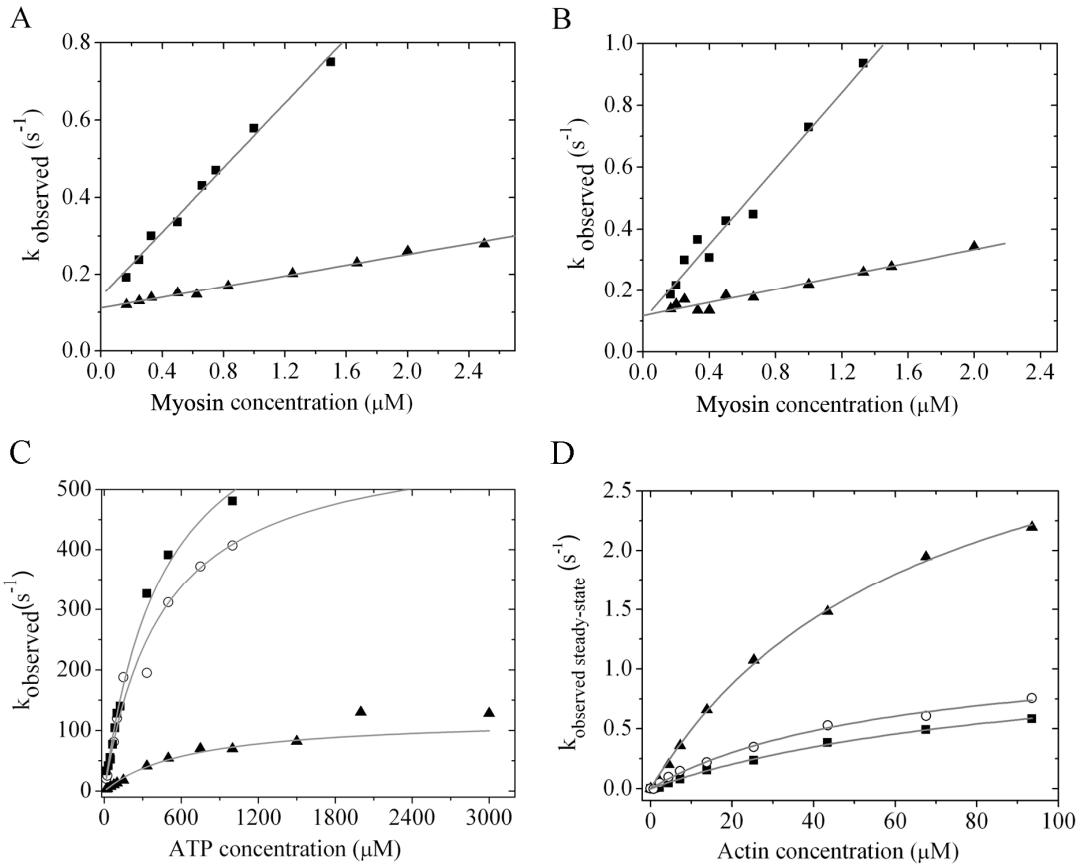

Figure 26. The effect of the mutations in the presence of actin. **A** and **B:** myosin concentration dependence of the observed rate of the acto-myosin association of $M_{F481A,F482A}$ and M_{F652A} respectively, in the absence (■) and presence (▲) of MgADP at 20 ˚C. Myosin was mixed with 0.05 μM pyrene-labeled actin and its fluorescence is followed. The fitted exponentials to the signal change gave the observed rate constants. The actin affinities listed in Table 6. **C:** MgATP-induced acto-myosin dissociation of M_{W501+} (▲), $M_{F481A,F482A}$ (○), and M_{F652A} (■). 1.5 μM pyrene-labeled actin was preincubated with 1 μM motor domain and mixed with different ATP concentrations in a stopped-flow at 20 ˚C. The observed rate of the fitted exponentials plotted against MgATP concentration. The parameters of the fitted hyperbola are presented in Table 6. **D:** actin-activated ATP-ase activity of M_{W501+} (▲), $M_{F481A,F482A}$ (○), and M_{F652A} (■).Hyperbolas were fitted on the data, the received parameters are presented in Table 6. This experiment was carried out in a low-ionic buffer (see Material and methods).

affinity ($K_{d,A}$) of $M_{F481A,F482A}$ and M_{F652A} decreased by 10 and 5 times respectively. In the presence of ADP the actin affinity of the mutants ($K_{d,DA}$) compared to the wild type weakened similarly as in its absence thus, the thermodynamic coupling ratios did not change significantly.

The ATP-induced acto-myosin dissociation also shows that the mutations make the acto-myosin interaction weaker. Pyrene-labeled acto-myosin complex was mixed with ATP up to 1mM in the stopped-flow. Hyperbola were fitted to the MgATP concentration dependences of the observed rate constants (Figure 26C). We found that the second order rate constants of MgATP binding and the maximum rates of the dissociation were several times larger in case of the mutants than in M_{W501+} (Table 6). On the contrary, the actin activated ATP-ase activities measured by pyruvate-kinase/lactate-dehydrogenase coupled assay show that in spite of the fact that the V_{max} values of the mutants are decreased compared to the M_{W501+}, the half saturation (K_m) does not differ significantly (Table 6 and Figure 26D). The latter parameter shows that in weak binding states actin affinity is not perturbed by the mutations. However, the former experiments reveal that the strong binding states show decreased affinities.

Discussion

It has been known for a while that the nucleotide binding site controls the state of the lever arm through the conformation of the switch 2 loop. However, the molecular mechanism of the communication between these two sites has not been fully understood yet. A recent *in silico* simulation composed a structural trajectory for the priming of the lever arm (recovery step) between the two end states of the conformational change. The results suggested that closure of switch 2 and 25 ° rotation of the converter domain are coupled by a seesaw-like movement of the relay helix (16). The N-terminal part of the relay helix moves towards the ATP due to the pulling of switch 2 closure to which the C-terminal of the helix reacts as a seesaw and moves toward the opposite direction. According to the simulated structural trajectory this seesaw-like movement of the relay helix is followed by a second phase in which the resulting converter rotation provokes a further 40 ° rotation. This later movement cannot be tolerated by the relay helix, thus the C-terminal region of the relay helix

unwinds or kinks initiated by the break of the intra-helical hydrogen bond 486-490. Fischer *et al.* explained the order of these two phases by the fact that the second phase is sterically hindered until the side chain rearrangements of the seesaw movement (62). However, such a direct structural trajectory of the recovery step neglects the dynamic behavior of the protein that allows it to populate the neighboring conformational space along the suggested trajectory. Recent umbrella sampling simulation showed a wider range of the possible conformations during the recovery step (30), letting conformations different from the main stream of the reaction trajectory suggested by Fischer *et al.* be populated (16)).

Nevertheless, the simulated structural trajectory reveals key residues, which can be essential in conducting the information of switch 2 state toward the converter region. Fischer *et al* suggested that a hydrophobic cluster (Phe-481/Phe-482/Phe-652) at the middle of the relay helix serves as the pivoting point of the relay seesaw during the recovery step (16). To check experimentally the necessity of the appointed residues they were mutated to dysfunctional residues.

We made two different mutant constructs ($M_{F481A,F482A}$ and M_{F652A}) with a single Trp-501 background. The two mutant myosin construct behave astonishingly identically. Their Trp-501 residues report that their fluorescence states are very similar, and all of the reaction steps of their enzyme cycles are changed by the mutations in the same mode and magnitude (see Table 4, 5, and 6). Fluorescence experiments show that the mutations have no effect on the lever arm conformations in the apo and pre-recovery states however, nucleotide binds to the mutants more slowly. On the contrary, the changed Trp-501 fluorescence of the mutants upon ADP.AlF_4 binding indicates that the conformation of the relay helix is perturbed in the post-recovery state. Interestingly, the mutants can hydrolyze ATP in this changed post-recovery conformation. We can state that the switch 2 is closed in this conformation just like in the wild type because the closed conformation of switch 2 is required for hydrolysis to be effective (6, 34). Hence, we judge that the lack of the phenylalanine fulcrum diverts the relay helix into a changed conformation upon switch 2 closure. This perturbed conformation is energetically less favorable, as indicated by the dramatically suppressed equilibrium constants of the recovery step. The conformation of the relay helix in this state resembles to its pre-recovery conformation, since Trp-501 remains on the surface of the motor domain, which is a characteristic of the pre-recovery conformation (58). This indicates that the movement of the relay helix is

impeded at the beginning of the reaction trajectory of the recovery step. Hence, it is likely that, although switch 2 closes, the relay seesaw cannot tilt in the absence of its pivoting point. In other words, the information of switch 2 closure cannot get to the C-terminal of the relay helix; therefore, the energetic landscape of the converter/lever arm region remains similar to that of the pre-recovery state.

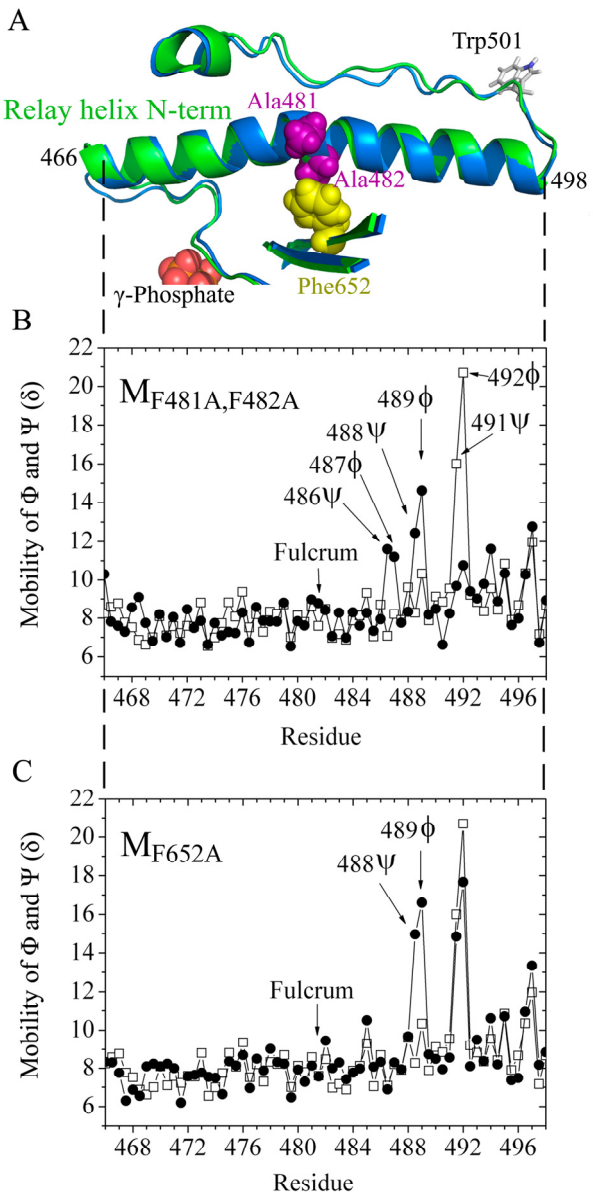

Figure 27. The effect of the mutations on the pre-recovery structure revealed by molecular dynamics simulation. The mutations F481A/F482A or F652A were introduced into the pre-recovery structure and molecular dynamics simulations were performed. **A:** The effect of the F481A/F482A mutations on the relay region conformation (wild type green, mutant blue). **B** and **C:** average amplitude of the torsion angle (Φ and Ψ) changes (δ) during the equilibrium phase of the molecular dynamics simulation of $M_{F481A,F482A}$ (●) and M_{F652A} (●) respectively, compared to the wild type (□). The two constructs show similar changes in the mobilities. The structural demonstration of the consecutive residues represented on the x-axis of graphs B and C.

We also performed *in silico* molecular dynamic simulations on the wild type motor domain and on the two mutated constructs [13]. These results are consistent with the experimental data. The relay helix structure in the pre-recovery conformation is not perturbed by the mutations. (Figure 27A) However, the post-recovery conformation is unstable and the helical structure at the kink region of the relay helix collapses into a distorted local energy minimum (Figure 28).

[13] Since the construction of these experiments were done by Zenhui Yang, I present these results just in the discussion section. The design of the experiments and the analyses of the data were carried out by me.

This result also shows that the phenylalanine fulcrum is essential for the right post-recovery lever arm conformation.

We also investigated the dynamics of the relay helix, and checked how the elimination of the pivoting point influences it. We collected the main-chain torsion angle Φ and Ψ of all residues in the relay helix during the equilibrium phase of the molecular dynamics simulation. Figures 27B and C show the average amplitudes of the torsion angle changes (δ) of the relay helix residues in the pre-recovery states of the wild type and the mutants. In the wild type motor domain most of the torsion angles have very similar mobilities, and this δ value is also characteristic of other helical residues in the motor domain. However, there is a highly mobile part in the relay helix (Ψ491/Φ492) exactly in the kink region. The ramachandran plots of these highly mobile residues show that Ψ491/Φ492 angles are located even outside of the favored α_R region of a central helix residue(31) however, other residues do not show such phenomena (Appendix figure 3). The high mobilities of Ψ491/Φ492 and their distorted position in the ramachandran plot indicate that this part of the kink region is strained in the pre-recovery state. Furthermore, we could perform the same analysis on a structure representing a state that is situated halfway on the reaction trajectory of the recovery step, since we also modeled *in silico* a structural trajectory for the recovery step. This state is picked up after the seesaw-like movement of the relay helix (first phase of the recovery step) but before the unwinding (kinking) of the relay helix (second phase of the recovery step). In this state the torsion angles of the whole kink region (486-492) behave similarly to the Ψ491/Φ492 in the pre-recovery state. This finding indicates that the seesaw movement increases the instability of the kink region, which is indicative of the presence of strain in this region. This strain leads finally to the unwinding of the helix.

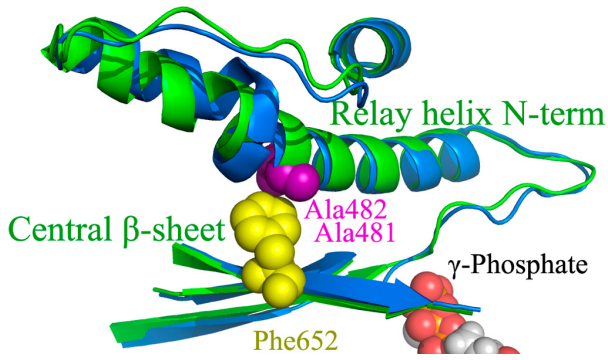

Figure 28. Comparison of the post-recovery relay region of the wild type and the mutation F481A/F482A. Molecular dynamics simulations were applied to achieve energetically lower conformations.

The mutations have intriguing effects on the dynamics of the relay helix. Interestingly, at the eliminated pivoting point the mobilities of the torsion angles are

not changed. However, they are increased by more than 50% at positions four (Ψ486/Φ487) and six (Ψ488/Φ489) amino acid away from the mutations in $M_{F481A,F482A}$. At the same time, the mobilities of the Ψ491/Φ492 torsion angles are dropped to the half of that of the wild type and they become similar to other torsion angles of the relay helix residues (Figure 27B). Even their ramachandran plots become similar to that of other relaxed helical residue (Appendix figure 3). On the other hand, Ψ488/Φ489 angles of $M_{F481A,F482A}$ tend to move out from the relaxed region to a similar region of the Ramachandran plot to what is populated by the Ψ491/Φ492 in the wild type, indicating that now these residues become strained. A similar effect was found in case of M_{F652A} (Figure 27C).

These findings indicate that the lack of the pivoting point shifts the strained part of the kink region by a few amino acids (Ψ486/Φ487 and Ψ488/Φ489) in the pre-recovery state. In other words, the elimination of the fulcrum rearranges strains along the relay helix, even at the beginning of the reaction trajectory of the recovery step. However, the produced strain in the kink region is supposed to be essential to the formation of the post-recovery state, and we also found that the tension is increasing in the kink region during the seesaw movement in the wild type myosin.

In summary, the mutational analysis proved the essential role of the relay fulcrum during the recovery step, even at the beginning of the reaction trajectory (16). Therefore, in the light of the structural data the pivoting role of the fulcrum and the seesaw-like tilt of the relay helix is seems to be a potential mechanism which conducts the closure of switch 2 to the converter domain and transforms the energetic landscape of the relay/converter/lever arm region to make the primed lever arm position more favorable.

Furthermore, the detailed cognition of the relay movement during the recovery step, helps us to identify those conformational changes that can lead to the triggering of the power stroke (see (43) and Chapter 4).

Chapter 3

Step 3 – The mechanism that allows actin rebinding to the post-hydrolytic primed motor domain

Introduction

Although the combination of the structural and kinetic investigations has led to a wide knowledge in the workings of steps 1 and 2 of the Lymn-Taylor model, steps 3 and 4 that lead to the rigor complex are still poorly understood (18).

In step 3, actin has to bind back to myosin having primed lever arm and MgADP.P_i in the nucleotide binding pocket to achieve force generation. The priming of the lever arm, the recovery step is a fast (k_{obs}~1000s-1) equilibrium step (K_{3a}~1) when MgATP is in the nucleotide binding site (step 3 in Scheme 7). Since this step is fully reversible both the pre- and post-recovery positions of the lever arm are populated (58). If the lever arm movement in MgADP.P_i (reverse recovery step, step 4 in scheme 7) was also a fast equilibrium step, actin would bind to myosin with a great chance after the reversal of the lever arm swing (to the $M^{\dagger}$.MgADP.P_i state). However, this results in a futile cycle [14] and the hydrolysis of ATP without force generation is avoidibly "uneconomic".

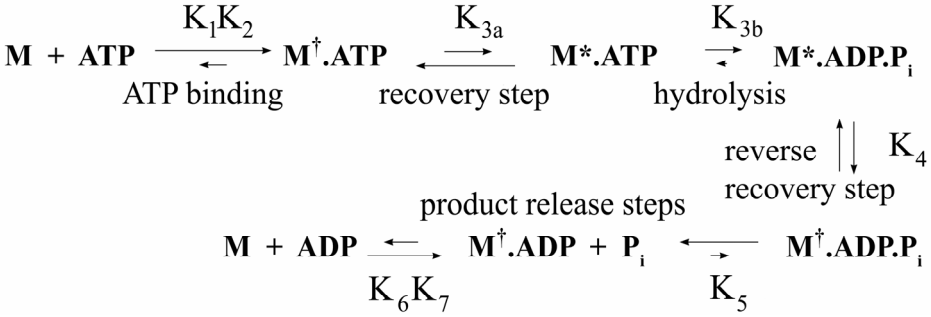

Scheme 7. The ATP-ase cycle of myosin in the absence of actin. † and * correspond to the low and high fluorescent states of Trp-501.

[14] An enzyme cycle without force generation.

Thus the question arises how myosin maximizes the chance of actin rebinding to myosin after hydrolysis, but before the reverse recovery step. Does hydrolysis (or the lever arm priming) influence the actin binding region in order to change the weak actin affinity in ATP (46)? If this was the case, there would be a hydrolysis (or lever arm priming) dependent communication between the nucleotide binding site and the actin binding region. However such a mechanism has not been observed. Moreover, the actin affinity in MgADP.P_i is seems to be as weak as in the MgATP-bound form, inducing immediate acto-myosin dissociation (41). Consequently, the lever arm movement has to be somehow different in MgADP.P_i, in order to maximize the chance of actin rebinding to myosin with MgADP.P_i and primed lever arm. However, the lever arm movement in MgADP.P_i has not been a well-characterized process [15].

There are two different possibilities to maximize the fraction of M*ADP.P_i, to which actin has to bind. According to the first scenario the equilibrium constant of the lever arm movement in MgADP.P_i is pushed absolutely to the primed M*MgADP.P_i state (K_4<<1) and the relative fraction of $M^{\dagger}$MgADP.P_i state is very low (46). This allows the lever arm movement to be a fast step and the subsequent Pi release has to be the rate limiting step of the cycle (22). Alternatively, actin binds with great probability to the myosin having primed lever arm if the lever arm movement in MgADP.P_i is a slow step. More exactly, the forward rate of the reverse recovery step is much slower than the rate of actin binding. According to this scenario the rate limiting step of the cycle is this step, and the subsequent Pi release is a fast step. In other words, the question is weather a thermodynamic or a kinetic barrier “blocks” the lever arm in the primed state, waiting for actin binding. The two scenarios cannot be distinguished easily by kinetic experiments, but they mean very different activation mechanisms of the ATP-ase cycle upon actin binding.

Recently, experimental evidence was found for the entitlement of the later case (27), presented in details in Máté Gyimesi’s PhD thesis. Two single tryptophan motor domain constructs were used to investigate the kinetics of P_i binding, release steps, and that of the lever arm movement in MgADP.P_i (step 4 and 5 in Scheme 7). One of the constructs contains a tryptophan in the relay helix (M_{W501+} construct) and senses the lever arm movement, while the other one (M_{W129+}) is sensible to the

[15] These conformational changes in fact belong to the second step of the Lymn-Taylor model, but the conclusions to be derived are strictly coupled to the understanding of actin rebinding to myosin.

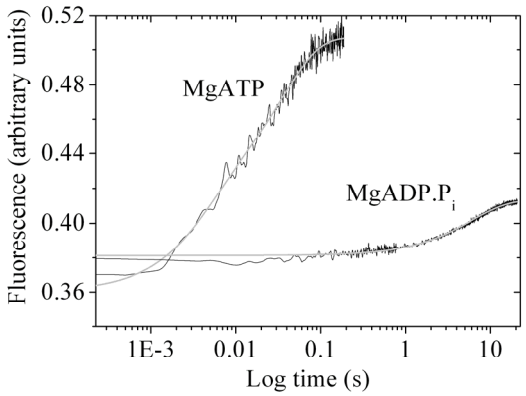

Figure 29. Stopped-flow records of the reactions of M_{W501+} with MgATP and MgADP.P_i. The fluorescence enhancement upon MgATP binding has two phases (kobs>150 s^{-1} and 25 s^{-1}), upon MgADP.P_i binding it is a slow single-phase fluorescence enhancement (0.2 s^{-1}).

nucleotide binding steps. Both constructs pre-incubated with MgADP were mixed and titrated with P_i in stopped-flow, and they were also mixed with MgADP after pre-incubation with saturating amount of P_i. The kinetic analysis revealed that the slow step is the lever arm movement in MgADP.P_i, and not the P_i release step (Figure 29), and that the forward rate of step 4 (reverse recovery step, k_{4+} in scheme 7) is equal with the steady-state turnover rate of the basal ATP-ase cycle (0.05s^{-1}). Furthermore, the P_i binding and release steps were significantly faster and K_4 was found to be 0.3.

Based on these findings, the main difference between the lever arm movements in MgADP.P_i and MgATP is not in the equilibrium constants. However, the observed rate of the recovery step in ATP is faster with four orders of magnitude than the reverse recovery step in MgADP.P_i. Consequently, there must be a conformational change induced by the hydrolysis step (step 3c in scheme 7) before the reversal swing of the lever arm. This supposed rearrangement in the active site lowers the rate of the lever arm movement most likely by increasing its activation energy. However, the coordinates of the primed lever arm state structures with MgATP (MgADP,BeF_x) or MgADP.P_i (MgADP.AlF_4, MgADP.VO_4) analogues do not manifest any difference in this region.

Recently, *in silico* molecular dynamics simulations on a structure having primed lever arm and ATP or ADP.P_i in its nucleotide binding site revealed some conformational differences (46). A small displacement of the cleaved γ-phosphate moves the switch 2 loop less than 1 Å away from its pre-hydrolytic position. This

movement pushes the side-chain of Asn-475, which reacts to it by turning away (Figure 30B). This side-chain movement of Asn-475 allows the formation of a hydrogen bond between Asn-475 and Tyr-573 residues. This newly formed hydrogen bond is supposed to block Tyr-573, not allowing it to move back to its pre-recovery conformation. Hence Tyr-573 cannot be involved in the conformational change of the recovery step in MgADP.P_i. On the contrary, in the MgATP-bound myosin Tyr-573 moves or wedges between the relay helix and the SH1 helix during the recovery step (46, 47) (Figure 30AB). According to this concept, the blocked wedge mechanism of Tyr-573 can be the reason for the decreased rate of the recovery step in MgADP.P_i. However, this hypothesis requires experimental validation.

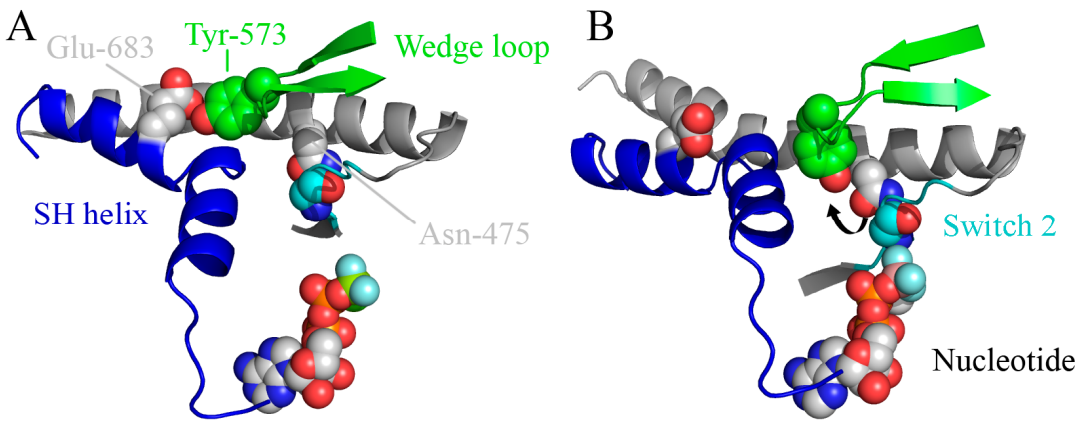

Figure 30. Action of Tyr-573 during the recovery step and after ATP hydrolysis. **A** and **B** parts of the figure are the pre- and post-recovery conformations of the *Dictyostelium* myosin II motor domain. (PDB code: 1MMA, 1VOM, respectively). During the recovery step Tyr-573 wedges against the relay helix and the SH helix. Based on molecular dynamics simulation of an ADP.$_{Pi}$ containing post-recovery structure, Asn-475 rotates due to hydrolysis (black arrow in part B) and makes a hydrogen bond with Tyr-573 (46).

Nevertheless, scheme 8 shows the kinetic model of the acto-myosin interaction (19). Step 0 is the formation of the initial collision complex that is followed by a series of conformational changes (step 1 and 2). The collision complex formation is strongly influenced by the ionic strength, as it is driven by charge-charge interactions between actin and some of the actin binding surface loops of myosin (18). The next conformational change results in the so-called weak binding acto-myosin complex (state 3 in Lymn-Taylor model, A-state in scheme 8). The interaction between actin and myosin in this state is very weak (Kd=50uM), since

$$A + M(Nu) \underset{}{\overset{K_0\ K_1}{\rightleftharpoons}} AM^{A}(Nu) \overset{K_2}{\rightleftharpoons} AM^{R}(Nu)$$

Actin binding Weak-to-strong transition

Scheme 8. Kinetic scheme of actin binding (19).

there is ADP.P_i in the nucleotide binding pocket. Because the existing structural data is very limited on this state, mainly mutational studies mapped which surface loops are involved in these interactions (28, 67). A computational rigid docking study was recently published that shows an exact actin binding surface of myosin with opened cleft (67) (see Chapter 4). Additionally, this state is also hardly investigable kinetically because the stable production of the acto-MgM.ADP.P_i ternary complex requires extreme concentrations (100 μM actin and 100 mM P_i). Otherwise, the weak interaction appears just transiently, since the next conformational transition in scheme 8 (K_2) leads immediately to P_i release and to strong acto-myosin interaction (step 4 in Lymn-Taylor model, R-state in scheme 8). These are responsible for the fact that this weakly interacting complex is the less discovered state in the Lynm-Taylor model.

Aims

Our aim was to investigate experimentally the role of Tyr-573 in slowing down the rate of the lever arm movement in ADP.P_i (reverse recovery step), to allow the fast actin rebinding to myosin having primed lever arm. We introduced a mutation into the M_{W501+} construct by mutating the tyrosine to phenylalanine at this position. This mutation inhibits very specifically the hydrogen bond mediated interactions of this residue. In the pre-recovery state this forms a hydrogen bond with Glu-683 (SH1 helix). This bond breaks during the recovery step and Tyr-573 rotates toward the nucleotide binding site to form its supposed post-hydrolytic interaction with Asn-475 (46). This later interaction is also inhibited by the elimination of the hydroxyl group.

By the use of Trp-501 fluorescence we are able to follow the lever arm movement in MgATP and MgADP.P_i and to detect the effects of the mutation on these steps. Naturally, the effect of the mutation should be very specific, otherwise the right interpretation of the data is almost impossible.

Results

Steady-state fluorescence Trp-501 in M_{Y573F}

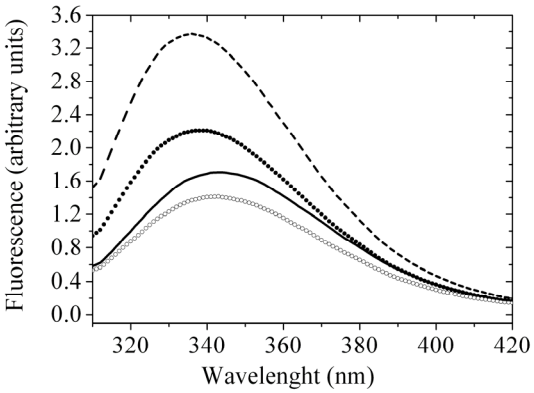

Figure 31. Fluorescence emission spectra of 3 μM M_{Y573F} in the absence (—) and in the presence of 0.5 mM MgADP (◦◦◦), or 0.5 mM MgATP (•••), or MgADP.AlF_4 (---) at 20 °C. Tryptophan was excited at 297 nm. All of them have the same intensity as M_{W501+}, except the MgATP bound, which has lower fluorescence.

In order to analyze the effects of the mutation on the conformations of the lever arm, we measured the steady-state fluorescence emission spectra of Trp-501 in M_{Y573F} at 20 °C in the presence of different nucleotides and compared them to that of M_{W501+} (Figure 31). In the absence of nucleotide the emission spectra of the mutant and the wild type are very similar (emission maximum at 343 nm and 342 nm of M_{Y573F} and M_{W501+}, respectively). Upon MgADP binding both constructs show 17% quench and 2 nm blue shift, indicating that the mutation has no effect on the pre-recovery conformation. The binding of the MgADP.P_i analogue MgADP.AlF_4, which induces the high fluorescence post-recovery state of M_{W501+}, results in 130% higher fluorescence intensity than that of the pre-recovery MgADP-bound state. In the case of the M_{W501+}.MgADP.AlF_4 this increase is 120%, and the spectrum has the same emission maximum as in case of the mutant (335 nm), indicating that the mutation does not have an effect on the primed lever arm conformation either. In contrast, the MgATP-induced fluorescence enhancement of the M_{Y573F} is significantly smaller (55% compared to the MgADP state) than that of the M_{W501+} (100%). In M_{W501+} the MgATP-bound myosin is an equilibrium mixture of the low (pre-recovery) and the high (post-recovery) fluorescent states and this is presumably also valid for the mutant. Thus, the lower fluorescence of the M_{Y573F}.MgATP complex might be caused by the more populated low fluorescent $M^{\dagger}$MgATP state, which is most likely due to the shifted equilibrium constant of the recovery step or the hydrolysis step.

Transient kinetic characterization of the lever arm movement of M_{Y573F} in ATP and ADP.P_i

The kinetics of MgADP binding to M_{Y573F} (Step 1 and 2 in Sceme 7) can be characterized by following the fluorescence signal of Trp-501 in stopped-flow device (see also Chapter 2). At 20 °C, the fluorescence quench induced by MgADP binding under pseudo first-order conditions could be fitted with a single exponential function. The MgADP concentration dependence of the observed rate constant shows two-step-binding kinetics of an induced-fit mechanism [16]. The second order rate constant of MgADP binding to M_{Y573F} is the same as in the case of the wild type (Table 7) (1.7 $\mu M^{-1}s^{-1}$ and 1.5 $\mu M^{-1}s^{-1}$ of M_{Y573F} and M_{W501+}, respectively), however, k_{+2} of the mutant is a bit slower (Table 7). We also measured the MgADP off-rate of M_{Y573F} ($k_{off\ MgADP}$=2 s^{-1}) by MgADP chasing experiment, which is approximately two-times slower than that of the wild type ($k_{off\ MgADP}$=5 s^{-1}).

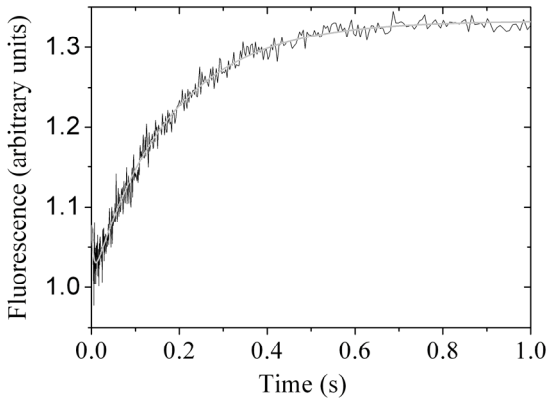

Figure 32. Stopped-flow record of the reaction of M_{Y573F} (1.5 μM) and MgATP (1 mM). The fluorescence change has two phases, an initial quench, which is the binding (k_{obs}=250 s^{-1}), and a fluorescence enhancement with an observed rate 6 s^{-1}

At 20 °C, MgATP binding to M_{Y573F} is accompanied by the same fluorescence quench as MgADP binding, but now it is followed by the fluorescence enhancement coupled with the recovery step (Figure 32). The subsequent fluorescence enhancement has only a single phase with an observed rate 6 s^{-1}. On the contrary, the fluorescence enhancement of M_{W501+} upon ATP binding has two phases (Figure 24D). The fast phase is the recovery step (>150 s^{-1}), which is followed by a slower phase corresponding to the hydrolysis step ($k_{obs}=(K_{3a}/(1+K_{3a}))xk_{3b}+k_{-3b}$=25 s^{-1}).

We also measured the kinetics of the reverse recovery step, the lever arm movement in ADP.P_i. M_{Y573F} pre-incubated with ADP was mixed with P_i in stopped-flow 17 A small fluorescence enhancement could be observed upon P_i binding to M_{Y573F}MgADP, just like in the case of M_{W501+}, however with a smaller amplitude. This might be the consequence of a bigger K_4 than in the M_{W501+} (note that

K_4=$M^{\dagger}$.MgADP.P_i/M*.MgADP.P_i). The single exponential fitted to the record shows that the observed rate of the transition is faster than in the wild type (0.3 s^{-1} and 0.2 s^{-1} of M_{Y573F} and M_{W501+} respectively).

---

[16] Since these experiments are carried out by László Végner, I do not present the figures of these experiemnts.

[17] Because of the high ionic strength of 25 mM P_i less NaCl was added to the P_i buffer in order to keep the ionic strength constant (see Materials and Methods). Then, before measurement the buffer was autoclaved at 120 ˚C to eliminate the pyrophosphate contamination that inhibits P_i binding to myosin (27).

Since the turnover rate of the enzyme cycle of M_{W501+} is equal with the forward rate of the reverse recovery step in MgADP.P_i, we also measured the turnover rate of M_{Y573F} with a multiple turnover experiment. M_{Y573F} was mixed with MgATP, being 5 fold molar excess and Trp-501 fluorescence was followed. When all the MgATP was hydrolyzed the fluorescence was dropped down to the fluorescence level of the MgADP-bound form [18]. The calculated turnover rate is 0.28 s^{-1}, which is 6 times faster than that of the wild type (58), and almost equal with the calculated rate of k_{+4} from the P_i binding of the M_{Y573F}. MgADP.

Characterization of the ATP hydrolysis step of M_{Y573F}

The hydrolytic activity of M_{Y573F} was determined by quenched-flow multiple turnover experiments using ^{32}P-labeled ATP (Figure 33). An initial burst phase of the P_i production was detected followed by a steady-state phase similar to the wild type. The amplitude of the burst phase gives the steady-state ratio of the pre- and the post-hydrolytic states, so the apparent equilibrium constant of the hydrolysis step ($^{app}K_{hydrolysis}$= M*.MgADP.P_i/($M^{\dagger}$.MgATP+M*.MgATP)). The amplitude of the burst phase of M_{Y573F} is 0.3 P_i/motor domain, the same as that of the M_{W501+}, and thus their $^{app}K_{hydrolysis}$ are also the same (Table 7). The fitted exponential on the burst phase shows that the observed rate of the P_i burst is slower than in M_{W501+} ($k_{observed\ hydrolysis}$ 6 s^{-1} and 25 s^{-1} of M_{Y573F} and M_{W501+} respectively), and its observed rate constant is identical to the rate constants of the ATP induced fluorescence enhancement. As it was mentioned in the previous chapter, in M_{W501+} the second phase of the fluorescence enhancement has the same rate constant as the observed rate constant of the P_i burst. However, the equilibrium constant of the recovery step (K_{3a}) influences the rate of the

forward reaction of the hydrolysis step ($k_{obs}=(K_{3a}/(1+K_{3a}))xk_{3b}+k_{-3b}=25\ s^{-1}$). Consequently, the lower the K_{3a}, the slower the observed rate of the hydrolysis step. A further scenario that explains the slower observed hydrolysis rate is that the recovery step determines directly the observed rate of the hydrolysis and the subsequent hydrolysis is faster. Since the fast phase of the fluorescence enhancement in M_{Y573F} cannot be detected, this scenario cannot be excluded. The steady-state phase, corresponding to the turnover rate of the enzyme cycle (k_{4+} in Scheme 7), is faster in the mutant, being in line with the previously determined activity of M_{Y573F}.

[18] Since M_{Y573F} is not saturated with MgADP in the presence of 15 μM MgADP, its fluorescence level is indeed between the fluorescence level of the apo and MgADP-bound forms.

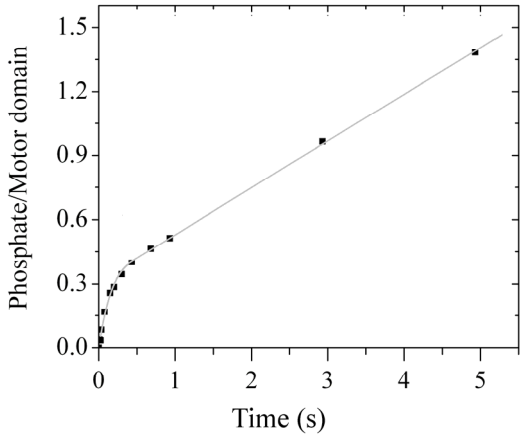

Figure 33. Phosphate production of M_{Y573F} . 20 μM motor domains and 160 μM γ^{32}P-ATP were rapidly mixed by quench-flow at 20˚C. The time course shows an initial burst phase followed by a steady-state phase. The relative amplitude of the burst phase is 0.4. Kinetic data are presented in Table 7.

Determination of K_{3a} and K_{3b} of M_{Y573F}

Based on the Trp-501 fluorescence and quench-flow experiments we can state that the mutation does not change basically the enzyme cycle of myosin represented by Scheme 7, similarly to the other relay mutants presented in Chapter 2. Moreover, the Y573F mutation does not even perturb the conformations of the relay region. However, the apparent equilibrium constant of the recovery step shows significant change. The ratio of the high and low fluorescent states gives $^{app}K_{recovery\text{-}step}=M^*_{(total)}/M^{\dagger}.ADP$, which can be calculated by the steady-state fluorescence emission spectra: $M^{\dagger}=(F_{MgADP.AlF4}-F_{ATP})/(F_{MgADP.AlF4}-F_{MgADP})$ and $(M^*_{(total)}=(F_{MgATP}-F_{MgADP})/(F_{MgADP.AlF4}-F_{MgADP})$, where F is the fluorescence intensities at the emission maximums. $^{app}K_{recovery\text{-}step}$ of M_{Y573F} is 0.68, which is 7.8 times smaller than that of M_{W501+} (5.3). Since the quench-flow experiment determines the steady-state fraction of the M*.MgADP.P_i state, the steady-state ratio of the three populated states ($M^{\dagger}$.MgATP, M*.MgATP and M*.MgADP.P_i) are known: $M^*.MgATP=M^*_{(total)}-M^*.MgADP.P_i$. Interestingly, $M^*_{(total)}$ (40%) is almost equal

with M*.MgADP.P_i (43%), which means that the steady-state fraction of M*.MgATP is undetectably small. Based on these findings, the equilibrium constants of the recovery step (K_{3a}) and the hydrolysis step (K_{3b}) can only be estimated (Table 7). For K_{3a} the upper limit is around the error of the measurement ($K_{3a}<0.1$), which means it bears a large perturbation, as it is almost 30 times smaller than in the M_{W501+}. On the contrary, the mutation does not lower the amplitude of the P_i bursts. Consequently, K_{3b} of M_{Y573F} deviates significantly from that of the M_{W501+}, since a much bigger K_{3b} (M*.MgADP.P_i /M*.MgATP) has to compensate the much less M*.MgATP in order to produce the same amount of M*.MgADP.P_i. According to this, K_{3b} of M_{Y573F} is at least 5.7, which is 10 times bigger than that of the M_{W501+}.

Discussion

Our recent kinetic investigation proved that the rate limiting step of the basal ATP-ase cycle of *Dictyostelium* myosin II is the reverse recovery step in MgADP.P_i (27). Consequently, the observed rate of this lever arm movement is slower with four orders of magnitude than the recovery step in MgATP. This means that, hydrolysis somehow lowers the rate of the lever arm movement. However, there is only a single molecular dynamics simulation that reveals the existence of a hydrolysis sensing conformational change in the nucleotide binding site (46). According to this model, the Tyr-573 is wedging against the relay helix during the recovery step in MgATP but its wedge action is blocked by a hydrogen bond (between Tyr-573 and Asn-475) after the hydrolysis. We introduced the Y573F mutation into the M_{W501+} construct in order to inhibit the hydrogen bond mediated interactions of this residue. In the pre-recovery state, Tyr-573 forms a hydrogen bond with Glu-683 (SH1 helix), which breaks during the recovery step and Tyr-573 rotates toward the nucleotide binding site to form its supposed post-hydrolytic hydrogen bond with Asn-475 (46).

If this structural model is right, we expect that the elimination of the pre-recovery hydrogen bond perturbs the wedge action of the tyrosine during the recovery step in MgATP. The lack of this interaction between Glu-683 and Tyr-573 might have the consequence that Tyr-573 is not coordinated properly and situated in a different position, which makes it dysfunctional. Alternatively, the role of this interaction is not just the coordination of the tyrosine, but also the mediation of a conformational

change from one site to the other. The importance of the interaction between the wedge loop and the SH1 helix is also implied by the fact that in myosin V and VI, in which this residue is not tyrosine but phenylalanine, the lack of the hydrogen bond mediated interaction between Glu-683 and Tyr-573 is recovered by a hydrophobic interaction between these residues. However, in myosin II the SH1 helix is too far from the phenyl ring of the phenylalanine to make such an interaction. Nevertheless, we expect that during the recovery step the mutation mimics the blocked wedge mechanism of Tyr-573 in MgADP.P_i by perturbing the wedge action of the tyrosine and hence, it should decrease the rate of the recovery step inMg ATP.

Furthermore, the mutation also is supposed to demolish the post-hydrolytic interaction of Tyr-573 and Asn-475, which releases the tyrosine from its post-hydrolytic blocked state. This should mimic the recovery step in MgATP, if the phenylalanine is functional to some extent. Consequently, the rate of the lever arm movement in MgADP.P_i should be increased in the mutant.

By using Trp-501 fluorescence, we judged that the Y573F mutation does affect neither the pre-recovery nor the post-recovery structure of the lever arm, because both the MgADP and MgADP.AlF_4-bound states have the same fluorescence as the wild type. However, the equilibrium constant of the recovery step is so dramatically suppressed (K_{3a}=2.7 and <0.1 in M_{W501+} and M_{Y573F} respectively) as the steady-state fraction of M*MgATP can not be detected. Regardless of this fact, the amplitude of the burst of the hydrolytic Pi production in M_{Y573F} is equal with that of the wild type. Consequently the mutation also affects the equilibrium constant of the hydrolysis step (K_{3b}=0.55 and <5.7 in M_{W501+} and M_{Y573F}, respectively). The fact that the hydrolysis is also perturbed by the mutation supports the concept that Tyr-573 has a role in the nucleotide binding site in the post-recovery state. The lack of its hydroxyl group might influence the state of switch 2 or Asn-475, which push the equilibrium of the hydrolysis toward the M*MgADP.P_i state.

Unfortunately, the kinetics of the recovery step in MgATP cannot be investigated directly, since the equilibrium constant of the recovery step is too small. However, the fact that K_{3a} decreased almost 30 times in the mutant indicates that the ratio of the forward and reverse rate of the recovery step is dramatically changed ($K=k_{forward}/k_{reverse}$). We can only estimate the lower limit of the observed rate of the recovery step to be 6 s^{-1}, since this is the observed rate of the subsequent hydrolysis step. If the observed rate of the recovery step is 6 s^{-1}, the hydrolysis can be the faster

step. Since $k_{observed\ 3a}=k_{forward}+k_{reverse}>6s^{-1}$ and $K_{3a}=k_{forward}/k_{reverse}<0.1$ in M_{Y573F}, the lower limit of $k_{forward}$ and $k_{reverse}$ are 0.5 s^{-1} and 5.5 s^{-1}, respectively. However, if the recovery step is faster than the hydrolysis step, the dramatic reduction of K_{3a} is also able to decrease the observed rate of the hydrolysis step, as it was demonstrated previously (57), since $k_{observed\ hydrolysis}=K_{3a}/(1+K_{3a})xk_{3b+}+k_{3b-}$. An upper limit, however, for the observed rate of the recovery step cannot be determined. Furthermore, the turnover rate, so the rate of the reverse recovery step of the M_{Y573F} is increased 6 times compared to M_{W501+}, and K_4 is decreased.

Consequently, the mutation specifically perturbs the energetics of the recovery step and the hydrolysis step. However, the effect of the mutation on the rate of the recovery step cannot be determined, since the small K_{3a} does not allow the investigation of the kinetics of the recovery step. In spite of the perturbed energetics of the recovery step and hydrolysis steps is a good indication of the supposed action of the Tyr-573 (46), we cannot prove directly that the different behavior of Tyr-573 during the lever arm movement in MgATP and MgADP.P_i is what causes the large difference in the kinetics of the two steps.

According to the presented models, the maximization of the chance that actin rebinds to myosin having primed lever arm and MgADP.P_i in the nucleotide binding site is due to a complex bidirectional communication between the nucleotide binding site and the lever arm. First, the switch 2 closer is coupled to the priming of the lever arm. If the lever arm is primed, MgATP can be hydrolyzed, but hydrolysis affects the conformation of the switch 2 loop and its surroundings, which dramatically lowers the rate of the lever arm movement, in order to let actin bind back with a great chance to myosin being in the proper state.

The other consequence of the fact that the rate limiting step of the basal ATP-ase cycle of *Dictyostelium* myosin II is the reverse recovery step in MgADP.P_i is that, actin has to activate the rate of the lever arm movement during the actin activated ATP-ase cycle. Chapter 4 below presents our new model on this activation.

Chapter 4

Step 4 - Communication path from the actin binding region toward the lever arm

Introduction

In step 4 of the Lymn-Taylor model the weak-to-strong transition of actin binding (K_2 in scheme 8), leading to the strongly-bound rigor state (R-state in scheme 8) (19), induces the power stroke and the hydrolytic products release. Today, this step remains the less understood one. The exact sequence of the reaction steps and the structural changes are not unambiguous, because the mechanical events are not really integrated into the biochemical reaction steps (73).

The major conformational change that can be observed during the weak-to-strong transition of actin binding is the actin binding cleft closure between the lower and upper 50 kDa subdomains, as it was first proposed many years ago (70). The apo structure of myosin V performing closed cleft fits perfectly into the cryo-filtered electron microscopic envelop of the actin filament "decorated" with strongly bound myosin heads (36). Consequently, when the cleft is closed the acto-myosin interaction is strong (K_d<0.1 μM)

$$A + M(Nu) \underset{}{\overset{K_0\ K_1}{\rightleftharpoons}} AM^{A}(Nu) \overset{K_2}{\rightleftharpoons} AM^{R}(Nu)$$

Actin binding Weak-to-strong transition

Scheme 8. Kinetic scheme of actin binding (19).

and when it is opened the interaction is weak (K_d=50 μM). Since cleft movement is an equilibrium step (K_2 in Scheme 8), the equilibrium constant of this transition determines the actual actin affinity of myosin, which varies significantly in different nucleotides. If the acto-myosin interaction is strong, K_2 is pushed predominantly toward the R-state (K_2>100), such as in nucleotide absence, while in weak interaction (MgATP state) K_2 is absolutely pushed to the A-state (K2<<1) (19). In MgADP and MgADP.P_i K_2 is thought to be intermediate however, in case of MgADP.P_i the concepts are controversial (18, 46, 71).

Nevertheless, the apo structures suggest that cleft closure might be the consequence of the rotation of the upper 50 kDa subdomain, which is accompanied by the torsion of the core β-sheet (13, 71). The strands that carry switch 1 and 2 bear the greatest conformational change upon β-sheet twist, resulting in the opening of the nucleotide binding pocket (Figure 34) (13). As presented in Chapter 1, the equilibrium constant between the two states of switch 1 is strongly coupled with that of the actin binding cleft, explaining the nucleotide controlled acto-myosin interaction (41). Accordingly, the same coupling is responsible for the accelerated product release steps upon actin binding. The opening of switch 1 creates an exit route known as the "backdoor" for P_i release (83). Furthermore, switch 2 opening might be able to trigger the power stroke by pushing back the N-terminal end of the relay helix into its pre-recovery conformation, since the closer of switch 2 induces the priming of the lever

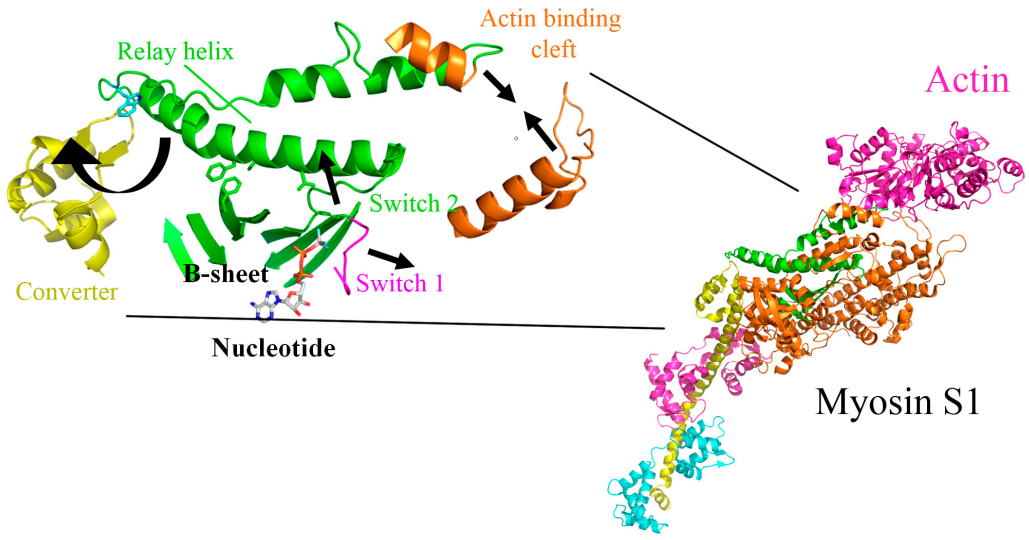

Figure 34. The presupposed conformational cascade during the weak-to-strong transition of actin binding to the myosin having primed lever arm. Actin binding cleft closure causes the torsion of the central B-sheet, especially those strands that carry switch 1 and switch 2, leading to the opening of the nucleotide binding site. While switch 1 opening is believed to result in the opening of the 'backdoor', leading to Pi release, switch 2 opening might induce the power stroke (13, 35).

arm (see Chapter 2). According to this structural model, the closing of the actin binding cleft opens the nucleotide binding pocket, which is likely to be followed by immediate P_i release, and at the same time the power stroke is also induced (37, 71, 81, 83). On the contrary, growing evidence from muscle fiber and single molecule experiments reveal that the power stroke happens first and then follows the P_i release step.

Many years ago, Huxley and Simmons found during their pioneering work that psoas muscle fibers respond to rapid length steps by a force-generating process with multi exponential decay. A fast phase (k_{obs}=1000s^{-1}) of this response (phase 2) was later identified as the power stroke of the actin-bound myosin (39, 53). Furthermore, a slower phase (phase 4) is found to be closely associated with P_i release step, as this step is the most sensitive to the presence of P_i (69). These findings make the basis of a recently produced kinetic model, stating that the power stroke is likely to precede the P_i release step (73, 74, 77, 85) (Scheme 9). However, direct evidence has not been found (15).

Nevertheless, the question arises, if the power stroke happens first and then the P_i release, how can actin trigger the power stroke without primary nucleotide binding site opening. The closed switch 1 and 2 are likely to be necessary to hold the P_i in the nucleotide binding site. And where does the conformational change, inducing the power stroke, come from? The response to this might reveal a direct communication pathway between the actin binding site and the relay helix.

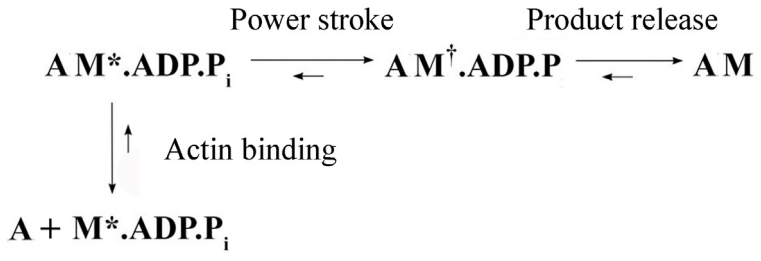

Scheme 9. Actin rebinding to myosin having primed lever arm (*), leading to the rigor acto-myosin complex (steps 3, 4 in the Lymn-Taylor model). † and * correspond to the low and high fluorescent states of Trp-501 and to the lever arm up and down states respectively. Muscle fiber and single molecule experiments reveal that the power stroke precedes P_i release in myosin II (74, 85).

Recently we found that the rate limiting step of the basal ATP-ase cycle of *Dictyostelium* myosin II is a lever arm swing in MgADP.P_i (the forward reaction of the reverse recovery step in Scheme 7 (27)) and not the P_i release step (37). Since the rate limiting step of the actin activated enzyme cycle is faster with two orders of magnitude, the rate of this lever arm

movement has to be accelerated by actin binding. But it is still a question how actin can accelerate the rate of the reverse recovery step in MgADP.P_i.

Aims

The integration of the mechanical step into the structural model is in contradiction with the muscle fiber kinetics (85). The weak-to-strong transition of actin binding can hardly induce the power stroke before P_i release according to the accepted structural models. However, our structural and kinetic understanding of the lever arm movement has improved in recent years (see Chapter 2 and (27)). These findings prompted us to reinvestigate the concept on actin activation in order to build a structural model that fits into the kinetic data derived from muscle fiber and single molecule experiments (74).

Results

A structural model for the activation of the power stroke

As it was presented in Chapter 2, a potential structural trajectory between the end states of the recovery step was composed by using computational simulation (16). In this transition the relay helix moves in a seesaw-like fashion, coupling switch 2 closure with the rotation of the lever-arm. When switch 2 closes, it pulls down the relay helix near to its N-terminal end through a hydrogen bond between Gly-457 and Asn-475 (Figure 20). The relay helix reacts as a seesaw, since it is supported at the middle, and its C-terminal end swings upwards.

By comparing the pre- and post-recovery structures, we found that when switch 2 closure pulls down the N-terminal region of the relay helix, the helix situated at the opposite side of the relay (in relation to switch 2) moves together with the relay helix (Figure 35). This helix is the N-terminal helix in the so-called helix-loop-helix motif, which is the main actin binding region of the lower 50 kDa subdomain (18). This helix is disrupted by an additional loop called proline-rich loop, which is the edge of the actin binding surface (36).

The relay helix and the N-terminal helix of the helix-loop-helix motif interact through extensive hydrophobic interactions (Figure 36, such as between Tyr-473/Ile-417, Glu-476/Ile-514). Those residues that transmit the movement between the two helixes are located half turn away from Asn-475 (Tyr-473, Lys-477). Consequently, certain parts of this helix, such as the prolin-rich loop move almost as much as the N-terminal of the relay helix at position 475 (1-1.5 Å) during the recovery step. The importance of the connection between the two helixes is revealed by the fact that the residues are highly conserved. Residues between the positions 475 and 478 (NEKL) are essential in all myosin isoforms, as are a couple of other conserved hydrophobic residues (Ile-514, Ile-517).

The coupled movement of the two helixes during the forward direction of the recovery step reveals that they might move together in the reverse direction as well. Consequently, in the post-recovery or pre-power stroke state a pull on the proline-rich loop from the opposite direction of switch 2 closure would be able to pull back the N-terminal segment of the relay helix to its pre-recovery position (Figure 36, red arrow), which is thought to lead to the rotation of the lever arm. The question arises whether actin binding is able to make the appropriate pull on the prolin-rich loop in order to accelerate the reverse recovery step.

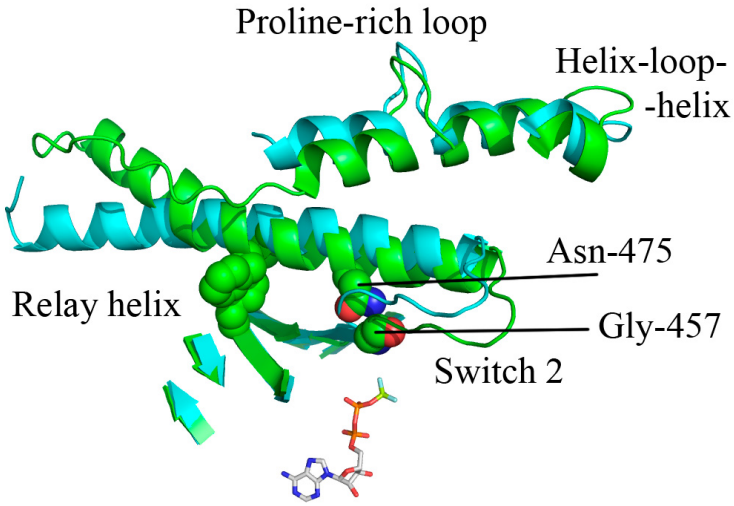

Figure 35. Pre- (blue) and post-recovery (green) structures of the relay region aligned to each other (PDB code: 1MMD and IVOM respectively). Switch 2 closure pulls done not just the N-terminal of the relay region during the recovery step but the first helix of the helix-loop-helix motif containing the proline-rich loop.

In order to investigate experimentally the role of the proline-rich loop in actin binding and in the activation of the rate of the lever arm movement, we introduced mutations into the M_{W501+} construct, which perturbed the role of the proline-rich loop. Since the majority of the mutational experiments in this project are not my own work, I wrote these results into the discussion section.

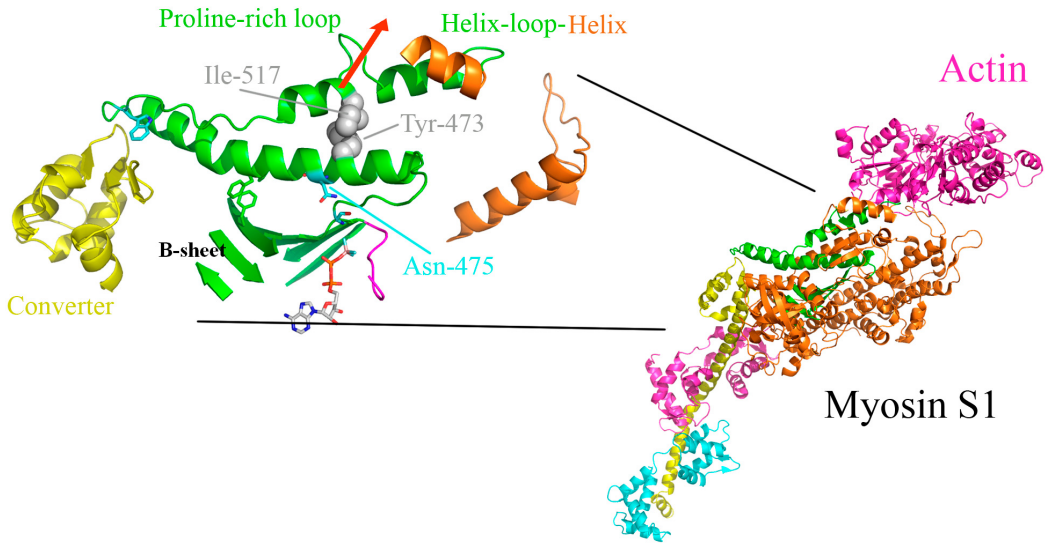

Figure 36. The activation of the power stroke through the proline-rich loop. A pull on the proline-rich loop from the direction opposite of switch 2 closure (red arrow) might lift back the relay helix N-terminal region into its pre-recovery position, leading to the power stroke. The proline-rich loop and the relay helix move together due to hydrophobic interactions, such as between Tyr-473-Ile-517.

Discussion

Growing evidence from muscle fiber and single molecule experiments show that the power stroke happens first in the force generating acto-myosin complex and the P_i release step only follows it (39, 73, 74, 85). However, the current structural model induces the power stroke through the opening of the nucleotide binding site (13, 71), which is likely to be coupled with immediate P_i release. Hence, our aim was to find a conformational change that induces the power stroke without primary nucleotide binding site opening. Consequently, this conformational change must be a direct communication pathway between the actin binding region and the lever arm.

Holmes *et al.* suggested that the central β-sheet torsion displaces the phenylalanine fulcrum of the relay helix at the third strand (numbering from the N-terminal subdomain) (see Chapter 2), thus allowing the relay helix to straighten and the lever arm to return to the pre-recovery position without primary switch 2 opening (22, 36). However, the β-sheet torsion of myosin V does not show any conformational change of this strand (13), and our experimental results show that the eliminated relay

fulcrum does not inhibit the actin activation of the lever arm movement (see Chapter 2 and (43)).

Alternatively, the opening of switch 1 and 2 is followed by a slow P_i release step and a much faster power stroke. This would manifest in an observed subsequent P_i release, although the nucleotide binding site opening occurs first and then the power stroke (76). In that case, the direct communication between the actin binding site and the lever arm is needless. However, from a totally opened nucleotide binding site P_i release is likely to be a diffusion-limited process, except if the P_i group is still buried and inhibited in its release. In spite of the fact that we still do not know the structure of the open nucleotide binding site in the acto-myosin complex, the opened switch 1 in the rigor-like structure creates an exit route for the P_i (83), contradicting this concept. Nevertheless, direct evidence for the order of the two steps and their relative rates has not been found.

Upon comparing the pre- and post-recovery structures of the *Dictyostelium* myosin II motor domain, we found that when switch 2 closes the helix-loop-helix motif, and particularly the proline-rich loop, move together with the N-terminal of the relay helix. We suppose that this proline-rich loop is the nearest actin binding site to the relay region (36) and an actin induced pull from the opposite direction of switch 2 closure on this loop can initiate the power stroke, without previous nucleotide binding site opening.

In order to investigate experimentally the role of the proline-rich loop in the activation of the lever arm movement, we made two mutant constructs in M_{W501+}. The prolin-rich loop seems to have two functional parts. These are a conserved positive charge at the tip of the loop on the one hand and at least 1 or 2 hydrophobic residues in it, depending on the myosin isoform, on the other hand. Based on this, we replaced the positive charge to a negative one in one construct (R520Q, M_{R520Q}) and we deleted the whole proline-rich loop in the other one (519-523, $M_{\Delta \text{ proline-rich loop}}$). We designed the later construct with great care by using protein homology modeling. The most important requirement was not to perturb the other actin binding regions of the helix-loop-helix motif, otherwise we could not have distinguished which effect can be assigned to which region. This mutant contains a continuous helix in place of the helix-breaking proline-rich loop according to the computational modeling.

Both constructs show very specific changes (experimental results not shown). The Trp-501 signal shows that the nucleotide binding steps and the lever arm

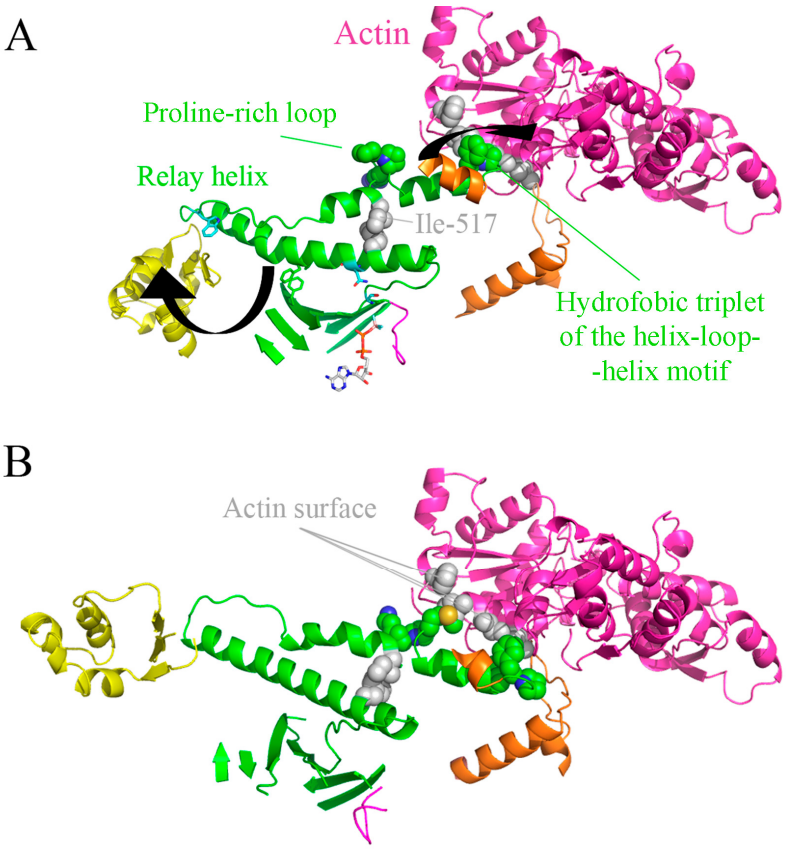

Figure 37. Computational docking structure of the weakly (**A**) and strongly (**B**) bound acto-myosin complex with open and closed actin binding cleft respectively. Figure **A** shows an illustration of the published structure (68) with *Dictyostelium* myosin II structure having primed lever arm and open actin binding cleft. Figure **B** shows the rigor acto-myosin structure of the chicken skeletal myosin II having closed actin binding cleft (36). During the transition from the structure presented in part A to that in B, the power stroke and the weak-to-strong transition of actin binding have to occur (black arrows). The proline-rich loop and the helix-loop-helix motif bind to the actin surface in a different position. In the weak binding complex a hydrophobic triplet (spacefill) in the loop region between the two helixes of the helix-loop-helix binds to hydrophobic residues (Ile-341, Ile-345) on actin surface 5 Å away from its binding site in the rigor complex (Ile-345, Leu-349).

movements in the absence of actin are not perturbed by the mutations. The lever arm can be primed like in the wild-type and the forward rate of the reverse recovery step in MgADP.P_i (the turnover rate) is also the same as that of the wild type. Furthermore, the mutations have some moderate effect on actin binding, proving that the proline-rich loop is a real actin binding loop. However, the mutations do not perturb the basic mechanism of actin binding. The main perturbation caused by the mutations is the total abolishment of the actin activation of the ATP-ase cycle. Since the actin activated turnover rate of the mutant is slower with at least two orders of magnitude than that of the M_{W501+}, this effect can not be explained by the small reduction in actin affinity, indicating that there must be a further function that is “knocked out”, confirming the supposed role for the prolin-rich loop.

Other results also support that the proline-rich loop is an actin binding site (36, 45, 67, 68). Myosin II structures having open and closed actin binding clefts were fitted onto the surface of three actin monomers by *in silico* rigid docking (36, 68). In spite of the fact that these docking experiments neglect the conformational changes derived from the interaction itself, they show us a possible binding surface for the weakly and strongly interacting complexes. Onishi and Morales found that the major difference between them is in the position of the lower 50 kDa subdomain on the first actin monomer however, the upper 50 kDa subdomain binds to the same region (68) (Figure 37). Since the primary actin binding site of the lower 50 kDa subdomain is the helix-loop-helix motif (510-546) (18), this region also changes its position on the actin surface. In the weak binding state, the edge of the helix-loop-helix motif binds 5 Å away from its position in the strongly interacting complex. Consequently, the interactions of the proline-rich loop also change during the weak-to-strong transition. In the weak binding complex the proline-rich loop interacts only with the N-terminal region of actin (68), but in the strong binding complex it is allowed to interact with hydrophobic residues on the actin surface (Ile-349, Phe-352). The interaction with the negatively charged N-terminal actin region is performed by Arg-520, while the hydrophobic side-chains of the proline-rich loop interact with the hydrophobic residues of the actin surface.

Due to the fact that the proline-rich loop and the relay helix move together, the conformational rearrangements of the actin binding region might induce a strain that lifts back the N-terminal segment of the relay region to its pre-recovery position, leading to the acceleration of the rate limiting reverse recovery step. Moreover, through the interaction of the Arg-520 and the N-terminal segment of actin, the relay helix might sense the presence of actin even in the weakly interacting complex. The R520Q mutation in itself abolishes the actin activation of the myosin ATP-ase cycle and a similar effect was found when an actin mutant without the interacting N-terminal region was used (63).

Accordingly, the direct communication between the actin binding region and the relay helix allows the acceleration of the rate of the reverse recovery step before P_i release, before or at the beginning of the reaction trajectory of the actin binding cleft closure. However, the intermediates of the transition are still not known.

Nevertheless, in MgADP.P_i the actin binding of myosin is thought to be a fast step but the acto-myosin interaction is weak (85). If the P_i release is a later event of

the actin activated ATP-ase cycle, the power stroke must happen through weakly interacting states. It is an interesting question, how the priming of the lever arm, the recovery step, happens detached from actin, but the power stroke occurs in actin-bound states, despite the fact that acto-myosin interaction in MgADP.P_i is as weak as in the MgATP-bound form. The answer to this question lies in kinetics. Scheme 10 shows the presupposed reaction mechanism of the second half of the ATP-ase cycle (27). The modeling of this mechanism shows that the predominant reaction flux happens through the actin-bound route, even at low actin concentration (5 μM), despite the weak acto-myosin interaction in MgADP.P_i (Kd=50 μM). This is a consequence of the slow lever arm movement in MgADP.P_i, which is activated by actin to a much faster step (from 0.05 s^{-1} to at least 4 s^{-1}). Consequently, the fast actin-bound reaction pathway empties the M*MgADP.P_i population before significant futile lever arm movement happens through the detached route. Thus, the answer to the question why the lever arm movement happens detached from actin in ATP, but attached in MgADP.P_i, is that the rate of the lever arm movement in MgADP.P_i is activated by actin, while in MgATP it is not (27).

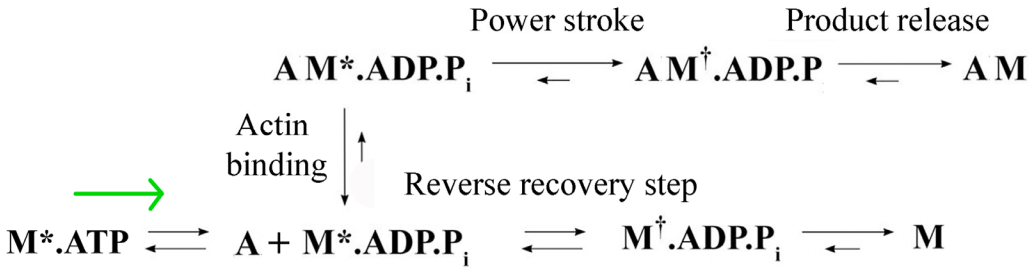

Scheme 10. Actin activated ATP-ase cycle of myosin II. † and * correspond to the low and high fluorescent states of Trp-501.

Final Conclusion

We used site-specific fluorescence signals placed in functional regions of *Dictyostelium* myosin II motor domain in combination with transient kinetic measurements. By the use of this technique we investigated the communication mechanisms of the nucleotide binding site, the actin binding region, and the lever arm of the myosin motor domain. These studies have a significant contribution to the understanding of the working of myosin. In this section it is presented how our results show the process of the ATP-ase cycle of myosin.

The starting process is the MgATP binding to the acto-myosin complex that, accompanied by a large free energy change, is driving forward the ATP-ase cycle (2). The first MgATP-induced conformational change is the open-closed transition of switch 1 loop in the nucleotide binding site (41). Since switch 1 loop is a hinge region between the lower and upper 50 kDa subdomains, its closure is coupled with the opening of the actin binding cleft, resulting in low actin affinity and acto-myosin dissociation (9, 33, 41, 71). The subsequent MgATP-induced conformational change is the open-closed transition of switch 2, which is coupled with the priming of the lever arm. This step is a fast equilibrium step (56). The conformational change of switch 2 closure is transmitted toward the lever arm by the seesaw-like movement of the relay helix, which is converted to a rotating movement by the converter domain (16, 43). Myosin with closed switch 2 is the catalytically active conformation, which inhibits the wasteful ATP hydrolysis without force generation (32). The hydrolysis must be accompanied by a conformational change, turning the lever arm movement in MgADP.P_i to a slow equilibrium step (27). However, the hydrolysis dependent

change of the nucleotide binding site is not really understood. The slow lever arm movement in MgADP.P_i allows actin to rebind to the myosin with primed lever arm (27). Since the acto-myosin interaction is a fast but weak process in MgADP.P_i, actin has to activate the rate of the ATP-ase cycle to make the actin-bound reaction path dominant (27). Since the rate limiting step is the forward direction of the reverse recovery step, actin has to activate the rate of the lever arm movement (27), but it has to do this without primary nucleotide binding site opening and P_i release (39, 73, 74, 85). This means that the power stroke has to be induced before the weak-to-strong transition of actin binding, which opens switch 1 loop (41). Consequently, a direct communication pathway is required between the actin binding region and the lever arm (43). Our results show that an actin-induced pull on the proline-rich loop is able to activate the rate of the lever arm movement without primary P_i release by lifting back the relay seesaw. The subsequent weak-to-strong transition of actin binding results in hydrolytic product release and the formation of the starting rigor acto-myosin complex (33).

Material and Methods

All chemical reagents were purchased from Sigma-Aldrich Chemical Co. (St. Louis, MO), except for the nucleotides (Roche Co., USA), the γ^{32}P-ATP (Izinta Ltd., Hungary), and the 3'-(N-methyl-anthraniloyl)-2'-deoxy-ATP (Jena Bioscience GmbH, Germany).

Protein engineering: All mutations were introduced into mutated forms of the *Dictyostelium discoideum* myosin II motor domain M761 cDNA fragment containing a C-terminal His-Tag (58). F239W (M_{W239+}) and F242W (M_{W242+}) mutations were introduced by megaprimer-based PCR strategy into the tryptophan null mutant M761 fragment (W36F, W432F, W501F, W584F) published previously (58). F481A,F482A, F652A, Y573F, R520Q, deletion of 519-523 (proline-rich loop deletion mutant) mutations were introduced into single tryptophan containing M_{W501+} (W36F, W432F, W584F) motor domain construct (58) with the same strategy. The mutant PCR products were ligated into pDXA-3H extrachromosomal shuttle vector containing one of the mentioned open reading frame of the M761 fragments (60). DH5 α *E. coli* strain was used to amplify the plasmids. Plasmids were isolated with QIAprep spin miniprep kit (Qiagen) and were electroporated into *Dictyostelium discoideum* AX2-ORF+ cells.

Protein expression and purification: AX2-ORF+ cells were cultured in 20 ml HL5 medium (ForMedium) containing 12.4 g/l glucose, 100 unit/ml penicillin, 0.1mg/ml streptomycin, and 15mg/l geneticin at 21 ˚C in cell culture dishes. Protein purification starts from 4 l 1x10^7 cell/ml cell culture, having grown for 1 weak in shacking incubator. Cells are harvested with 2700 rpm in a Beckman J2-MC centrifuge for 7 min and washed (140 mM NaCl, 2.7 mM KCl, 10.1 mM $Na_2HPO_4x7H_2O$, 18 mM KH_2PO_4, pH 7.3). Cells (40g) are lysated in 240 ml 50 mM Tis-HCl, 2 mM EDTA, 0.2 mM EGTA, 5 mM benzamidine, 40 μg/ml PMSF, 3 DTT, 0.3V/V% triton pH 8.0 by using an ultrasound sonicator for 10 min. After an 1 hour incubation on ice, the lysate is centrifuged with 50,000 rpm for 60 min at 4°C in a Beckman L7-65 Ultracentrifuge. Pellet is homogenized in 100 ml 50 mM HEPES pH 7.3, 30 mM K-acetate, 10 mM Mg-acetate, 5 mM benzamidine, and 40 μg/ml PMSF, and 3 mM β-mercaptoethanol. The received solution is centrifuged again with 50,000 rpm for 45 min at 4°C. Pellet is homogenized again in the previous buffer, but containing

additional 10 mM ATP and 10 mM $MgCl_2$ and centrifuged again with 50,000 rpm for 60 min at 4°C. The supernatant is purified by using His-tagged chromatography: loaded onto 15 ml Ni-NTA (Qiagen) column and washed with 50 ml 50 mM HEPES pH 7.3, 30 mM K-acetate, 3 mM β-mercaptoethanol, 5 mM benzamidine, 50 ml 50 mM HEPES pH 7.3, 300 mM K-acetate, 3 mM β-mercaptoethanol, 5 mM benzamidine, ~80 ml 50 mM imidazol in first washing buffer (the exact required volume is monitored with Bredford reagent). The elution is done with 0.5 M imidazol pH 7.3 with 3 mM β-mercaptoethanol, 5 mM benzamidine. Preparations were dialyzed against an assay buffer (40 Mm NaCl, 20 mM HEPES, pH 7.3, 2 mM MgCl and 2mM mercaptoethanol) in which most of the experiments were performed, otherwise noted. Actin preparation and pyrene labeling were done as described in (11, 82).

Steady-state fluorescence measurements were carried out with a Fluoromax Spex-320 fluorimeter equipped with a 150 W Xe lamp. The samples containing 3 μM motor domain constructs were excited at 295 nm with 2 nm bandwidth excitation and emission slits when tryptophan fluorescence was detected. The emission spectra of the fluorescence were detected in 310-420 nm range. During acrylamide quenching experiments the time courses of tryptophan fluorescence were detected at 340 nm and the 3 μM motor domains were titrated with acrylamide in a 0.05-0.4 mM concentration range. The optical settings were the same when ATP hydrolysis activities of the motor domain constructs were measured following Trp fluorescence change: the running out of the five fold molar excess ATP decreases the fluorescence. If a mutant construct has the same fluorescence level when MgATP or MgADP binds to it, its activity was measured with pyruvate kinase (PK) lactate dehydrogenase (LDH) coupled assay described in the next paragraph. The temperature dependence of the fluorescence detected at 340 nm was measured by heating the sample from 6°C to 26°C and the recorded fluorescence intensities were assigned to discreet temperature values. ADP.AlF_4 and ADP.BeF_x substrates were done by mixing the motor domain with 0.1 mM MgADP, 4 mM NaF, and 0.1 mM $BeCl_2$ or $AlCl_3$.

Actin activated ATP-ase activities were determined by using pyruvate kinase (PK) lactate dehydrogenase (LDH) coupled assay. 2% LDH/PK, 1mM PEP, 1mM ATP, 200 μM NADH was mixed with the 0.5 μM motor domain construct and titrated with

actin up to 100 μM in a buffer containing 5mM HEPES pH 7.2, 1 mM MgCl, 1 mM KCl. The absorbance change was detected at 340 nm (decreasing NADH) in a Shimadzu UV-2101 PC photometer.

Stopped-flow measurements were carried out on a BioLogic SFM-300/400 (BioLogic SAS, France) or on a KinTek SF-2004 (KinTec Corporation, USA) stopped-flow fluorimeter, equipped with 150 W Super-quiet Hg-Xe lamps (Hamamatsu Photonics, UK). Tryptophan was excited at 297 nm, where mercury lamps have an emission peak. Slits were 4 nm and a 340 nm interference filter (Corion CFS-001999 9L134) was used on the emission side. Pyrene was excited at 365 nm, the emission was detected through a WG420 cut-off filter (Comar Instruments, UK). Light scattering was measured at 340 nm. Mant-nucleotide was also excited at 365 nm and fluorescence was detected through the WG420 cut-off filter. During chasing experiment the mant-ADP (10 μM) preincubated with myosin was chased with ATP (1 mM). The dead time of the BioLogic stopped-flow is 0.2 and 2 ms if the μFC-08 and the FC-15 cuvette is used, respectively, and that of the KinTec SF-2004 was determined to be 1ms, at 18ml/s flow-rate. All concentrations noted are post-mix concentrations, and all experiments were carried out at 20 °C, unless otherwise stated.

Temperature-jump/stopped-flow measurements were carried out by using a temperature-jump accessory for a BioLogic SFM-300/400 stopped-flow (BioLogic SAS, France). 5 μM motor domain solution kept at 20 ˚C was mixed with hot ATP solution and Trp-501 fluorescence was measured at different temperatures up to 55 ˚C. The amplitude of the signal change lost in the dead time was determined by measuring the fluorescence level of the “apo” solution at each temperature. The principles of the method are described in the Appendix and in (42).

Temperature-jump experiments were carried out by using a TJ-64 System (Hi-Tech Scientific, Salisbury, U.K.) as in (56), but fluorescence was detected through the 340 nm interference filter.

Quench-flow experiments were carried out by using γ^{32}P-ATP radioactive nucleotide as a signal for the hydrolytic activity on a RQF-3 quench-flow apparatus (KinTec Corporation, USA). The ATP was applied in 5-10 fold molar excess in multiple

turnover experiments, and the hydrolyzed Pi was separated from the nucleotide by using coal solution as it is described in (86). The radioactivity of the γ^{32}P hydrolytic product was measured with a Wallac 1409 Liquid Scintillation Counter (PerkinElmer, Inc, USA). The indicated concentrations are post-mix concentrations.

Molecular dynamics simulations: InsightII 2000 software was used for generating the missing parts of 1MMD pre-recovery *Dictyostelium* myosin II motor domain structure. ADP.BeF_x was replaced with ATP by changing the BeF_x to Pi group. By averaging the coordinates of 125 structures picked up at each 2 ps time point of the equilibrium phase of the simulation, we visualized a relaxed conformation. For the post-recovery state, Jon Kull's unpublished structure was used which has exactly the same conformation as 1VOM, but contains all the residues. The BeF_x was also replaced by a Pi group. Mutations F481A, F482A, or F652A were introduced into these structures and further molecular dynamics simulation were done in the same way. Constant volume periodic boundaries were used with the box dimensions of 134.7 Å. Then the structures were solvated by TIP3P water with 12 Å cut-off value. Finally, the system was mechanically minimized with parm03 parameters and equilibrated for 2ns at 300 K by SHAKE algorithm with 2 fs time steps in AMBER9 program. Temperature control parameters were set up based on Berendsen's method. We determined the amplitude (δ) of the torsional mobility of the Φ, Ψ angles according to

$$\delta = \sqrt{\frac{\sum (x - \bar{x})^2}{n - 1}}$$

, where x is the actual torsion angle, $\bar{x}$ the average of all the Φ or Ψ angles of the given residue, and n the number of data points. The experiments were repeated three times and averaged, each based on 125 collected structures picked up at each 2 ps time point from 250 ps-long equilibrium phases.

Appendix

Temperature-jump/stopped-flow

The own-developed temperature-jump/stopped-flow apparatus allows us to study fast enzyme reactions at high temperatures, even above the denaturation temperature of the enzyme (42). The temperature-jump/stopped-flow apparatus is a redesigned conventional stopped-flow that is able to increase the temperature of the sample even by 60ºC on the submillisecond time scale during the mixing of the reactants. With this technique the kinetics of the enzyme reactions, which are faster than the denaturation process, can be investigated. In addition, it allows us to investigate the kinetics of many human enzymes at our physiological temperature which are instable in solution at 37 ˚C. Furthermore, it allows us to study the progress of heat-induced protein unfolding, which was impossible until now in case of fast denaturation processes.

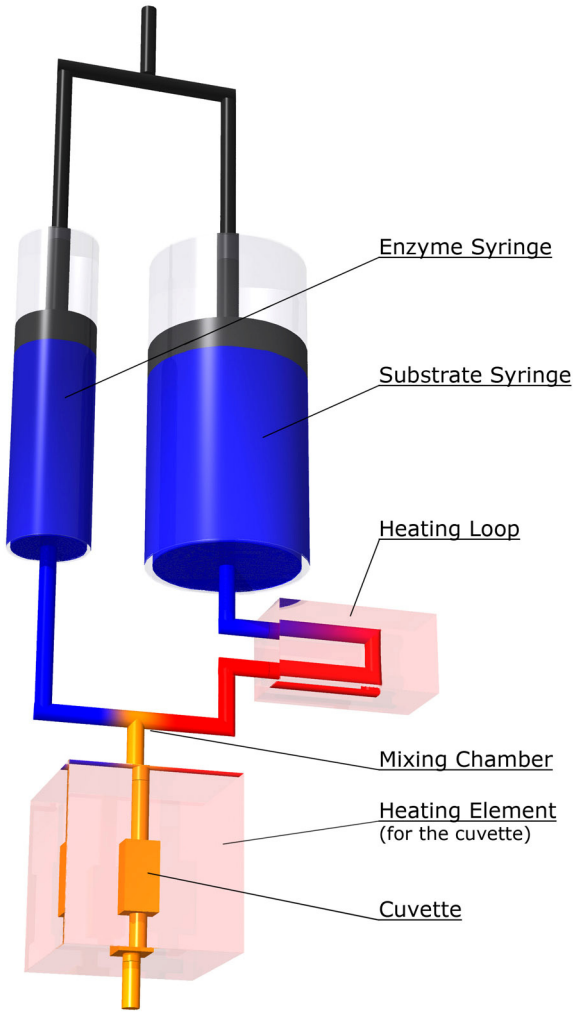

Appendix figure 1. Schematic view of the temperature-jump/stopped-flow instrument. The colors indicate the temperature of the solution inside the instrument.

Principle of the temperature-jump/stopped-flow

In a stopped-flow instrument the progression of a reaction can be observed through an optical signal. The reactants are rapidly pushed from two syringes (A and B) into a small mixing chamber from which the reaction mixture flows into the observation cuvette. While the reaction mixture reaches the cuvette, the progression of the reaction cannot be detected typically for 0.5-

1 ms, being the dead time of the instrument. In a conventional stopped-flow the syringes and the cuvette house are kept on the same temperature by a water circulator. In that case the applied experimental temperature range is limited by the temperature sensitivity of the reactants. The *temperature-jump/stopped-flow* apparatus oversteps this limitation. Appendix figure 1 shows the schematic view of the instrument. The enzyme (syringe A) and its substrate (syringe B) are stored at native temperature by using water bath temperature control. The temperature of the cuvette can be adjusted by an additional heating element in a wide temperature range (5-80 ˚C). Furthermore, a second heating element is inserted between the substrate syringe (syringe B) and the mixing chamber. This heating element is able to increase the temperature of the substrate solution even to a higher temperature than the temperature of the cuvette (note that the substrate must be non-heat-sensitive). Accordingly, when the reactants are pushed to the cuvette, a cold enzyme solution (syringe A) can be mixed with a high-temperature substrate solution (syringe B), resulting in an immediate temperature increase for the enzyme solution (temperature-jump). The temperature of the cuvette is adjusted to the temperature of the developing temperature of the reaction mixture, in order to keep the reaction mixture at a constant temperature during the reaction. Since the mixing of the reactant solutions yields the temperature jump, the dead time of the stopped-flow remains around 1 ms.

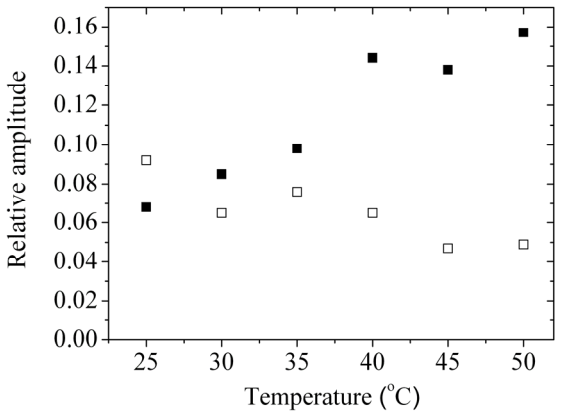

Appendix Figure 2. Temperature dependence of the amplitudes of the two phases of the M_{W501+} fluorescence enhancement upon the reaction with MgATP. The fast phase (■) is the recovery step, the slow phase (□) corresponds to the hydrolysis step. The measurement of the reaction at extreme temperatures was allowed by the temperature-jump/stopped-flow instrument

The reaction of M_{W501+} and MgATP above the denaturation temperature of the myosin

By the use of the temperature-jump/stopped-flow instrument, the reaction of M_{W501+} and MgATP was measured between 20 and 55 ˚C. The fluorescence increase has two phases at every temperature. The signal change lost in the dead time of the instrument was determined by measuring the fluorescence level of the apo M_{W501+} at each temperature. Thus the

relative amplitude of the two phases can be determined (Appendix figure 2). The higher the temperature, the bigger the relative amplitude of the fast phase corresponding to the recovery step. This confirms the finding that the fluorescence increase of M_{W501+} has two phases at 20 ˚C. Consequently K_{3a} was underestimated previously (58).

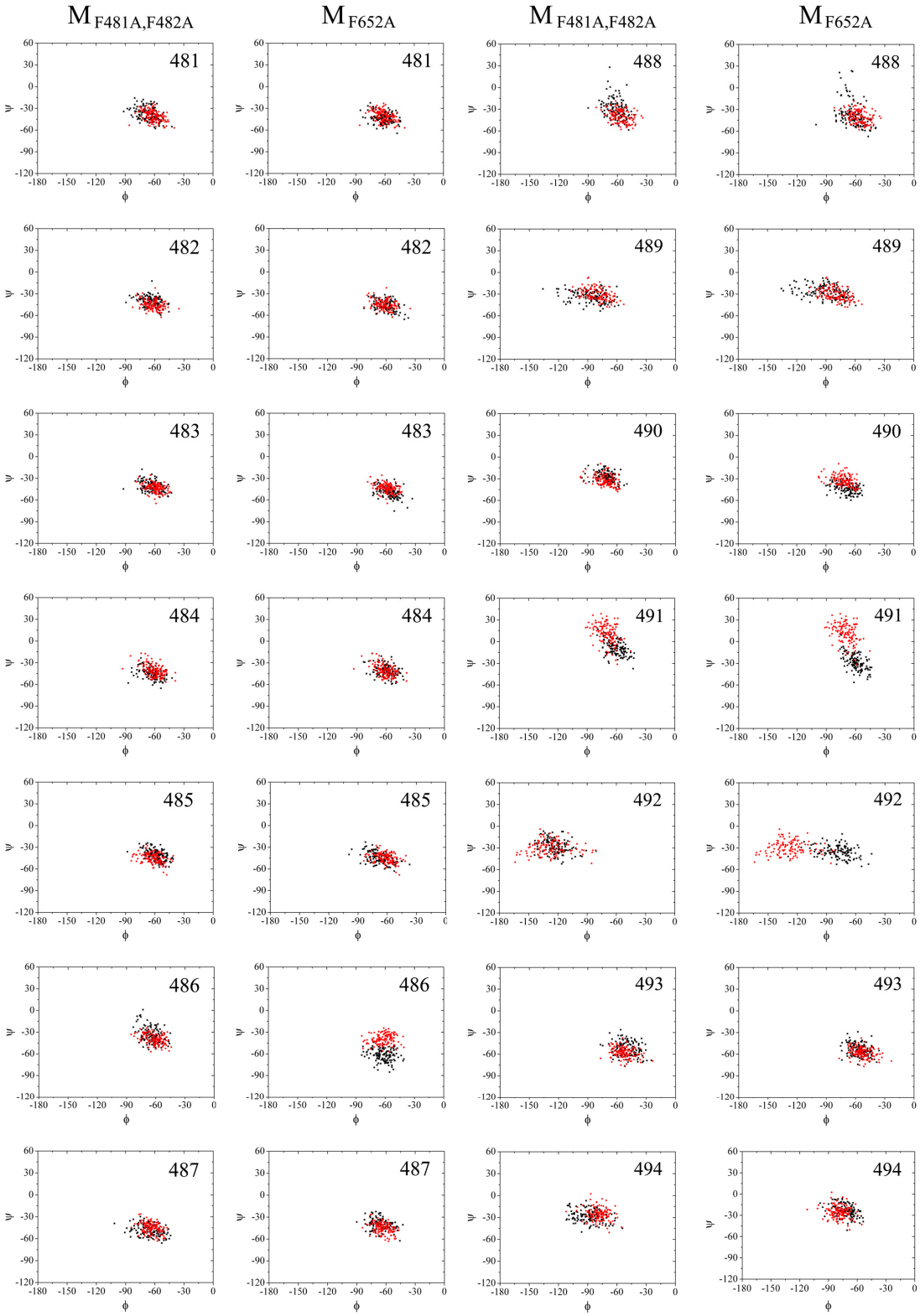

Appendix Figure 3. Ramachandran plots of the relay helix residues in the pre-recovery structures of $M_{F481A,F482A}$ and M_{F652A} (black) compared to that of the wild type (red). The Φ, Ψ angles belong to 125 collected structures picked up at each 2 ps time point from the 250 ps-long equilibrium phases of the molecular dynamic simulations.

Tables

Table 1. Kinetic data of nucleotide binding of M_{239+} and M_{242+}
Rate constants of nucleotide binding of M_{W239+} in the presence and absence of Mg^{2+} based on stopped-flow experiments. k_{on} were determined from the slope of the initial linear part of the plots of k_{obs} versus ligand concentration. $k_{induced\ fit}$ are the maximum observed rate constants from the hyperbole fitting of the same plots. k_{off} are determined from the intercepts of the initial linear part of the plots.

ligand	rate constant	M_{W239+}			M_{W242+}	Wild type*
		20 °C	12 °C	5 °C	5 °C	20 °C
MgATP	k_{on} ($\mu M^{-1}s^{-1}$)	1.4	-	0.87	2.1	0.66
	$k_{induced\ fit}$ (s^{-1})	1100	-	450	400	-
MgADP	k_{on} ($\mu M^{-1}s^{-1}$)	3.9.	4.1	3.4	0.82	1.4
	$k_{induced\ fit}$ (s^{-1})	>>1000	1000-1500	800	300	400
	k_{off} (s^{-1})	-	30	10	41	7.9
	K_D (μM)	-	7.3	2.9	50	5.6
	$K_{iso,observed}$	-	55	32	-	-
ADP	k_{on} ($\mu M^{-1}s^{-1}$)	12	-	-	-	-
	$k_{induced\ fit}$ (s^{-1})	>>1000	-	-	-	-
	k_{off} (s^{-1})	50	-	-	-	-
	K_D (μM)	4.2	-	-	-	-

* published in (58)

Table 2. Elementally rate constants of switch 1 isomerization and that of the MgADP binding to M_{W239+}.

rate constant	Data analysed	20°C	12°C	5°C
$k_{iso\ switch\ 1,\ forward}$ (s^{-1})	Mg^{2+} binding/ dissociation	20	6	≈1
$k_{iso\ switch\ 1,\ backward}$ (s^{-1})		29	18	12
$K_{iso\ switch\ 1}$		0.7	0.3	≈0.1
$k_{iso\ switch\ 1,\ forward}$ (s^{-1})	MgADP binding	-	23	3
$k_{iso\ switch\ 1,\ backward}$ (s^{-1})		-	32	29
k_{1on} ($\mu M^{-1}s^{-1}$)		3.8	3.5	3.3
k_{2on} ($\mu M^{-1}s^{-1}$)		2.7	0.57	≈0.15

Table 3. Switch 1 fluorescence states assigned to structural states.

Relative fluorescence intensities of Trp-239	Ligands bound to myosin	Structural states	Nomenclature
High fluorescence (*M): 113% (360 nm *)	Actin and/or MgADP	1W7I	-Weak ADP-bound state -Open switch 1
Intermediate fluorescence (M): 100% (350 nm)	None (Apo state)	1W8J, 1Q5G	Apo
Low fluorescence (†M): 63% (340 nm)	-Nucleotides or analog in which the γ-phosphate site is occupied (ATP, ADP.Pi, AMP.PNP) - MgADP	1W7J, 1MMA, 1MMD, 1MMG, 1MMN, 1MND, 1MNE, 1VOM	-Closed switch 1
Lowest fluorescence (††M): 55% (349 nm)	Mg^{2+}-free ADP		

Table 4 Stern-Volmer constants of the acrylamide quenching experiments of 3µM M_{W501+}, $M_{F481A,F482A}$, and M_{F652A}. They were titrated with up to 0.4 M acrylamide in the absence and presence of different nucleotides at 20 °C (Supplemental Figure 2). In M_{W501+} the difference in the Stern-Volmer constants of the up ($MgADP.AlF_4$) and the down (MgADP) lever arm states is significantly larger than the mutants'.

	Stern-Volmer constant (M^{-1})		
Nucleotide	**M_{W501+}**	**$M_{F481A,F482A}$**	**M_{F652A}**
none	4.11 ± 0.09	4.10 ± 0.08	3.77 ± 0.08
ADP	3.73 ± 0.07	3.70 ± 0.08	3.34 ± 0.12
ATP	3.20 ± 0.08	3.74 ± 0.08	3.26 ± 0.10
$ADP.AlF_4$	2.98 ± 0.04	3.58 ± 0.07	3.15 ± 0.07

Table 5 Rate constants and equilibrium constants of some reaction steps in Scheme 1 of M_{W501+}, $M_{F481A,F482A}$, and M_{F652A}. K_{3a}=M*.ATP/M†.ATP and K_{3b}=M*.ADP.P_i/M*.ATP were calculated from the amplitude of the P_i burst ($^{apparent}K_{hydrolysis}$=M*.ADP.$P_i$/(M†.ATP+M*.ATP)) and the amplitude of the fluorescence enhancement upon ATP binding ($^{apparent}K_{recovery\ step}$=(M*.ATP+M*.ADP.$P_i$)/M†ATP and M*.ATP=M*$_{(total)}$-M*.ADP.$P_i$). All parameters were measured at 20 °C, otherwise stated.

Parameters of Scheme 1	Nucleotide	M_{W501+}	$M_{F481A,F482A}$	M_{F652A}
K_1k_{+2} ($\mu M^{-1}s^{-1}$)	MgADP	1.50	0.33	0.30
k_{+6} (s^{-1})	Mg mant-ADP	3.5	0.36	0.4
K_1k_{+2} ($\mu M^{-1}s^{-1}$) (6 °C)	MgATP	0.80	0.15	0.13
k_{+2} (s^{-1}) (6 °C)		400	170	126
$^{app}K_{recovery\ step}$		5.25	0.27	0.14
$^{app}K_{hydrolysis}$		0.43	0.11	0.05
$K_{3a\ (recovery\ step)}$		2.7	0.14	0.09
$K_{3b\ (hydrolysis)}$		0.55	0.91	0.66
$k_{observed\ hydrolysis}$ (s^{-1})		25.0	5.3	2.2
k_{4+} (s^{-1})		0.05	0.14	0.07

Table 6 Kinetic and thermodynamic parameters of the actin-myosin interaction and actin activation of M_{W501+}, $M_{F481A,F482A}$, and M_{F652A}. Data signed with * are published in (28).

experiment	parameter	M_{W501+}	$M_{F481A,F482A}$	M_{F652A}
ATP induced actin-myosin dissociation	K_1k_{+2} ($\mu M^{-1}s^{-1}$) of ATP	0.18	1.3	1.5
	k_{max} (s^{-1})	121	600	700
Actin binding	k_{+A} ($\mu M^{-1}s^{-1}$)	1.60 ± 0.04*	0.41 ± 0.05	0.61 ± 0.04
	k_{-A} (s^{-1})	0.047 ± 0.002*	0.14 ± 0.01	0.1 ± 0.03
	$K_{d,A}$ (μM)	0.03*	0.34	0.16
	k_{+DA} ($M^{-1}s^{-1}$)	0.22 ± 0.02*	0.07 ± 0.002	0.12 ±
	k_{-DA} (s^{-1})	0.027 ± 0.002*	0.11 ± 0.003	0.108 ± 0.008
	$K_{d,DA}$ (μM)	0.12*	1.57	0.90
Actin-activated ATP-ase activity	v_{max} (s^{-1})	3.8	1.2	1.2
	K_M (μM)	67	61	98

Table 7.

Table 7 Rate constants and equilibrium constants of some reaction steps in Scheme 1 of $\mathbf{M_{W501+}}$ and $\mathbf{M_{Y573F}}$. K_{3a}=M*.ATP/M†.ATP and K_{3b}=M*.ADP.P_i/M*.ATP were calculated from the amplitude of the P_i burst ($^{apparent}K_{hydrolysis}$=M*.ADP.$P_i$/(M†.ATP+M*.ATP)) and the amplitude of the fluorescence enhancement upon ATP binding ($^{apparent}K_{recovery\ step}$=(M*.ATP+M*.ADP.$P_i$)/M†ATP and M*.ATP=M*$_{(total)}$-M*.ADP.$P_i$). All parameters were measured at 20 °C.

Parameters of Scheme 1	Nucleotide	$\mathbf{M_{W501+}}$	$\mathbf{M_{Y573F}}$
K_1k_{+2} ($\mu M^{-1}s^{-1}$)	MgADP	1.50	1.7
k_{+6} (s^{-1})		5	2.5
$^{app}K_{recovery\ step}$		5.25	0.68
$^{app}K_{hydrolysis}$		0.43	0.4
$K_{3a\ (recovery\ step)}$		2.7	<0.1
$K_{3b\ (hydrolysis)}$		0.55	>5.7
$k_{observed\ hydrolysis}$ (s^{-1})		25.0	6
k_{4+} (s^{-1})		0.05	0.28

Abbreviations

A	actin
Ala, A	alanine amino acid
Asn, N	asparagine amino acid
Arg, R	arginine amino acid
ATP-ase	adenosine 5’ triphosphatase
EDTA	ethylene diamine tetraacetic acid
EGTA	ethylene glycol tetraacetic acid
Glu, E	glutamate amino acid
GPCRs	G-protein-coupled receptors
HEPES	4-(2-hydroxyethyl)-1-piperazineethanesulfonic acid
M	myosin
MgADP	magnesium adenosine 5’ diphosphate
MgADP.P_i	magnesium adenosine 5’ diphosphate and inorganic phosphate
MgATP	magnesium adenosine 5’ triphosphate
MgGDP	magnesium guanosine 5’ diphosphate
MgGTP	magnesium guanosine 5’ triphosphate
mant-	N-methyl anthraniloyl
NADH	nicotin amide adenine dinucleotide
NTP-ase	nucleoside triphosphatase
obs	observed
P_i	inorganic phosphate group
PEP	phosphoenol pyruvate
Phe, F	phenylalanine amino acid
PK/LDH	pyruvate kinase / lactate dehydrogenase
Tyr, Y	tyrosine
Trp, W	tryptophan

References

1. Bagshaw, C. R., J. F. Eccleston, F. Eckstein, R. S. Goody, H. Gutfreund, and D. R. Trentham. 1974. The magnesium ion-dependent adenosine triphosphatase of myosin. Two-step processes of adenosine triphosphate association and adenosine diphosphate dissociation. Biochem. J. 141: 351-364.

2. Bagshaw, C. R., and D. R. Trentham. 1974. The characterization of myosin-product complexes and of product-release steps during the magnesium ion-dependent adenosine triphosphatase reaction. Biochem. J. 141: 331-349.

3. Baker, J. P., and M. A. Titus. 1998. Myosins: matching functions with motors. Curr. Opin. Cell Biol. 10: 80-86.

4. Balint, M., F. A. Sreter, I. Wolf, B. Nagy, and J. GERGELY. 1975. The substructure of heavy meromyosin. The effect of Ca2+ and Mg2+ on the tryptic fragmentation of heavy meromyosin. J. Biol. Chem. 250: 6168-6177.

5. Banga I., Erdõs T., Gerendás M, Mommaerts W.F.H.M., Straub F.B., and Szent-Györgyi A. 1941. Myosin and Muscular Contraction.

6. Bauer, C. B., H. M. Holden, J. B. Thoden, R. Smith, and I. Rayment. 2000. X-ray structures of the apo and MgATP-bound states of Dictyostelium discoideum myosin motor domain. J. Biol. Chem. 275: 38494-38499.

7. Choi, I. G., and S. H. Kim. 2006. Evolution of protein structural classes and protein sequence families. Proc. Natl. Acad. Sci. U. S. A 103: 14056-14061.

8. Collins, F. S., and A. D. Barker. 2007. Mapping the cancer genome. Pinpointing the genes involved in cancer will help chart a new course across the complex landscape of human malignancies. Sci. Am. 296: 50-57.

9. Conibear, P. B., C. R. Bagshaw, P. G. Fajer, M. Kovacs, and A. Malnasi-Csizmadia. 2003. Myosin cleft movement and its coupling to actomyosin dissociation. Nat. Struct. Biol. 10: 831-835.

10. Conibear, P. B., A. Malnasi-Csizmadia, and C. R. Bagshaw. 2004. The effect of F-actin on the relay helix position of myosin II, as revealed by tryptophan fluorescence, and its implications for mechanochemical coupling. Biochemistry 43: 15404-15417.

11. Cooper, J. A., S. B. Walker, and T. D. Pollard. 1983. Pyrene actin: documentation of the validity of a sensitive assay for actin polymerization. J. Muscle Res. Cell Motil. 4: 253-262.

12. Coureux, P. D., H. L. Sweeney, and A. Houdusse. 2004. Three myosin V structures delineate essential features of chemo-mechanical transduction. EMBO J. 23: 4527-4537.

13. Coureux, P. D., A. L. Wells, J. Menetrey, C. M. Yengo, C. A. Morris, H. L. Sweeney, and A. Houdusse. 2003. A structural state of the myosin V motor without bound nucleotide. Nature 425: 419-423.

14. Cremo, C. R., and M. A. Geeves. 1998. Interaction of actin and ADP with the head domain of smooth muscle myosin: implications for strain-dependent ADP release in smooth muscle. Biochemistry 37: 1969-1978.

15. Davis, J. S., and N. D. Epstein. 2007. Mechanism of tension generation in muscle: an analysis of the forward and reverse rate constants. Biophys. J 92: 2865-2874.

16. Fischer, S., B. Windshugel, D. Horak, K. C. Holmes, and J. C. Smith. 2005. Structural mechanism of the recovery stroke in the myosin molecular motor. Proc. Natl. Acad. Sci. U. S. A 102: 6873-6878.

17. Fisher, A. J., C. A. Smith, J. B. Thoden, R. Smith, K. Sutoh, H. M. Holden, and I. Rayment. 1995. X-ray structures of the myosin motor domain of Dictyostelium discoideum complexed with MgADP.BeFx and MgADP.AlF4-. Biochemistry 34: 8960-8972.

18. Geeves, M. A., R. Fedorov, and D. J. Manstein. 2005. Molecular mechanism of actomyosin-based motility. Cell Mol. Life Sci. 62: 1462-1477.

19. Geeves, M. A., R. S. Goody, and H. Gutfreund. 1984. Kinetics of acto-S1 interaction as a guide to a model for the crossbridge cycle. J Muscle Res. Cell Motil. 5: 351-361.

20. Geeves, M. A., and K. C. Holmes. 1999. Structural mechanism of muscle contraction. Annu. Rev. Biochem. 68: 687-728.

21. Geeves, M. A., and K. C. Holmes. 1999. Structural mechanism of muscle contraction. Annu. Rev. Biochem. 68: 687-728.

22. Geeves, M. A., and K. C. Holmes. 2005. The molecular mechanism of muscle contraction. Adv. Protein Chem. 71: 161-193.

23. GERGELY, J., M. A. GOUVEA, and D. KARIBIAN. 1955. Fragmentation of myosin by chymotrypsin. J. Biol. Chem. 212: 165-177.

24. Geyer, M., T. Schweins, C. Herrmann, T. Prisner, A. Wittinghofer, and H. R. Kalbitzer. 1996. Conformational transitions in p21ras and in its complexes with the effector protein Raf-RBD and the GTPase activating protein GAP. Biochemistry 35: 10308-10320.

25. Goody, R. S., and W. Hofmann-Goody. 2002. Exchange factors, effectors, GAPs and motor proteins: common thermodynamic and kinetic principles for different functions. Eur. Biophys. J 31: 268-274.

26. Gulick, A. M., C. B. Bauer, J. B. Thoden, and I. Rayment. 1997. X-ray structures of the MgADP, MgATPgammaS, and MgAMPPNP complexes of

the Dictyostelium discoideum myosin motor domain. Biochemistry 36: 11619-11628.

27. Gyimesi, M., B. Kintses, A. Bodor, A. Perczel, S. Fischer, C. R. Bagshaw, and A. Malnasi-Csizmadia. 2008. The mechanism of the reverse recovery-step, phosphate release, and actin activation of Dictyostelium myosin II. J. Biol. Chem.

28. Gyimesi, M., A. K. Tsaturyan, M. S. Kellermayer, and A. Malnasi-Csizmadia. 2008. Kinetic characterization of the function of myosin loop 4 in the actin-myosin interaction. Biochemistry 47: 283-291.

29. Hannemann, D. E., W. Cao, A. O. Olivares, J. P. Robblee, and E. M. De La Cruz. 2005. Magnesium, ADP, and actin binding linkage of myosin V: evidence for multiple myosin V-ADP and actomyosin V-ADP states. Biochemistry 44: 8826-8840.

30. Harris, M. J., and H. J. Woo. 2008. Energetics of subdomain movements and fluorescence probe solvation environment change in ATP-bound myosin. Eur. Biophys. J.

31. Ho, B. K., A. Thomas, and R. Brasseur. 2003. Revisiting the Ramachandran plot: hard-sphere repulsion, electrostatics, and H-bonding in the alpha-helix. Protein Sci. 12: 2508-2522.

32. Holmes, K. C. 1997. The swinging lever-arm hypothesis of muscle contraction. Curr. Biol. 7: R112-R118.

33. Holmes, K. C., I. Angert, F. J. Kull, W. Jahn, and R. R. Schroder. 2003. Electron cryo-microscopy shows how strong binding of myosin to actin releases nucleotide. Nature 425: 423-427.

34. Holmes, K. C., and M. A. Geeves. 2000. The structural basis of muscle contraction. Philos. Trans. R. Soc. Lond B Biol. Sci. 355: 419-431.

35. Holmes, K. C., and R. R. Schroder. 2003. Switch 1 opens on strong binding to actin. Molecular and cellular aspects of muscle contraction. Adv. Exp. Med. Biol. 538: 159-166.

36. Holmes, K. C., R. R. Schroder, H. L. Sweeney, and A. Houdusse. 2004. The structure of the rigor complex and its implications for the power stroke. Philos. Trans. R. Soc. Lond B Biol. Sci. 359: 1819-1828.

37. Houdusse, A., and H. L. Sweeney. 2001. Myosin motors: missing structures and hidden springs. Curr. Opin. Struct. Biol 11: 182-194.

38. Huxley, H. E. 1969. The mechanism of muscular contraction. Science 164: 1356-1365.

39. Irving, M., V. Lombardi, G. Piazzesi, and M. A. Ferenczi. 1992. Myosin head movements are synchronous with the elementary force-generating process in muscle. Nature 357: 156-158.

40. Itzen, A., O. Pylypenko, R. S. Goody, K. Alexandrov, and A. Rak. 2006. Nucleotide exchange via local protein unfolding--structure of Rab8 in complex with MSS4. EMBO J 25: 1445-1455.

41. Kintses, B., M. Gyimesi, D. S. Pearson, M. A. Geeves, W. Zeng, C. R. Bagshaw, and A. Malnasi-Csizmadia. 2007. Reversible movement of switch 1 loop of myosin determines actin interaction. EMBO J. 26: 265-274.

42. Kintses, B., Z. Simon, M. Gyimesi, J. Toth, B. Jelinek, C. Niedetzky, M. Kovacs, and A. Malnasi-Csizmadia. 2006. Enzyme kinetics above denaturation temperature: a temperature-jump/stopped-flow apparatus. Biophys. J. 91: 4605-4610.

43. Kintses, B., Z. Yang, and A. Malnasi-Csizmadia. 2008. Experimental investigation of the seesaw mechanism of the relay region that moves the myosin lever arm. J Biol Chem.

44. Klebe, C., H. Prinz, A. Wittinghofer, and R. S. Goody. 1995. The kinetic mechanism of Ran--nucleotide exchange catalyzed by RCC1. Biochemistry 34: 12543-12552.

45. Kojima, S., K. Konishi, K. Katoh, K. Fujiwara, H. M. Martinez, M. F. Morales, and H. Onishi. 2001. Functional roles of ionic and hydrophobic surface loops in smooth muscle myosin: their interactions with actin. Biochemistry 40: 657-664.

46. Koppole, S., J. C. Smith, and S. Fischer. 2006. Simulations of the myosin II motor reveal a nucleotide-state sensing element that controls the recovery stroke. J. Mol. Biol. 361: 604-616.

47. Koppole, S., J. C. Smith, and S. Fischer. 2007. The structural coupling between ATPase activation and recovery stroke in the myosin II motor. Structure. 15: 825-837.

48. Koshland, D. E. 1958. Application of a Theory of Enzyme Specificity to Protein Synthesis. Proc. Natl. Acad. Sci. U. S. A 44: 98-104.

49. Kull, F. J., R. D. Vale, and R. J. Fletterick. 1998. The case for a common ancestor: kinesin and myosin motor proteins and G proteins. J Muscle Res. Cell Motil. 19: 877-886.

50. Kumar, S., B. Ma, C. J. Tsai, N. Sinha, and R. Nussinov. 2000. Folding and binding cascades: dynamic landscapes and population shifts. Protein Sci. 9: 10-19.

51. Kurzawa, S. E., D. J. Manstein, and M. A. Geeves. 1997. Dictyostelium discoideum myosin II: characterization of functional myosin motor fragments. Biochemistry 36: 317-323.

52. Leipe, D. D., Y. I. Wolf, E. V. Koonin, and L. Aravind. 2002. Classification and evolution of P-loop GTPases and related ATPases. J. Mol. Biol. 317: 41-72.

53. Lombardi, V., G. Piazzesi, M. A. Ferenczi, H. Thirlwell, I. Dobbie, and M. Irving. 1995. Elastic distortion of myosin heads and repriming of the working stroke in muscle. Nature 374: 553-555.

54. Lymn, R. W., and E. W. Taylor. 1971. Mechanism of adenosine triphosphate hydrolysis by actomyosin. Biochemistry 10: 4617-4624.

55. Malnasi-Csizmadia, A., J. L. Dickens, W. Zeng, and C. R. Bagshaw. 2005. Switch movements and the myosin crossbridge stroke. J. Muscle Res. Cell Motil. 1-7.

56. Malnasi-Csizmadia, A., D. S. Pearson, M. Kovacs, R. J. Woolley, M. A. Geeves, and C. R. Bagshaw. 2001. Kinetic resolution of a conformational transition and the ATP hydrolysis step using relaxation methods with a Dictyostelium myosin II mutant containing a single tryptophan residue. Biochemistry 40: 12727-12737.

57. Malnasi-Csizmadia, A., J. Toth, D. S. Pearson, C. Hetenyi, L. Nyitray, M. A. Geeves, C. R. Bagshaw, and M. Kovacs. 2007. Selective perturbation of the myosin recovery stroke by point mutations at the base of the lever arm affects ATP hydrolysis and phosphate release. J. Biol. Chem. 282: 17658-17664.

58. Malnasi-Csizmadia, A., R. J. Woolley, and C. R. Bagshaw. 2000. Resolution of conformational states of Dictyostelium myosin II motor domain using tryptophan (W501) mutants: implications for the open-closed transition identified by crystallography. Biochemistry 39: 16135-16146.

59. Manstein, D. J., K. M. Ruppel, and J.A. Spudich. 1989. Expression and characterization of a functional myosin head fragment in Dictyostelium discoideum. Science 246: 656-658.

60. Manstein, D. J., H. P. Schuster, P. Morandini, and D. M. Hunt. 1995. Cloning vectors for the production of proteins in Dictyostelium discoideum. Gene 162: 129-134.

61. Mermall, V., P. L. Post, and M. S. Mooseker. 1998. Unconventional myosins in cell movement, membrane traffic, and signal transduction. Science 279: 527-533.

62. Mesentean, S., S. Koppole, J. C. Smith, and S. Fischer. 2007. The principal motions involved in the coupling mechanism of the recovery stroke of the myosin motor. J. Mol. Biol. 367: 591-602.

63. Miller, C. J., W. W. Wong, E. Bobkova, P. A. Rubenstein, and E. Reisler. 1996. Mutational analysis of the role of the N terminus of actin in actomyosin interactions. Comparison with other mutant actins and implications for the cross-bridge cycle. Biochemistry 35: 16557-16565.

64. Monod, J., J. WYMAN, and J. P. CHANGEUX. 1965. ON THE NATURE OF ALLOSTERIC TRANSITIONS: A PLAUSIBLE MODEL. J. Mol. Biol. 12: 88-118.

65. Naber, N., T. J. Minehardt, S. Rice, X. Chen, J. Grammer, M. Matuska, R. D. Vale, P. A. Kollman, R. Car, R. G. Yount, R. Cooke, and E. Pate. 2003. Closing of the nucleotide pocket of kinesin-family motors upon binding to microtubules. Science 300: 798-801.

66. Najmoutin GA, and et al. 2005. Heterotrimeric G-protein alpha-subunit adopts a "preactivated" conformation when associated with betagamma-subunits. 38071-38080.

67. Onishi, H., S. V. Mikhailenko, and M. F. Morales. 2006. Toward understanding actin activation of myosin ATPase: the role of myosin surface loops. Proc. Natl. Acad. Sci. U. S. A 103: 6136-6141.

68. Onishi, H., and M. F. Morales. 2007. A closer look at energy transduction in muscle. Proc. Natl. Acad. Sci. U. S. A 104: 12714-12719.

69. Ranatunga, K. W., M. E. Coupland, and G. Mutungi. 2002. An asymmetry in the phosphate dependence of tension transients induced by length perturbation in mammalian (rabbit psoas) muscle fibres. J Physiol 542: 899-910.

70. Rayment, I., W. R. Rypniewski, K. Schmidt-Base, R. Smith, D. R. Tomchick, M. M. Benning, D. A. Winkelmann, G. Wesenberg, and H. M. Holden. 1993. Three-dimensional structure of myosin subfragment-1: a molecular motor. Science 261: 50-58.

71. Reubold, T. F., S. Eschenburg, A. Becker, F. J. Kull, and D. J. Manstein. 2003. A structural model for actin-induced nucleotide release in myosin. Nat. Struct. Biol. 10: 826-830.

72. Rosenfeld, S. S., A. Houdusse, and H. L. Sweeney. 2005. Magnesium regulates ADP dissociation from myosin V. J. Biol. Chem. 280: 6072-6079.

73. Siththanandan, V. B., J. L. Donnelly, and M. A. Ferenczi. 2006. Effect of strain on actomyosin kinetics in isometric muscle fibers. Biophys. J 90: 3653-3665.

74. Sleep, J., M. Irving, and K. Burton. 2005. The ATP hydrolysis and phosphate release steps control the time course of force development in rabbit skeletal muscle. J Physiol 563: 671-687.

75. Smith, C. A., and I. Rayment. 1996. X-ray structure of the magnesium(II).ADP.vanadate complex of the Dictyostelium discoideum myosin motor domain to 1.9 A resolution. Biochemistry 35: 5404-5417.

76. Smith, D. A., M. A. Geeves, J. Sleep, and S. M. Mijailovich. 2008. Towards a unified theory of muscle contraction. I: foundations. Ann. Biomed. Eng 36: 1624-1640.

77. Smith, D. A., and J. Sleep. 2004. Mechanokinetics of rapid tension recovery in muscle: the Myosin working stroke is followed by a slower release of phosphate. Biophys. J 87: 442-456.

78. Spoerner, M., T. Graf, B. Konig, and H. R. Kalbitzer. 2005. A novel mechanism for the modulation of the Ras-effector interaction by small molecules. Biochem. Biophys. Res. Commun. 334: 709-713.

79. Spoerner, M., C. Herrmann, I. R. Vetter, H. R. Kalbitzer, and A. Wittinghofer. 2001. Dynamic properties of the Ras switch I region and its importance for binding to effectors. Proc. Natl. Acad. Sci. U. S. A 98: 4944-4949.

80. Spoerner, M., A. Nuehs, C. Herrmann, G. Steiner, and H. R. Kalbitzer. 2007. Slow conformational dynamics of the guanine nucleotide-binding protein Ras complexed with the GTP analogue GTPgammaS. FEBS J 274: 1419-1433.

81. Spudich, J. A. 2001. The myosin swinging cross-bridge model. Nat. Rev. Mol. Cell Biol 2: 387-392.

82. Spudich, J. A., and S. Watt. 1971. The regulation of rabbit skeletal muscle contraction. I. Biochemical studies of the interaction of the tropomyosin-troponin complex with actin and the proteolytic fragments of myosin. J. Biol. Chem. 246: 4866-4871.

83. Sweeney, H. L., and A. Houdusse. 2004. The motor mechanism of myosin V: insights for muscle contraction. Philos. Trans. R. Soc. Lond B Biol Sci. 359: 1829-1841.

84. Szent-Gyorgyi, A. G. 2004. The early history of the biochemistry of muscle contraction. J. Gen. Physiol 123: 631-641.

85. Takagi, Y., H. Shuman, and Y. E. Goldman. 2004. Coupling between phosphate release and force generation in muscle actomyosin. Philos. Trans. R. Soc. Lond B Biol Sci. 359: 1913-1920.

86. Toth, J., B. Varga, M. Kovacs, A. Malnasi-Csizmadia, and B. G. Vertessy. 2007. Kinetic mechanism of human dUTPase, an essential nucleotide pyrophosphatase enzyme. J. Biol. Chem. 282: 33572-33582.

87. Weijland, A., and A. Parmeggiani. 1993. Toward a model for the interaction between elongation factor Tu and the ribosome. Science 259: 1311-1314.

88. Ye, M., F. Shima, S. Muraoka, J. Liao, H. Okamoto, M. Yamamoto, A. Tamura, N. Yagi, T. Ueki, and T. Kataoka. 2005. Crystal structure of M-Ras reveals a GTP-bound "off" state conformation of Ras family small GTPases. J Biol Chem. 280: 31267-31275.

89. Yu, H., L. Ma, Y. Yang, and Q. Cui. 2007. Mechanochemical coupling in the myosin motor domain. I. Insights from equilibrium active-site simulations. PLoS. Comput. Biol. 3: e21.

90. Yu, H., L. Ma, Y. Yang, and Q. Cui. 2007. Mechanochemical coupling in the myosin motor domain. II. Analysis of critical residues. PLoS. Comput. Biol. 3: e23.

91. Zeng, W., P. B. Conibear, J. L. Dickens, R. A. Cowie, S. Wakelin, A. Malnasi-Csizmadia, and C. R. Bagshaw. 2004. Dynamics of actomyosin interactions in relation to the cross-bridge cycle. Philos. Trans. R. Soc. Lond B Biol. Sci. 359: 1843-1855.